Reports File Posted 9/25

GEORGIA INSTITUTE OF TECHNOLOGY
OFFICE OF RESEARCH ADMINISTRATION

RESEARCH PROJECT INITIATION

Date: October 16, 1973

Project Title: Study of Multiple Hologram Recording in Lithium Niobate

Project No: E-21-633

Principal Investigator: Dr. W. R. Callen & Dr. T. K. Gaylord

Sponsor: NASA - Marshall Space Flight Center

Agreement Period: From 10/1/73 Until 10/31/74

Type Agreement: NAS8-30246

Amount:
$8,976 NASA funds (E-21-633)
5,225 GIT Contrib. (E-21-323)
$14,201 TOTAL

Reports Required:
Monthly Progress Reports; Final Technical Report

Sponsor Contact Person (s):

Technical Matters
Mr. Joseph H. Kerr or
Mr. E. H. Pitts
NASA-Marshall Space Flight Center
ATTN: S&E-ASTR-IA
Marshall Space Flight Center, Alabama 35812

Contractual Matters
(Thru ORA)
Mr. R. J. Whitcomb (ACO)
ONR Resident Representative
Campus

Assigned to: Electrical Engineering

COPIES TO:

- Principal Investigator
- School Director
- Dean of the College
- Director, Research Administration
- Director, Financial Affairs (2)
- Security-Reports-Property Office
- Patent Coordinator
- Library
- Rich Electronic Computer Center
- Photographic Laboratory
- Project File
- Other

RA-3 (6-71)

Reports File Rec'd

GEORGIA INSTITUTE OF TECHNOLOGY

OFFICE OF RESEARCH ADMINISTRATION

Board

RESEARCH PROJECT TERMINATION

Date: November 20, 1974

Project Title: Study of Multiple Hologram Recording in Lithium Niobate

Project No: E-21-633

Principal Investigator: Dr. W. R. Callen & Dr. T. K. Gaylord

Sponsor: NASA - Marshall Space Flight Center

Effective Termination Date: 10/31/74

Clearance of Accounting Charges: 10/31/74

Grant Closeout items remaining:

1. Final Report of Inventions
2. Government Property Inventory & Related Certificate
3. Classified Material Certificate

None

Assigned to Electrical Engineering

COPIES TO:

Principal Investigator
School Director
Dean of the College
Director of Research Administration
Associate Controller (2)
Security-Reports-Property Office
Patent and Inventions Coordinator

Library, Technical Reports Section
Rich Electronic Computer Center
Photographic Laboratory
Terminated Project File No. _____
Other _____

E-21-633

GEORGIA INSTITUTE OF TECHNOLOGY
ATLANTA, GEORGIA 30332

SCHOOL OF
ELECTRICAL ENGINEERING

November 7, 1973

Mr. J. H. Kerr
S & E-ASTR-IA
NASA/Marshall Space Flight Center

Title: "Study of Multiple Hologram Recording in Lithium Niobate"

Subject: Monthly Letter Report No. 1 on Contract NAS8-30246 for the Period 1 October 1973 to 31 November 1973.

Dear Sir:

Activities during the first month of the subject contract included organizational and planning sessions. A thorough review of optical recording and optical memory systems is planned. A number of equipment orders were planned and an inquiry about the purchase of iron-doped lithium niobate was sent.

Expenditures and man-hours effort during the first reporting period are:

Technical effort - 84 man-hours	$739
Materials and Supplies	0
Equipment	188
Total Expenditure to Date	$927

Next month's activities will include setting up some of the basic experimental procedures that are necessary for the investigation.

The projected expenditures and man-hours effort for the remainder of the program are:

Technical Effort	$5,674
Materials and Supplies	513
Equipment	1,862
	$8,049

Respectfully submitted,

W. R. Callen
T. K. Gaylord
Project Directors

WRC TKG/kfc

cc: J. Weaver

E-21-633

GEORGIA INSTITUTE OF TECHNOLOGY
ATLANTA, GEORGIA 30332

SCHOOL OF
ELECTRICAL ENGINEERING

December 7, 1973

Mr. J. H. Kerr
S & E-ASTR-IA
NASA/Marshall Space Flight Center
Marshall Space Flight Center, Alabama 35812

Title: "Study of Multiple Hologram Recording in Lithium Niobate"

Subject: Monthly Letter Report No. 2 on Contract NAS8-30246 for the Period 1 November 1973 to 1 December 1973.

Dear Sir:

Activities during the second month of the subject contract included extensive fine tuning and adjustment of the argon laser. Excellent amplitude and frequency stability were obtained.

Expenditures and man-hours effort during the first two reporting periods are:

Technical Effort - 168 man-hours	$1,478
Materials and Supplies	0
Equipment	188
Total Expenditure to Date	$1,666

Next month's activities will include the study and start of construction of an oven to contain the volume holographic storage material, and to control accurately its temperature.

The projected expenditures and man-hours effort for the remainder of the program are:

Technical Effort	$4,935
Materials and Supplies	513
Equipment	1,862
	$7,310

Respectfully submitted,

W. R. Callen
T. K. Gaylord
Project Directors

WRC TKG/kfc

cc: J. Weaver

GEORGIA INSTITUTE OF TECHNOLOGY
ATLANTA, GEORGIA 30332

SCHOOL OF
ELECTRICAL ENGINEERING

January 7, 1974

Mr. J. H. Kerr
S & E-ASTR-IA
NASA/Marshall Space Flight Center

Title: "Study of Multiple Hologram Recording in Lithium Niobate"

Subject: Monthly Letter Report No. 3 on Contract NAS8-30246 for the Period 1 December 1973 to 1 January 1974.

Dear Sir:

Activities during the third month of the subject contract included purchase and initial set-up of the basic experimental equipment. The report "Angular Selectivity of Lithium Niobate Volume Holograms"[1] was published in Journal of Applied Physics. These results show that the angular packing density of holograms in practice is in agreement with the theoretically calculated value--a very important result.

Expenditures and man-hours effort during the first three reporting periods are:

Technical effort - 252 man-hours	$ 2,217
Materials and Supplies	80
Equipment	1,264
Total Expenditure to Date	$ 3,561

Next month's activities will include continued effort on the experimental measurement of diffraction efficiency of lithium niobate holograms. This work is concentrating on the measurement of excess scattered light that is observed during the read-out process. Multiple holograms stored at present are being monitored periodically to determine if there are any changes in angular selectivity, scattered light output and diffraction efficiency.

---

[1] T. K. Gaylord and F. K. Tittel, "Angular selectivity of lithium niobate volume holograms," J. Appl. Physics, vol. 44, no. 10, pp. 4771-4773, October 1973.

Mr. J. H. Kerr
Contract NAS8-30246

January 7, 1974

The projected expenditures and man-hours effort for the remainder of the program are:

Techanical Effort	$ 4196
Materials and Supplies	433
Equipment	786
	$ 5415

Respectfully submitted,

W. R. Callen
T. K. Gaylord
Project Directors

WRC TKG/kfc

cc: J. Weaver

E-21-633

GEORGIA INSTITUTE OF TECHNOLOGY
ATLANTA, GEORGIA 30332

SCHOOL OF
ELECTRICAL ENGINEERING

February 7, 1974

Mr. J. H. Kerr
S & E-ASTR-IA
NASA/Marshall Space Flight Center
Marshall Space Flight Center, Alabama 35812

Title: "Study of Multiple Hologram Recording in Lithium Niobate"

Subject: Monthly Letter Report No. 4 on Contract NAS8-30246 for the Period 1 January 1974 to 1 February 1974.

Dear Sir:

Activities during the fourth month of the subject contract included a significant experimental and theoretical effort into the "scattered light problem" associated with optical recording in lithium niobate. This effort was done in conjunction with Robert Magnusson, one of Dr. Gaylord's graduate students. A preliminary theory has been developed by them and much of the past month has been spent experimentally testing these predicted results. Experiments, now largely completed, show a remarkably close agreement between theory and experiment. Light entering the crystal is scattered by a, so far, unknown scattering center. Due to the thickness of the crystal this light in turn interferes with the original laser beam and a holographic pattern is recorded. Upon reading illumination of the lithium niobate, this holographic pattern is reconstructed as a series of diffraction cones that give the impression of scattered light.

Expenditures and man-hours effort during the first four reporting periods are:

Technical Effort - 364 man-hours	$2,984
Materials and Supplies	109
Equipment	1,264
Total Expenditure to Date	$4,357

Next month's activities will include further experimental and theoretical investigations of the scattered light problem. Preliminary experimental efforts on multiple holographic storage are being formulated.

The projected expenditures and man-hours effort for the remainder of the program are:

Technical Effort	$3,429
Materials and Supplies	404
Equipment	786
	$4,619

Respectfully submitted,

W. R. Callen
T. K. Gaylord
Project Directors

WRC TKG/kfc

cc: J. Weaver

GEORGIA INSTITUTE OF TECHNOLOGY
ATLANTA, GEORGIA 30332

SCHOOL OF
ELECTRICAL ENGINEERING

March 7, 1974

Mr. J. H. Kerr
S & E-ASTR-IA
NASA/Marshall Space Flight Center
Marshall Space Flight Center, Alabama 35812

Title: "Study of Multiple Hologram Recording in Lithium Niobate"

Subject: Monthly Letter Report No. 5 on Contract NAS8-30246 for the Period 1 February 1974 to 1 March 1974.

Dear Sir:

Activities during the fifth month of the subject contract included the official announcement of experimental results[1] that have been acquired over a period of about one year. It has now been shown that very high writing sensitivities (defined in terms of the exposure per unit areas necessary to construct a 1% diffraction efficiency hologram) are attainable in lithium niobate. These sensitivities are much higher than any previously reported for any of the ferroelectrics. The sensitivity reported previously for lithium niobate was about 0.8 joules/cm^2. Our recent results show that only 2×10^{-3} joules/cm^2 are required to write a 1% efficient hologram in certain iron-doped crystals. This new high sensitivity even exceeds the recent monumental breakthrough with strontium barium niobate[2], in which the energy to write a hologram was reduced from 15 joules/cm^2 to 4×10^{-3} joules/cm^2. These results are extremely important to our effort, since lithium niobate is technologically a much more advanced material than is strontium barium niobate.

Expenditures and man-hours effort during the first five reporting periods are:

Technical Effort - 476 man-hours	$3,751
Materials and Supplies	116
Equipment	1,264
Total Expenditure to Date	$5,131

Next month's activities will include detailed experimental investigation of the problem of multiple hologram storage at a single crystal location.

---

[1] Applied Physics Letters, Vol. 24, pp. 130-131, February 1974.

[2] Optical Society of America Topical Meeting on Optical Storage of Digital Data, Aspen, Colorado, April 1973.

The projected expenditures and man-hours effort for the remainder of the program are:

Technical Effort	$2,662
Materials and Supplies	397
Equipment	786
Total Projected Expenditure for Completion of the Program	$3,845

Respectfully submitted,

W. R. Callen
T. K. Gaylord
Project Directors

WRC/TKG:bew

cc: J. Weaver

GEORGIA INSTITUTE OF TECHNOLOGY
ATLANTA, GEORGIA 30332

SCHOOL OF
ELECTRICAL ENGINEERING

April 7, 1974

Mr. J. H. Kerr
S & E-ASTR-IA
NASA/Marshall Space Flight Center
Marshall Space Flight Center, Alabama 35812

Title: "Study of Multiple Hologram Recording in Lithium Niobate"

Subject: Monthly Letter Report No. 6 on Contract NAS8-30246 for the Period 1 March 1974 to 1 April 1974.

Dear Sir:

Activities during the sixth month of the subject contract included the completion of the experimental and theoretical effort to explain the "scattered light" that appears when lithium niobate holograms are reconstructed. The final theoretical analysis is applicable to a two beam holographic configuration, in addition to the one beam exposure case that recently has been reported in the literature.[1] Scattered light within the lithium niobate interferes with the incident laser beams, and this interference pattern is recorded in addition to the two beam interference pattern. These experimental and theoretical results have been accepted for publication.[2]

Expenditures and man-hours effort during the first six reporting periods are:

Technical Effort - 588 man-hours	$4,508
Materials and Supplies	146
Equipment	1,264
Total Expenditure to Date	$5,918

Next month's activities will include continued effort on the problem of multiple hologram storage at a single crystal location.

---

[1] M. R. B. Forshaw, Applied Optics, Vol. 13, p. 2, 1974.

[2] R. Magnusson and T. K. Gaylord, Applied Optics, Vol. 13, 1974 (to appear).

The projected expenditures and man-hours effort for the remainder of the program are:

Technical Effort	$1,905
Materials and Supplies	367
Equipment	786
Total Projected Expenditure for Completion of the Program	$3,058

Respectfully submitted,

W. R. Callen
T. K. Gaylord
Project Directors

WRC TKG/kfc

cc: J. Weaver

GEORGIA INSTITUTE OF TECHNOLOGY
ATLANTA, GEORGIA 30332

SCHOOL OF
ELECTRICAL ENGINEERING

May 7, 1974

Mr. J. H. Kerr
S & E- ASTR-IA
NASA/Marshall Space Flight Center
Marshall Space Flight Center, Alabama 35812

Title: "Study of Multiple Hologram Recording in Lithium Niobate"

Subject: Monthly Letter Report No. 7 on Contact NAS8-30246 for the period 1 April 1974 to 1 May 1974.

Dear Sir:

Activities during the seventh month of the subject contract included an experimental investigation of multiple hologram storage in lithium niobate. In particular, several plane wave holograms were stored successfully at a single location in a sample of lithium niobate. When the holograms were played back, the holograms exhibited noticeable fine structure in the angular selectivity. This fine structure could, in some cases, indicate an optimal method of close packing of multiply stored holograms. The origin of the fine structure is under investigation.

Expenditures and man-hours effort during the first seven reporting periods are:

Technical Effort- 630 man-hours	$4,798
Materials and Supplies	167
Equipment	1,470
Total Expenditure to Date	$6,435

Next month's activities will include continued experimental effort on the problem of multiple hologram storage at a single crystal location.

The projected expenditures and man-hours effort for the remainder of the program are:

Technical Effort	$1,615
Materials and Supplies	346
Equipment	580
Total Projected Expenditure for Completion of the Program	$2,541

Respectfully submitted,

W. R. Callen
T. K. Gaylord
Project Directors

WRC,TKG/sb
cc: J. Weaver

GEORGIA INSTITUTE OF TECHNOLOGY
ATLANTA, GEORGIA 30332

SCHOOL OF
ELECTRICAL ENGINEERING

June 7, 1974

Mr. J. H. Kerr
S & E - ASTR - IA
NASA/Marshall Space Flight Center
Marshall Space Flight Center, Alabama 35812

Title: "Study of Multiple Hologram Recording in Lithium Niobate"

Subject: Monthly Letter Report No. 8 on Contract NAS8-30246 for the period 1 May 1974 to 1 June 1974.

Dear Sir:

Activities during the eighth month of the subject contract included a preliminary study of multi-port aspects of a proposed high capacity optical recorder. This would allow multiple users to access the stored data simultaneously, rather than sequentially. This possibility immediately indicates the potential of performing true parallel processing on the stored data. This will allow very efficient handling of the recorded data.

Expenditures and man-hours effort during the first eight reporting periods are:

Technical Effort - 672 man hours	$5,088
Materials and Supplies	395
Equipment	1,470
Total Expenditure to Date	$6,953

Next month's activities will include continued experimental and theoretical effort on the overall problem of multiple holographic storage.

The projected expenditures and man-hours effort for the remainder of the program are:

Technical Effort	$1,325
Materials and Supplies	118
Equipment	580
Total Projected Expenditure for Completion of the Program	$2,023

Respectfully submitted,

W. R. Callen
T. K. Gaylord
Project Directors

WRC TKG/kfc

cc: J. Weaver

File: E-21633

GEORGIA INSTITUTE OF TECHNOLOGY
ATLANTA, GEORGIA 30332

SCHOOL OF
ELECTRICAL ENGINEERING

July 7, 1974

Mr. J. H. Kerr
S & E-ASTR-IA
NASA/Marshall Space Flight Center
Marshall Space Flight Center, Alabama 35812

Title: "Study of Multiple Hologram Recording in Lithium Niobate"

Subject: Monthly Letter Report No. 9 on Contract NAS8-30246 for the period 1 June 1974 to 1 July 1974.

Dear Sir:

Activities during the ninth month of the subject contract included the culmination of a detailed analysis of the diffraction efficiency of thick holographic gratings with arbitrary shape.[1] A Fourier series representation of the grating is employed along with a coupled-mode theory of diffraction. The results obtained are in good agreement with the extention of Burckhardt's theory to nonsinusoidal gratings. The coupled-mode theory, however, is computationally simpler and more efficient. The results indicate the possibility that this type of analysis might be used in reverse to determine the grating shapes of thick grating holograms recorded in lithium niobate. Depending on which of the possible physical mechanisms is operative in a given situation (drift or diffusion), different grating shapes are generated.

Expenditures and man-hours effort during the first nine reporting periods are:

Technical Effort - 714 man-hours	$5,378
Materials and Supplies	425
Equipment	1,470
Total Expenditure to Date	$7,273

Next month's activities will include experimental effort on the problem of multiple hologram storage at a single crystal location.

---

[1] S. F. Su and T. K. Gaylord, "Calculation of Arbitrary Order Diffraction Efficiencies of Thick Gratings with Arbitrary Grating Shape," to be submitted to Journal of the Optical Society of America.

The projected expenditures and man-hours effort for the remainder of the program are:

Technical Effort	$1,035
Materials and Supplies	88
Equipment	580
Total Projected Expenditure for Completion of the Program	$1,703

Respectfully submitted,

W. R. Callen
T. K. Gaylord
Project Directors

WRC/TKG:km

cc: J. Weaver

GEORGIA INSTITUTE OF TECHNOLOGY
ATLANTA, GEORGIA 30332

SCHOOL OF
ELECTRICAL ENGINEERING

August 7, 1974

Mr. J. H. Kerr
S & E-ASTR-IA
NASA/Marshall Space Flight Center
Marshall Space Flight Center, Alabama 35812

Title: "Study of Multiple Hologram Recording in Lithium Niobate"

Subject: Monthly Letter Report No. 10 on Contract NAS8-30246 for the period 1 July 1974 to 1 August 1974.

Dear Sir:

Activities during the tenth month of the subject contract included the official announcement of the experimental results and theoretical explanation of the scattered light that appears during reconstruction of lithium niobate holograms.[1] In addition, a second article was published detailing the requirements for practical optical memories.[2] Types of page composers are compared, and the required writing energy densities for various optical recording materials are tabulated.

Expenditures and man-hours effort during the first ten reporting periods are:

Technical Effort - 736 man-hours	$5,723
Materials and Supplies	513
Equipment	1,675
Total Expenditure to Date	$7,911

Next month's activities will include continued effort on the general problem of multiple hologram storage at a single crystal location.

---

[1] R. Magnusson and T. K. Gaylord, "Laser Scattering Induced Holograms in Lithium Niobate," Applied Optics, Vol. 13, pp. 1545-1548, July 1974.

[2] T. K. Gaylord, "Optical Memories: Filling the Storage Gap," Optical Spectra, Vol. 8, pp. 29-34, June, 1974.

The projected expenditures and man-hours effort for the remainder of the program are:

Technical Effort	$ 690
Materials and Supplies	0
Equipment	375
Total Projected Expenditure for Completion of the Program	$1,065

Respectfully submitted,

W. R. Callen
T. K. Gaylord
Project Directors

WRC/TKG:kfc

cc: J. Weaver

GEORGIA INSTITUTE OF TECHNOLOGY
ATLANTA. GEORGIA 30332

SCHOOL OF
ELECTRICAL ENGINEERING

September 7, 1974

Mr. J. H. Kerr
S & E-ASTR-IA
NASA/Marshall Space Flight Center
Marshall Space Flight Center, Alabama 35812

Title: "Study of Multiple Hologram Recording in Lithium Niobate"

Subject: Monthly Letter Report No. 11 on Contract NAS8-30246 for the period 1 August 1974 to 1 September 1974.

Dear Sir:

Activities during the eleventh month of the subject contract included a detailed experimental and theoretical study of the angular positioning requirements of the lithium niobate crystal for reading out the stored hologram. Theoretical results were obtained using the coupled wave theory of Kogelnik and the matrix numerical theory of Burckhardt. Comparison to our experimental results shows fairly good agreement. Detailed graphs will be presented in the Final Report.

A study of the interference effects due to the uncoated crystal surfaces was undertaken. It was found that the diffraction efficiency could vary dramatically depending on the material thickness. Details will be presented in the Final Report.

Expenditures and man-hours effort during the first eleven reporting periods are:

Technical Effort - 758 man-hours	$6,068
Materials and Supplies	513
Equipment	2,035
Total Expenditure to Date	$8,616

Next month's activities will include the conclusion of our findings on the problem of multiple hologram storage in $LiNbO_3$.

The projected expenditures and man-hours effort for the remainder of the program are:

Technical Effort	$ 345
Materials and Supplies	0
Equipment	15
Total Projected Expenditure for Completion of the Program	$ 360

Respectfully submitted,

W. R. Callen
T. K. Gaylord
Project Directors

WRC/TKG:sbp

cc: J. Weaver

GEORGIA INSTITUTE OF TECHNOLOGY
ATLANTA, GEORGIA 30332

SCHOOL OF
ELECTRICAL ENGINEERING

November 7, 1974

Mr. J. H. Kerr
EF-13
NASA/Marshall Space Flight Center
Marshall Space Flight Center, Alabama 35812

Title: "Study of Multiple Hologram Recording in Lithium Niobate"

Subject: Monthly Letter Report No. 12 on Contract NAS8-30246 for the Period 1 October 1974 to 1 November 1974.

Dear Sir:

Activities during the twelfth month of the subject contract included the determination of optical requirements for evaluation of binary data page holograms. The necessary optics include two Fourier transform lenses, beam expander, data mask, film holder, five degree-of-freedom crystal mount, beam splitter and two mirrors.

Expenditures and man-hours effort during the first twelve reporting periods are:[1]

Technical Effort - 780 man-hours	$6,413
Materials and Supplies	513
Equipment	2,050
Total Expenditures to Date	$8,976

Next month's activities will include the determination of the mechanical requirements for the evaluation of binary data page holograms.

---

[1] Expenditure to date does not reflect funds of contract extension granted 1-23-75.

The projected expenditures and man-hours effort for the remainder of the program are:[2]

Technical Effort	$16,735
Materials and Supplies	1,500
Equipment	1,640
Travel	125
Total Project Expenditures for Completion of the Program	$20,000

Respectfully submitted,

W. R. Callen
T. K. Gaylord
Project Directors

WRC/TKG:gc

cc: J. Weaver

[2]Projected expenditure reflects contract extension granted 1-23-75.

GEORGIA INSTITUTE OF TECHNOLOGY
ATLANTA, GEORGIA 30332

SCHOOL OF
ELECTRICAL ENGINEERING

December 7, 1974

Mr. J. H. Kerr
EF-13
NASA/Marshall Space Flight Center
Marshall Space Flight Center, Alabama 35812

Title: "Study of Multiple Hologram Recording in Lithium Niobate"

Subject: Monthly Letter Report No. 13 on Contract NAS8-30246 for the Period 1 November 1974 to 1 December 1974.

Dear Sir:

Activities during the thirteenth month of the subject contract included the determination of mechanical requirements for the evaluation of binary data page holograms. Mechanical holders for the Fourier transform lenses, data mask positioner, collimator holder, beam splitter, and mirror mount interfaces are being designed.

Expenditures and man-hours effort during the first thirteen reporting periods are:[1]

Technical Effort - 780 man-hours	$6,413
Materials and Supplies	513
Equipment	2,050
Total Expenditures to Date	$8,976

Next month's activities will include the design of the overall system for evaluation of data page holograms in lithium niobate.

---

[1] Expenditure to date does not reflect funds of contract extension granted 1/23/75.

The projected expenditures and man-hours effort for the remainder of the program are:[2]

Technical Effort	$16,735
Materials and Supplies	1,500
Equipment	1,640
Travel	125
Total Projected Expenditures for Completion of the Program	$20,000

Respectfully submitted,

W. R. Callen
T. K. Gaylord
Project Directors

WRC/TKG:gc

cc: J. Weaver

[2]Projected expenditure reflects contract extension granted 1/23/75.

GEORGIA INSTITUTE OF TECHNOLOGY
ATLANTA, GEORGIA 30332

SCHOOL OF
ELECTRICAL ENGINEERING

January 7, 1975

Mr. J. H. Kerr
EF-13
NASA/Marshall Space Flight Center
Marshall Space Flight Center, Alabama 35812

Title: "Study of Multiple Hologram Recording in Lithium Niobate"

Subject: Monthly Letter Report No. 14 on Contract NAS8-30246 for the Period 1 December 1974 to 1 January 1975.

Dear Sir:

Activities during the fourteenth month of the subject contract included the design of the overall configuration for evaluation of data page holograms. A large optical breadboard is under construction for the prototype system. Materials have been obtained for optical interfaces, and these are currently being built.

Expenditures and man-hours effort during the first fourteen reporting periods are:[1]

Technical Effort - 780 man-hours	$6,413
Materials and Supplies	513
Equipment	2,050
Total Expenditures to Date	$8,976

Next month's activities will include testing of the mechanical-optical system for evaluation of the data page holograms and initial determination of experimental configuration for use of the frequency doubled Nd:YAG laser as a source for writing multiple holograms.

---

[1]Expenditure to date does not reflect funds of contract extension granted 1-23-75.

The projected expenditures and man-hours effort for the remainder of the program are:[2]

Technical Effort	$16,735
Materials and Supplies	1,500
Equipment	1,640
Travel	125
Total Projected Expenditure for Completion of the Program	$20,000

Respectfully submitted,

W. R. Callen
T. K. Gaylord
Project Directors

WRC/TKG:gc

cc: J. Weaver

[2]Projected expenditure reflects contract extension granted 1-23-75.

GEORGIA INSTITUTE OF TECHNOLOGY
ATLANTA, GEORGIA 30332

SCHOOL OF
ELECTRICAL ENGINEERING

February 7, 1975

Mr. J. H. Kerr
EF-13
NASA/Marshall Space Flight Center
Marshall Space Flight Center, Alabama 35812

Title: "Study of Multiple Hologram Recording in Lithium Niobate"

Subject: Monthly Letter Report No. 15 on Contract NAS8-30246 for the Period 1 January 1975 to 1 February 1975.

Dear Sir:

Activities during the fifteenth month of the subject contract included the completion of the construction of the Fourier transform lens mountings and the optical breadboard. The optical breadboard has been constructed to allow a wide variety of optical configurations to be tested with a minimum of set-up time. The preliminary design of the experimental configuration for use of the frequency doubled Nd:YAG laser as a source for writing multiple holograms has been completed.

Expenditures and man-hours effort during the first fifteen reporting periods are:

Technical Effort - 958 man-hours	$ 9,625
Materials and Supplies	1,049
Equipment	2,862
Travel	0
Total Expenditures to Date	$13,536

Next month's activities will include the design of a versatile mask holder and the preparation of photomask (data page) art work.

The projected expenditures for the remainder of the program are:

Technical Effort	$13,523
Materials and Supplies	1,078
Equipment	714
Travel	125
Total Projected Expenditures for Completion of the Program	$15,440

Respectfully submitted,

W. R. Callen
T. K. Gaylord
Project Directors

WRC/TKG:gc

cc: J. Weaver

GEORGIA INSTITUTE OF TECHNOLOGY
ATLANTA, GEORGIA 30332

SCHOOL OF
ELECTRICAL ENGINEERING

March 7, 1975

Mr. J. H. Kerr
EF-13
NASA/Marshall Space Flight Center
Marshall Space Flight Center, Alabama 35812

Title: "Study of Multiple Hologram Recording in Lithium Niobate"

Subject: Monthly Letter Report No. 16 on Contract NAS8-30246 for the Period 1 February 1975 to 1 March 1975.

Dear Sir:

Activities during the sixteenth month of the subject contract included the calculation of the limiting cases needed in the binary data pages to allow full testing of the lithium niobate holographic storage. Required data page configurations include 1) checker board, 2) alternate columns (or rows), and 3) random pattern. Art work to generate these input masks is currently being drawn.

Expenditures and man-hours effort during the first sixteen reporting periods are:

Technical Effort - 1,136 man-hours	$12,837
Materials and Supplies	1,212
Equipment	2,862
Travel	73
Total Expenditures to Date	$16,984

Next month's activities will include the preparation of glass substrate data pages from art work and the final design of the mask holder and the film plate holder.

The projected expenditures for the remainder of the program are:

Technical Effort	$10,311
Materials and Supplies	915
Equipment	714
Travel	52
Total Projected Expenditure for Completion of the Program	$11,992

Respectfully submitted,

W. R. Callen
T. K. Gaylord
Project Directors

WRC/TKG:gc

cc: J. Weaver

GEORGIA INSTITUTE OF TECHNOLOGY
ATLANTA, GEORGIA 30332

SCHOOL OF
ELECTRICAL ENGINEERING

April 7, 1975

Mr. J. H. Kerr
EF-13
NASA/Marshall Space Flight Center
Marshall Space Flight Center, Alabama 35812

Title: "Study of Multiple Hologram Recording in Lithium Niobate"

Subject: Monthly Letter Report No. 17 on Contract NAS8-30246 for the Period 1 March 1975 to 1 April 1975.

Dear Sir:

Activities during the seventeenth month of the subject contract included preliminary check-out of a small scale prototype system on the completed optical breadboard. The two inch spatially filtered collimator was tested and found to be satisfactory. Preliminary check-out of the 8 inch focal length Fourier transform lens indicated that qualitatively these lenses were satisfactory. The two dimensional Fourier transforms of a variety of transparency objects were obtained with these lenses. Some possible problems with astigmatism were noted.

Expenditures and man-hours effort during the first seventeen reporting periods are:

Technical Effort - 1,314 man-hours	$16,049
Materials and Supplies	1,640
Equipment	2,862
Travel	73
Total Expenditures to Date	$20,624

Next month's activities will include testing of inverse Fourier transforming and spatial filtering.

The projected expenditures for the remainder of the program are:

Technical Effort	$7,099
Materials and Supplies	487
Equipment	714
Travel	52
Total Projected Expenditures for Completion of the Program	$8,352

Respectfully submitted,

W. R. Callen
T. K. Gaylord
Project Directors

WRC/TKG:gc

cc: J. Weaver

E-21-633

GEORGIA INSTITUTE OF TECHNOLOGY
SCHOOL OF ELECTRICAL ENGINEERING
ATLANTA, GEORGIA 30332

PHONE: (404) 894-2901

May 7, 1975

Mr. J. H. Kerr
EF-13
NASA/Marshall Space Flight Center
Marshall Space Flight Center, Alabama 35812

Title: "Study of Multiple Hologram Recording in Lithium Niobate"

Subject: Monthly Letter Report No. 18 on Contract NAS8-30246 for the Period 1 April 1975 to 1 May 1975.

Dear Sir:

Activities during the eighteenth month of the subject contract included further check-out of the object beam optical system. This included Fourier transforming a two dimensional transparency with the first lens and inverse Fourier transforming with the second lens. Qualitative inspection of the original transparency and the image of the transparency through the object beam optical system showed good replication. A number of specialized test patterns (to simulate binary data) were ordered and were received.

Expenditures and man-hours effort during the first eighteen reporting periods are:

Technical Effort - 1,377 man-hours	$17,011
Materials and Supplies	1,640
Equipment	3,214
Travel	73
Total Expenditures to Date	$21,938

Next month's activities will include testing of the positioning sensitivity of the optical elements.

The projected expenditures for the remainder of the program are:

Technical Effort	$6,137
Materials and Supplies	487
Equipment	362
Travel	52
Total Projected Expenditures for Completion of the Program	$7,038

Respectfully submitted,

W. R. Callen
T. K. Gaylord
Project Directors

WRC/TKG:gc

cc: J. Weaver

E-21-633

GEORGIA INSTITUTE OF TECHNOLOGY
SCHOOL OF ELECTRICAL ENGINEERING
ATLANTA, GEORGIA 30332

PHONE: (404) 894-2901

June 7, 1975

Mr. J. H. Kerr
EF-13
NASA/Marshall Space Flight Center
Marshall Space Flight Center, Alabama 35812

Title: "Study of Multiple Hologram Recording in Lithium Niobate"

Subject: Monthly Letter Report No. 19 on Contract NAS8-30246 for the Period 1 May 1975 to 1 June 1975.

Dear Sir:

Activities during the nineteenth month of the subject contract included further testing of object beam and read-out optics. An extensive series of tests to determine the positioning sensitivity of spatial filters in the Fourier transform plane (filter plane) were undertaken. With the 8 inch focal length, f/5.6 transform lenses, the positioning was found to be very critical. A variety of realistic data page masks were completed this month.

Expenditures and man-hours effort during the first nineteen reporting periods are:

Technical Effort - 1,440 man-hours	$17,973
Materials and Supplies	1,643
Equipment	3,240
Travel	73
Total Expenditures to Date	$22,929

Next month's activities will include testing of the entire holographic optical system.

The projected expenditures for the remainder of the program are:

Technical Effort	$5,175
Materials and Supplies	484
Equipment	336
Travel	52
Total Projected Expenditures for Completion of the Program	$6,047

Respectfully submitted,

W. R. Callen
T. K. Gaylord
Project Directors

WRC/TKG:gc

cc: J. Weaver

E-21-633

GEORGIA INSTITUTE OF TECHNOLOGY
SCHOOL OF ELECTRICAL ENGINEERING
ATLANTA, GEORGIA 30332

PHONE: (404) 894-2901

July 7, 1975

Mr. J. H. Kerr
EF-13
NASA/Marshall Space Flight Center
Marshall Space Flight Center, Alabama 35812

Title: "Study of Multiple Hologram Recording in Lithium Niobate"

Subject: Monthly Letter Report No. 20 on Contract NAS8-30246 for the Period 1 June 1975 to 1 July 1975.

Dear Sir:

Activities during the twentieth month of the subject contract included completion of a major project to predict the index of refraction distribution within the lithium niobate storage crystals. This work has no been completed and represents an extension of J. J. Amodei's work (at RCA Laboratories). The holographic grating shape is now known as a function of physical mechanism for the entire recording process, not just for the initial-stage and final-stage (steady state) of recording. This information will be presented in detail in the Final Report, under the sub-heading "Unified Approach to the Formation of Phase Holograms in Lithium Niobate."

Expenditures and man-hours effort during the first twenty reporting periods are:

Technical Effort - 1,503 man-hours	$18,935
Materials and Supplies	1,975
Equipment	3,252
Travel	73
Total Expenditure to Date	$24,235

Next month's activities will include continued testing of the entire holographic optical system.

The projected expenditures for the remainder of the program are:

Technical Effort	$4,213
Materials and Supplies	152
Equipment	324
Travel	52
Total Projected Expenditure for Completion of the Program	$4,741

Respectfully submitted,

W. R. Callen
T. K. Gaylord
Project Directors

WRC/TKG:gc

cc: J. Weaver

E-21-633

GEORGIA INSTITUTE OF TECHNOLOGY
SCHOOL OF ELECTRICAL ENGINEERING
ATLANTA, GEORGIA 30332

PHONE: (404) 894-2901

August 7, 1975

Mr. J. H. Kerr
Mr. H. F. Smith
EF-13
NASA/Marshall Space Flight Center
Marshall Space Flight Center, Alabama 35812

Title: "Study of Multiple Hologram Recording in Lithium Niobate"

Subject: Monthly Letter Report No. 21 on Contract NAS8-30246 for the Period 1 July 1975 to 1 August 1975.

Dear Sirs:

Activities during the twenty-first month of the subject contract included testing of the holographic optical recording and readout system. This was done by placing input images in the experimental configuration and recording the Fourier transforms of the data patterns and the inverse Fourier transforms of the transformed data (producing a real and doubly inverted image of the input data). This was done for three limiting case data patterns: 1) alternate rows of "1"s and "0"s; 2) checkerboard pattern; and 3) a random array of "1"s and "0"s. The recorded intensity contours of the Fourier transforms were recorded and compared with theoretically determined patterns. These compared quite closely. The retransformed final doubly inverted images also were recorded for comparison to the originals. With the exception of a non-symmetrical bright spot, these retransformed images looked very good. The non-symmetrical bright spot is attributable to a slight wedge angle in the Kodak HRP plates and may require an aligned gate for removal. Complete pictoral results will be presented in our final report.

Expenditures and man-hours effort during the first twenty-one reporting periods are:

Technical Effort - 1,580 man-hours	$20,307
Materials and Supplies	2,025
Equipment	3,276
Travel	73
Total Expenditure to Date	$25,681

Next month's activities will include the completion of the description of general volume holography results by the dynamic theory.

The projected expenditures for the remainder of the program are:

Technical Effort	$ 2,841
Materials and Supplies	102
Equipment	300
Travel	52
Total Projected Expenditure for Completion of the Program	$ 3,295

Respectfully submitted.

W. R. Callen
T. K. Gaylord
Project Directors

WRC/TKG:gc

cc: J. Weaver

E-21-633

GEORGIA INSTITUTE OF TECHNOLOGY
SCHOOL OF ELECTRICAL ENGINEERING
ATLANTA, GEORGIA 30332

PHONE: (404) 894-2901

September 7, 1975

Mr. J. H. Kerr
Mr. H. F. Smith
EF-13
NASA/Marshall Space Flight Center
Marshall Space Flight Center, Alabama 35812

Title: "Study of Multiple Hologram Recording in Lithium Niobate"

Subject: Monthly Letter Report No. 22 on Contract NAS8-30246 for the Period 1 August 1975 to 1 September 1975.

Dear Sirs:

Activities during the twenty-second month of the subject contract included the completion of an important initial phase of a generalized theory to describe all experimental results of recording and reading in volume holography. We have acquired additional experimental results this month, and these results seem to be in qualitative agreement with the theoretical work just completed. The use of a dynamic (continuous feedback) approach allows the inclusion of the effects of a laser wave interfering with its own diffracted wave inside the recording medium due to the volume nature of the storage medium. This effect causes the continuous recording of another hologram that alters the initial one, producing a resultant grating that is not uniform through the thickness of the recording material. The reading and writing characteristics of such a hologram can vary dramatically, depending on the recording material and the experimental conditions. A large number of diverse types of writing, reading, and angular selectivity characteristics have been reported in the published literature (approximately 25 articles). The dynamic theory of thick hologram writing and reading is shown to predict qualitatively all of these various types of experimental behavior. Many rapidly-varying, experimental, writing and reading results (such as those we have observed in our laboratory) have previously informally been attributed to "experimental problems." It is apparent now that these results are "normal" for those conditions and should be expected. Our understanding of volume holography has been incomplete. Thus the dynamic theory has been shown by us (effort led by Robert Magnusson, a Ph.D. student) to be very powerful, (1) in determining the material and recording parameters needed to produce a certain desired hologram characteristic and (2) as a diagnostic tool to analyze the parameters of thick photosensitive recording materials.

This effort should be greatly expanded and applied to predict quantitative experimental results based on the parameters of significance that have emerged as a result of this initial study.

Expenditures and man-hours effort during the first twenty-two reporting periods are:

Technical Effort - 1,657 man-hours	$21,679
Materials and Supplies	2,127
Equipment	3,276
Travel	73
Total Expenditure to Date	$27,155

Next month's activities will include complete documentation of the research effort in an interim report.

The projected expenditures for the remainder of the program are:

Technical Effort	$ 1,469
Materials and Supplies	0
Equipment	300
Travel	52
Total Projected Expenditure for Completion of the Program	$ 1,821

Respectfully submitted,

W. R. Callen
T. K. Gaylord
Project Directors

WRC/TKG:gc

cc: J. Weaver

E #-21-633

GEORGIA INSTITUTE OF TECHNOLOGY
SCHOOL OF ELECTRICAL ENGINEERING
ATLANTA, GEORGIA 30332

PHONE: (404) 894-2901

October 7, 1975

Mr. J. H. Kerr
Mr. H. F. Smith
EF-13
NASA/Marshall Space Flight Center
Marshall Space Flight Center, Alabama 35812

Title: "Study of Multiple Hologram Recording in Lithium Niobate"

Subject: Monthly Letter Report No. 23 on Contract NAS8-30246 for the Period 1 September 1975 to 1 October 1975.

Dear Sirs:

Activities during the twenty-third month of the subject contract included a full scale test of the lithium niobate data recording system on the new vibration isolation table. A 15 mw HeNe laser was used for both writing and reading. A page of binary data was Fourier transformed with a lens, using a collimated laser beam. The Fourier transform was interfered with a plane reference beam. An iron doped crystal of lithium niobate was inserted into the intersection of the beams, and a hologram was recorded using an exposure time of a few seconds. Very clear reconstructed images were obtained after inverse transforming with a second lens. These images exhibited high spatial resolution.

Expenditures and man-hours effort during the first twenty-three reporting periods are:

Technical Effort - 1,741 man-hours	$23,148
Materials and Supplies	2,127
Equipment	3,276
Travel	125
Total Expenditure to Date	$28,676

Next month's activities will include further testing of the data recording system.

The projected expenditures for the remainder of the program are:

Technical Effort	0
Materials and Supplies	0
Equipment	$300
Travel	0
Total Projected Expenditure for Completion of the Program	$300

Respectfully submitted,

W. R. Callen
T. K. Gaylord
Project Directors

WRC/TKG:gc

cc: J. Weaver

E-21-633

GEORGIA INSTITUTE OF TECHNOLOGY
SCHOOL OF ELECTRICAL ENGINEERING
ATLANTA, GEORGIA 30332

PHONE: (404) 894-2901

November 7, 1975

Mr. J. H. Kerr
Mr. H. F. Smith
EF-13
NASA/Marshall Space Flight Center
Marshall Space Flight Center, Alabama 35812

Title: "Study of Multiple Hologram Recording in Lithium Niobate"

Subject: Monthly Letter Report No. 24 on Contract NAS8-30246 for the Period 1 October 1975 to 1 November 1975.

Dear Sirs:

Activities during the twenty-fourth month of the subject contract included the presentation of technical summaries of the Ph.D. thesis work of S. F. Su and R. Magnusson. This occurred at the Annual Meeting of the Optical Society of America on October 24 in Boston. Mr. Su's work was summarized under the title of "Refractive-Index Profiles and Arbitrary-Order Diffraction Efficiencies of Lithium Niobate Hologram Gratings," and an abstract appears in the J. Opt. Soc. Am., Vol. 65, p. 1220, October 1975. Mr. Magnusson's work was summarized under the title of "Application of Dynamic Theory to the Description of Experimental Volume Holography Results," and an abstract appears in the J. Opt. Soc. Am., Vol. 65, p. 1219, October 1975.

Expenditures and man-hours effort during the first twenty-four reporting periods are:

Technical Effort - 1,741 man-hours	$23,148
Materials and Supplies	2,127
Equipment	3,426
Travel	125
Total Expenditure to Date	$28,826

Next month's activities will include further study of a method to determine the refractive index profile of thick gratings in ferroelectric crystals.

The projected expenditures for the remainder of the program are:

Technical Effort	0
Materials and Supplies	0
Equipment	$150
Travel	0
Total Projected Expenditure for Completion of the Program	$150

Respectfully submitted,

W. R. Callen
T. K. Gaylord
Project Directors

WRC/TKG:gc

cc: J. Weaver

GEORGIA INSTITUTE OF TECHNOLOGY
SCHOOL OF ELECTRICAL ENGINEERING
ATLANTA, GEORGIA 30332

PHONE: (404) 894-2901

December 7, 1975

Mr. J. H. Kerr
Mr. H. F. Smith
EF-13
NASA/Marshall Space Flight Center
Marshall Space Flight Center, Alabama 35812

Title: "Study of Multiple Hologram Recording in Lithium Niobate"

Subject: Monthly Letter Report No. 25 on Contract NAS8-30246 for the Period 1 November 1975 to 1 December 1975.

Dear Sirs:

Activities during the twenty-fifth month of the subject contract included the finalizing of a method for determining the refractive index profile of unknown thick optically-induced refractive index gratings in ferroelectric crystals. This method, based on the coupled wave theory, requires only a knowledge of the fundamental and the higher-order diffraction efficiencies. This method quantitatively determines the extent to which various physical mechanisms (drift and diffusion) are present in the material.

Expenditures and man-hours effort during the first twenty-five reporting periods are:

Technical Effort - 1,741 man-hours	$23,148
Materials and Supplies	2,127
Equipment	3,576
Travel	125
Total Expenditure to Date	$28,976

Next month's activities will include the preparation of the Final Report.

The projected expenditures for the remainder of the program are:

Technical Effort	0
Materials and Supplies	0
Equipment	0
Travel	0
Total Projected Expenditure for Completion of the Program	0

Respectfully submitted,

W. R. Callen
T. K. Gaylord
Project Directors

WRC/TKG:gc

cc: J. Weaver

Contract NAS8–30246

STUDY OF MULTIPLE HOLOGRAM RECORDING IN LITHIUM NIOBATE

T. K. Gaylord and W.R. Callen
School of Electrical Engineering
Georgia Institute of Technology
Atlanta, Georgia 30332

October 1974

FINAL REPORT FOR PERIOD 1 OCTOBER 1973 – 31 OCTOBER 1974

Performed for

National Aeronautics and Space Administration
George C. Marshall Space Flight Center
Marshall Space Flight Center, Alabama 35812

SCHOOL OF ELECTRICAL ENGINEERING
Georgia Institute of Technology
Atlanta, Georgia 30332

FINAL REPORT

PROJECT NO. E-21-633

STUDY OF MULTIPLE HOLOGRAM RECORDING IN LITHIUM NIOBATE

by

T. K. Gaylord and W. R. Callen

RESEARCH CONTRACT NAS8-30246

1 October 1973 to 31 October 1974

Performed for

NATIONAL AERONAUTICS AND SPACE ADMINISTRATION
George C. Marshall Space Flight Center
Marshall Space Flight Center, Alabama 35812

ABSTRACT

The results of detailed experimental and theoretical considerations relating to multiple hologram recording in lithium niobate is reported. The following problem areas are identified and discussed: 1) the angular selectivity of the stored holograms, 2) interference effects due to the crystal surfaces, 3) beam divergence effects, 4) material recording sensitivity, and 5) scattered light from material inhomogeneities.

TABLE OF CONTENTS

LIST OF FIGURES

I. INTRODUCTION

A program to study high capacity recording in electro-optic crystals was undertaken. This study focused on the problems associated with very high capacity storage (through multiple hologram superposition) and the use of lithium niobate as the recording medium.

A number of important problem areas were identified and studied. These included: 1) the angular selectivity of the stored holograms, 2) interference effects due to the crystal surfaces, 3) beam divergence effects, 4) material recording sensitivity, and 5) scattered light from material inhomogeneities.

Single hologram and multiple hologram recording experiments were performed on a vibration isolation table with an argon laser using the experimental configuration shown in Fig. 1. Holograms were analyzed experimentally by reading them with laser light of 488.0nm, 514.5nm, and 632.8nm wavelength.

To properly interpret the above experimental results, a number of analytical studies were initiated to provide predictions of the read-out parameters of the volume holograms.

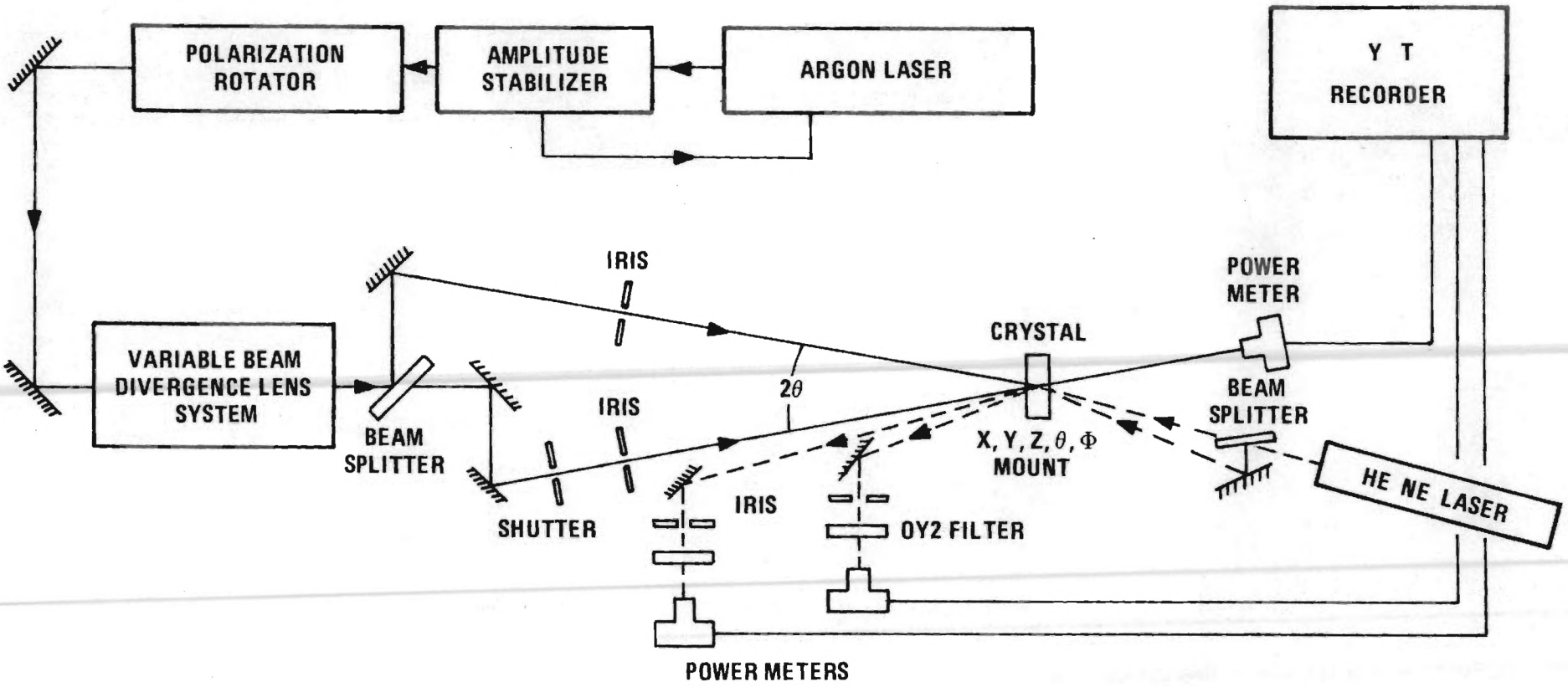

FIGURE 1. EXPERIMENTAL CONFIGURATION FOR MEASURING THE OPTICAL HOLOGRAPHIC STORAGE PROPERTIES OF FERROELECTRIC CRYSTALS.

II. ANGULAR SELECTIVITY

Because of the three-dimensional nature of the crystal, holograms recorded in lithium niobate are volume holograms. These holograms are produced directly (without processing) by the interference of laser beams of the appropriate wavelength intersecting in the crystal. The volume nature of this holographic storage is especially interesting since it indicates the possibility of very high capacity information storage.

Volume (thick) holograms exhibit a number of properties in addition to those possessed by two-dimensional (thin) holograms. Among these properties is angular selectivity—the need for the reference beam to illuminate the hologram at a precise angle in order to achieve reconstruction. Illumination outside of this angular corridor produces a rapidly decreasing intensity of the reconstructed data. To perform these diagnostic experiments plane wave holograms (caused by the interference of two plane waves) were used. Even though this is a special case, a general hologram may be constructed by the superposition of an infinite number of plane wave holograms. Reconstruction of a volume hologram [1] is possible (with half maximum diffracted power or greater) only over the range of wavelengths given by

$$\frac{\Delta\lambda}{\lambda} \simeq \cot\theta \, \frac{L}{t} \qquad (1)$$

and only over the range of angles given by

$$\Delta\theta \simeq A(\eta_o) n(\lambda, P) \, \frac{L}{t} \, , \qquad (2)$$

where $\Delta\lambda$ and $\Delta\theta$ are centered about the writing wavelength λ, and the writing angle, θ. The thickness of the hologram is given by t, L is the fringe

spacing of the fundamental grating ($L = \lambda/2\sin\theta$), $n(\lambda,P)$ is the appropriate index of refraction for the probing beam wavelength and polarization, and $A(\eta_o)$ is the angular selectivity coefficient (approximately equal to unity). These types of properties are in actuality just manifestations of the increased storage capacity of the volume storage medium.

The experimental configuration shown in Figure 1 was used to measure the angular selectivity and compare it with the theoretical value. Thicknesses from 1mm to 5mm were tested. Both iron-doped and nominally pure crystals of lithium niobate were used. The half-power angular widths were found to be in agreement with theoretically predicted values. These results show that the theoretical angular packing density of multiple holograms is achievable! This important finding was reported in Appl. Phys. Letters [2]. This publication gives experimental details as well as results and is reproduced here for completeness.

Additional experimental results have been obtained since Ref. 2 was published. These show a much more detailed comparison of theory and experiment for a broader range of reading angles. These data are shown in Figs. 2 and 3.

Angular selectivity of lithium niobate volume holograms

T. K. Gaylord

School of Electrical Engineering, Georgia Institute of Technology, Atlanta, Georgia 30332

F. K. Tittel

Electrical Engineering Department, Rice University, Houston, Texas 77001
(Received 29 May 1973)

The angular selectivities for the reconstruction of volume-phase holograms in doped and nominally pure $LiNbO_3$ crystals have been measured. The half-power angular widths for reading were found for the cases studied to be in agreement with theoretically predicted values.

It has been demonstrated that $LiNbO_3$ can be used as a recording material for volume-phase holograms.[1] These holograms are produced directly (without processing) by the interference of laser beams of the appropriate wavelength intersecting in the crystal. The volume nature of this holographic storage is especially interesting since it indicates the possibility of very-high-capacity information storage. Volume (thick) holograms exhibit a number of properties in addition to those possessed by two-dimensional (thin) holograms. Among these properties is angular selectivity—the need for the reference beam to illuminate the hologram at a precise angle in order to achieve reconstruction. Illumination outside of a narrow angular corridor produces a rapidly decreasing intensity of the reconstructed data.

A standard two-beam holographic configuration was used and plane-wave holograms were written. These holograms were reproductions of the original interference pattern, which has the geometry of a series of vertical planes, with an intensity variation perpendicular to the planes of $I(z) = 2I_0 \sin^2(\pi z/L)$, where I_0 is the intensity of each writing beam and L is the resultant grating spacing ($L = \lambda/2 \sin\phi_{\text{Bragg}}$).

Two poled single-domain $LiNbO_3$ crystals were used, one doped with 0.05 mole% iron and one nominally pure sample. The crystals were oriented as shown in Fig. 1 with their b-face surfaces perpendicular to the bisector of the writing beams and with the c axis in the plane of the writing beams. A frequency-doubled Nd:YAG laser (5300 Å) and an argon-ion laser operating at 5145 Å were used in these experiments to write the holograms.

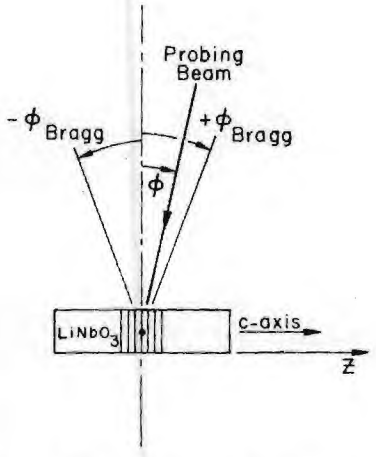

FIG. 1. Geometry of the writing and measuring configuration.

A HeNe laser (6328 Å) aligned to its corresponding Bragg angle was used to monitor the diffraction efficiency and to measure the angular selectivity. The polarization of the two writing beams was in the plane of these beams, while the polarization of the HeNe monitoring beam was perpendicular to the plane of incidence.

To measure the angular selectivity for reconstruction, the single HeNe probing beam was allowed to illuminate the hologram and the diffracted power was monitored. Then, by rotating the incident beam with respect to the crystal (varying the angle ϕ shown in Fig. 1), the variations in diffraction efficiency were measured. For the iron-doped $LiNbO_3$ crystal the measured angular selectivity is shown in Fig. 2.

Assuming that the sinusoidal interference pattern, $I(z)$, produced by the intersection of the two writing beams produces a sinusoidal variation in the index of refraction, then the diffraction efficiency of the volume grating hologram is given by[2] $\eta_0 = \sin^2(\pi \Delta n t/\lambda \cos\phi_{\text{Bragg}})$, where η_0 is the on-Bragg-angle diffraction efficiency, Δn is the peak value of the sinusoidal grating of index of refraction, and t is the length of the interaction region (thickness of the crystal for these cases). During the writing process Δn increases and a peak in the diffraction efficiency (predicted to be 100%) occurs when Δn reaches a value of $(\lambda \cos\phi_{\text{Bragg}})/2t$. A further increase in Δn causes the diffraction efficiency to decrease until a Δn of $(\lambda \cos\phi_{\text{Bragg}})/t$ is reached at which

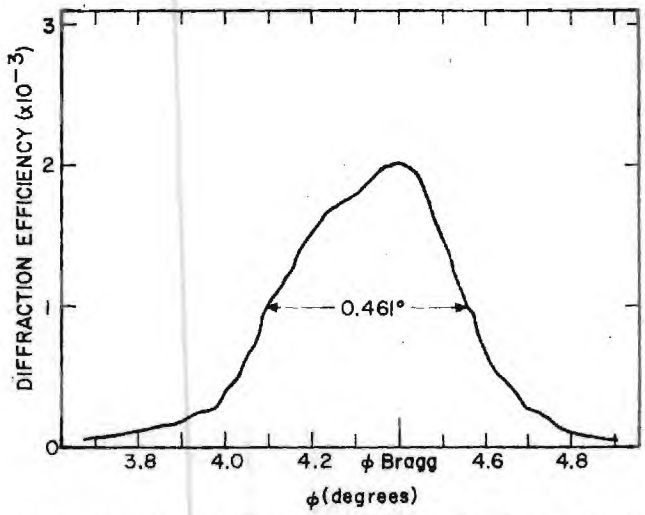

FIG. 2. Angular selectivity for reading of a hologram recorded in a 1-mm-thick iron-doped $LiNbO_3$ crystal using a writing wavelength of 5300 Å and a probing wavelength of 6328 Å.

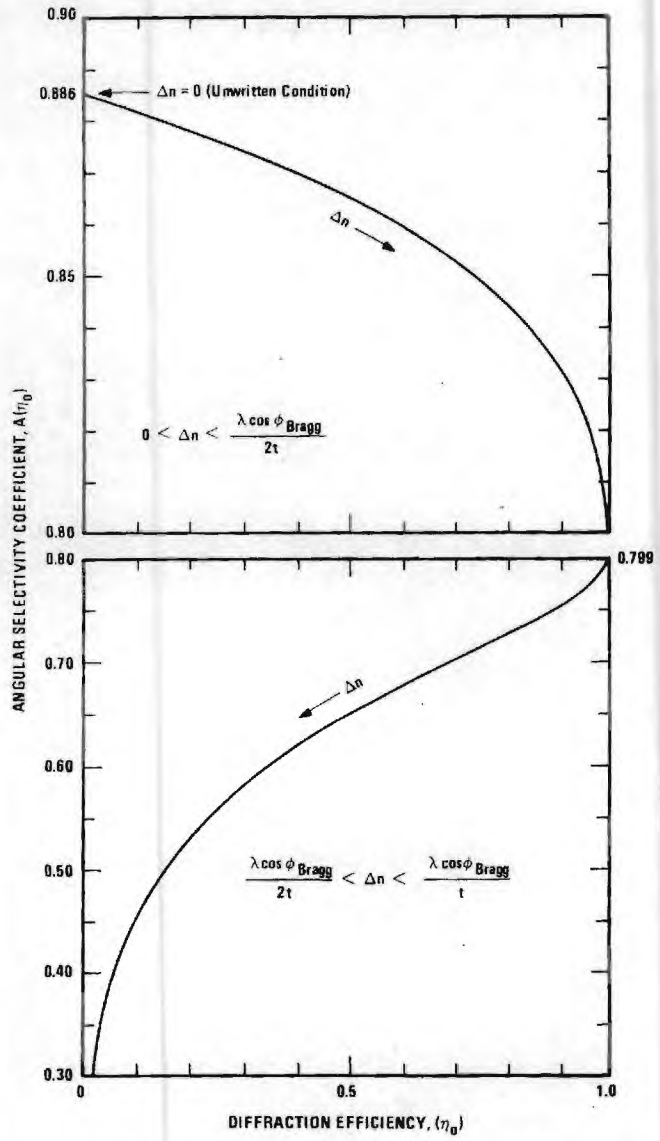

FIG. 3. The angular selectivity coefficient, $A(\eta_0)$, as a function of on-Bragg-angle diffraction efficiency, η_0.

time η_0 again begins to increase. This oscillatory behavior of the diffraction efficiency with exposure time has been experimentally observed.[3,4]

The theoretical angular selectivity for reading a volume hologram can be determined using the coupled-wave theory of Kogelnik.[2] For the full range of on-Bragg-angle diffraction efficiencies ($0 < \eta_0 < 1.00$), the half-power full angular width inside the crystal, $(\Delta\phi)_i$, can be determined by numerically solving Eqs. (42)—(45) in Ref. 2. The result is that $(\Delta\phi)_i = A(\eta_0)L/t$, where $A(\eta_0)$ is the angular selectivity coefficient. The half-power full angular width as measured from outside the crystal is thus

$$\Delta\phi \simeq A(\eta_0)n(\lambda, P)L/t \quad \text{rad}, \tag{1}$$

where $n(\lambda, P)$ is the appropriate index of refraction for the probing beam wavelength and polarization. The angular selectivity coefficient, $A(\eta_0)$, as determined by the coupled-wave theory is evaluated in Fig. 3.[5] As the change in index of refraction varies from zero (unwritten condition) to $(\lambda\cos\phi_{\text{Bragg}})/2t$ this factor changes from 0.886 to 0.799. This initial range of Δn values includes the relatively low diffraction efficiencies which correspond to practical holographic storage of information. For Δn beyond $(\lambda\cos\phi_{\text{Bragg}})/2t$, the angular selectivity coefficient decreases rapidly as shown in Fig. 3. Thus the angular corridor for reading narrows considerably with further exposure. Simultaneously, the diffraction efficiency increases at larger angular deviations from the Bragg angle as shown in Fig. 4. As the change in index of refraction, Δn, increases, these side lobe positions increase in diffraction efficiency and decrease their angular separation, $\Delta\phi$, from the exact Bragg angle. These side lobes coalesce at the Bragg angle ($\Delta\phi = 0$) when Δn increases to $1.5(\lambda\cos\phi_{\text{Bragg}})/t$ at which time the next set of side lobes are increasing in diffraction efficiency and moving toward the Bragg angle. Obviously for Δn greater than about $0.75(\lambda\cos\phi_{\text{Bragg}})/t$ the conventional notion of angular selectivity becomes ambiguous due to the presence of these side lobes.

Equation (1) assumes small angles of incidence. For the geometry of the experiments reported here, only a 0.24% error is introduced into this equation by the small-angle approximation. The more nearly exact expression for the half-power full angular width for reading for any angle of incidence is

$$\Delta\phi \simeq \sin^{-1}\{n(\lambda, P)\sin[(\phi_{\text{Bragg}})_i + \tfrac{1}{2}(\Delta\phi)_i]\} - \sin^{-1}\{n(\lambda, P)\sin[(\phi_{\text{Bragg}})_i - \tfrac{1}{2}(\Delta\phi)_i]\}, \tag{2}$$

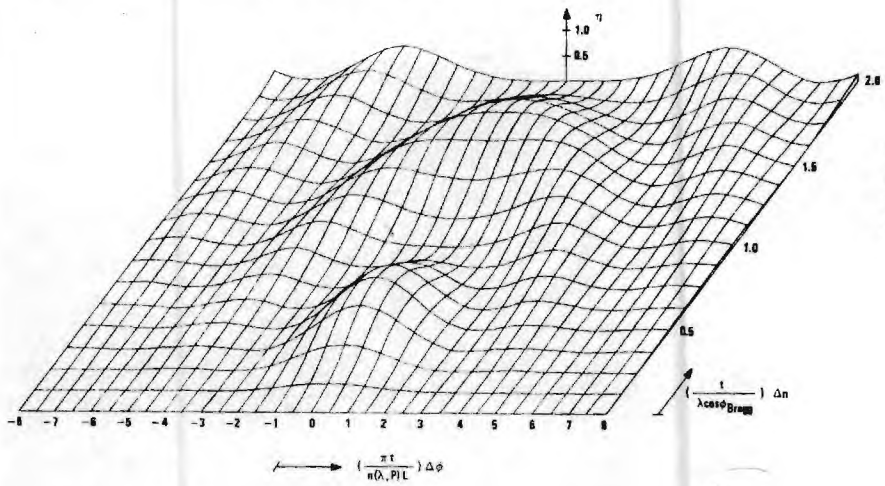

FIG. 4. Predicted variation of diffraction efficiency (η) with change in index of refraction (Δn) and angular deviation ($\Delta\phi$) from the exact Bragg angle.

where the angle of refraction $(\phi_{Bragg})_i = \sin^{-1}\{[1/n(\lambda, P)] \times \sin\phi_{Bragg}\}$. The HeNe probing beam ($\lambda = 6328$ Å) was polarized perpendicular to the c axis of the crystal (ordinary ray) and thus $n(\lambda, P) = 2.288$ for $LiNbO_3$. For the 1-mm-thick iron-doped $LiNbO_3$ sample, the measured half-power full angular width from Fig. 2 is seen to be $0.461^\circ \pm 0.004^\circ$. For the conditions of this experiment ($\phi_{Bragg} = 4.4^\circ$, $\lambda = 5300$ Å, and $\eta_0 = 2.0\times10^{-3}$) the calculated value from (2) is 0.402°. For the 5-mm-thick nominally pure $LiNbO_3$ crystal, the half-power angular width was measured to be $0.080^\circ \pm 0.004^\circ$ as compared to the calculated value from (2) for that experiment ($\phi_{Bragg} = 4.35^\circ$, $\lambda = 5145$ Å, and $\eta_0 = 1.1\times10^{-4}$) of 0.0789°. The deviations between the theoretical and experimental values were 14 and 1.6%, respectively. The agreement between theoretical and experimental values may be taken as an indication that the presence of divergence in the writing beams (writing beam divergence $= 0.143^\circ$ for the 5300-Å beams and 0.035° for the 5145-Å beams) does not have an appreciable effect on the resultant angular selectivity for reading. The presence of optical absorption has previously been shown to have very little effect on the angular selectivity of dielectric transmission holograms.[2]

In summary, the angular selectivity for the reconstruction of $LiNbO_3$ volume holograms has been measured and found to be in agreement with theoretical predictions. This information is of particular interest for high-capacity information storage applications since it indicates (1) a practical limit on the angular packing density of multiple holograms stored at a single location and (2) the required beam positioning accuracy to perform the process of reading.

*Work supported by the National Science Foundation.

[1]F. S. Chen, J. T. LaMacchia, and D. B. Fraser, Appl. Phys. Lett. **13,** 223 (1968).
[2]H. Kogelnik, Bell Syst. Tech. J. **48,** 2909 (1969).
[3]J. J. Amodei, W. Phillips, and D. L. Staebler, Appl. Opt. **11,** 390 (1972).
[4]A. Ishida, O. Mikami, S. Miyazawa, and M. Sumi, Appl. Phys. Lett. **21,** 192 (1972).
[5]The angular selectivity expression [Eq. (1)] has previously appeared in the literature without the index of refraction factor (Refs. 1 and 6) and without the $A(\eta_0)$ factor (Refs. 1 and 7).
[6]T. K. Gaylord, T. A. Rabson, and F. K. Tittel, Appl. Phys. Lett. **20,** 47 (1972).
[7]R. L. Townsend and J. T. LaMacchia, J. Appl. Phys. **41,** 5188 (1970).

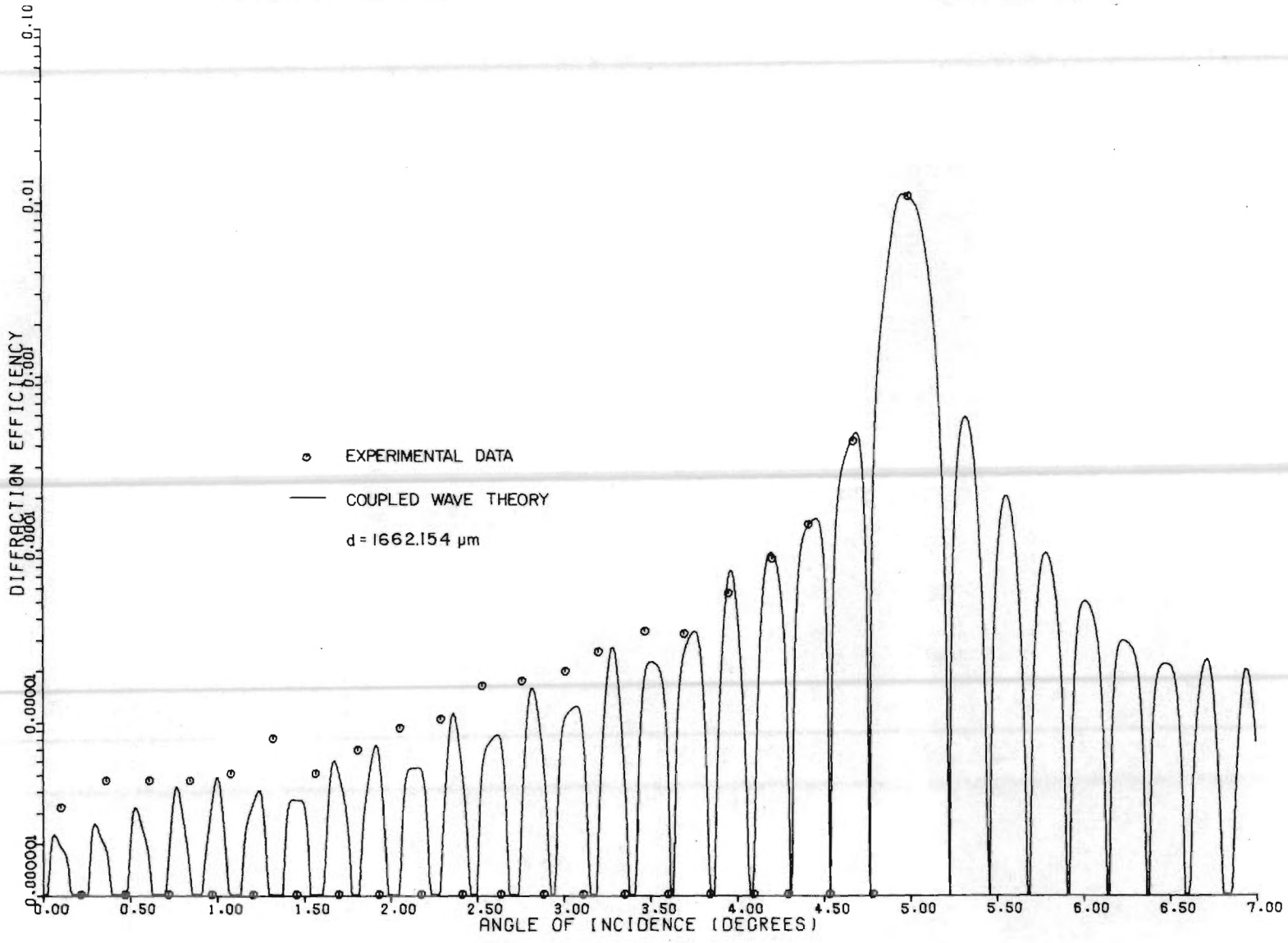

FIGURE 2. A COMPARISON OF ANGULAR SELECTIVITY EXPERIMENTAL DATA WITH RESULTS FROM THE COUPLED WAVE THEORY. The particular thickness chosen, d, yields the best fit close to the Bragg angle.

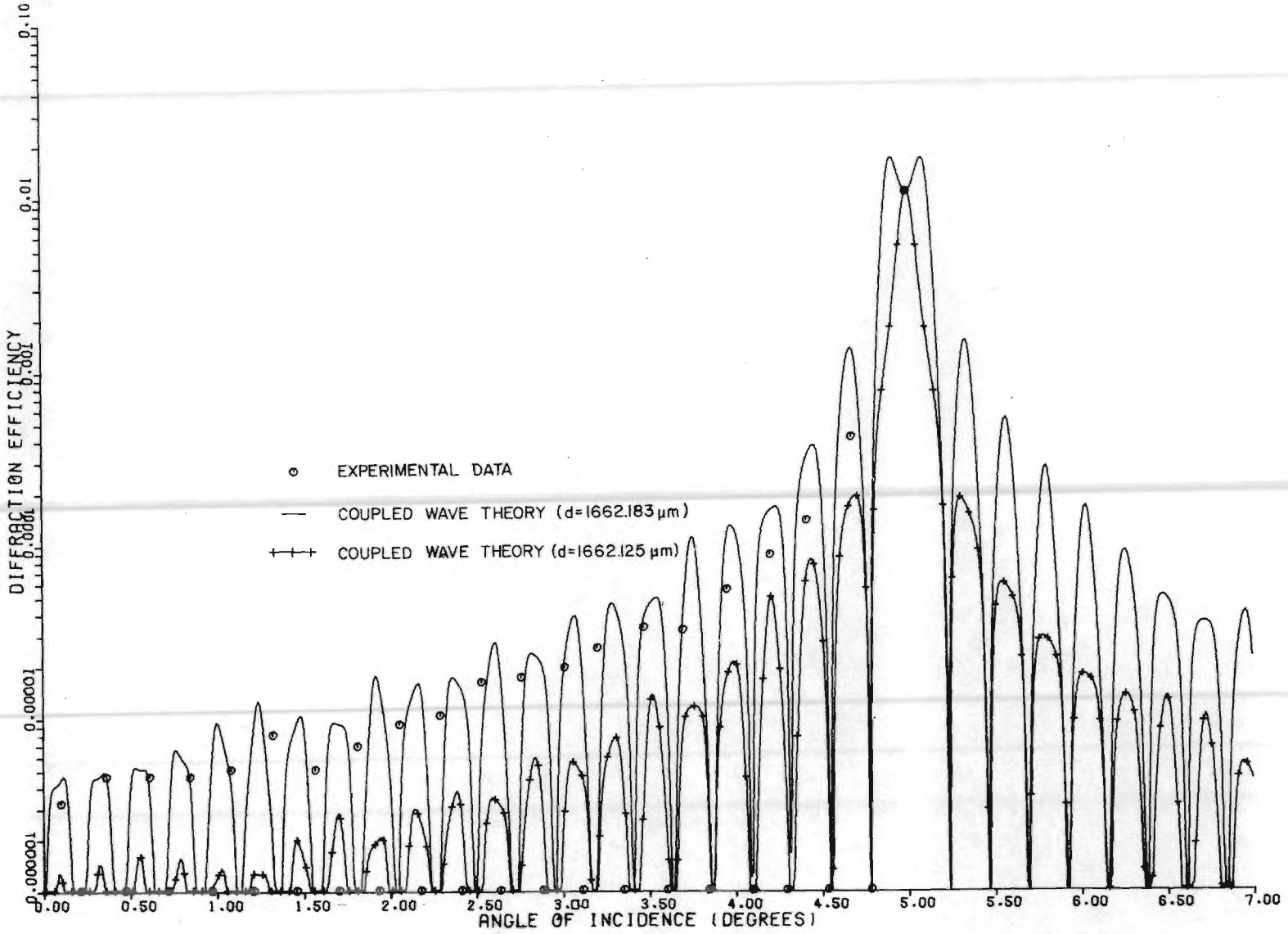

FIGURE 3. AMPLITUDE RANGE OF THEORETICAL ANGULAR SELECTIVITY DUE TO MINUTE THICKNESS VARIATIONS. The thickness used in producing the plain curve is that needed to obtain a minimum value of the transmittance factor on the Bragg angle ($\tau = 0.3$). The crossed curve corresponds to maximum transmittance ($\tau = 1.8$). The experimental data is seen to occur within these extremes.

III. SURFACE INTERFERENCE EFFECTS

Many analyses of hologram reconstruction do not account for boundary (surface) reflections. The diffraction efficiency results may be corrected to include boundary reflections by multiplying by a transmittance factor. This factor, τ, is developed by us in Ref. 3, a copy of which is included in this report. This factor is the same as the transmittance factor derived by Kogelnik and given as Eq. (8) in Ref. 4, but with νd in that equation replaced by the argument of the sine function in Eq. (27) in our paper [3].

From these results, we find that boundary reflections produced by the surfaces can considerably change the diffraction efficiency. The change can be an increase or a decrease depending on whether the transmittance factor is greater or less than unity. This effect has been studied by Cohen and Gordon [5]. For the grating parameters used here, τ is typically in the range 0.70 to 1.20. In practice, the boundary reflections can be eliminated by antireflection coatings on the surfaces of the gratings.

Calculated results showing the thickness dependence of τ for lithium niobate are shown in Fig. 4. The effect of τ as a function of reading angle is shown in Fig. 5.

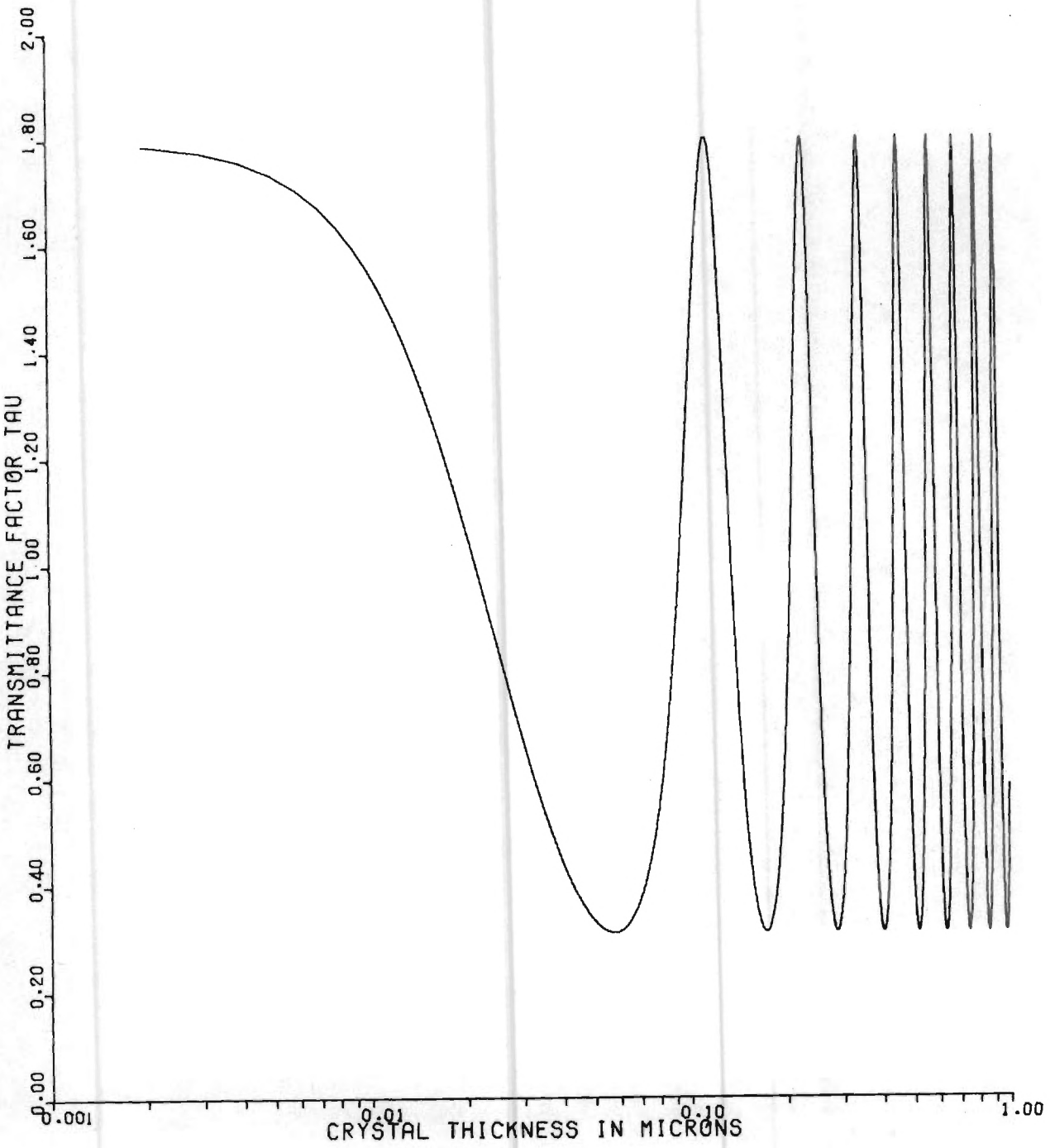

FIGURE 4. TRANSMITTANCE FACTOR, τ, AS A FUNCTION OF CRYSTAL THICKNESS.

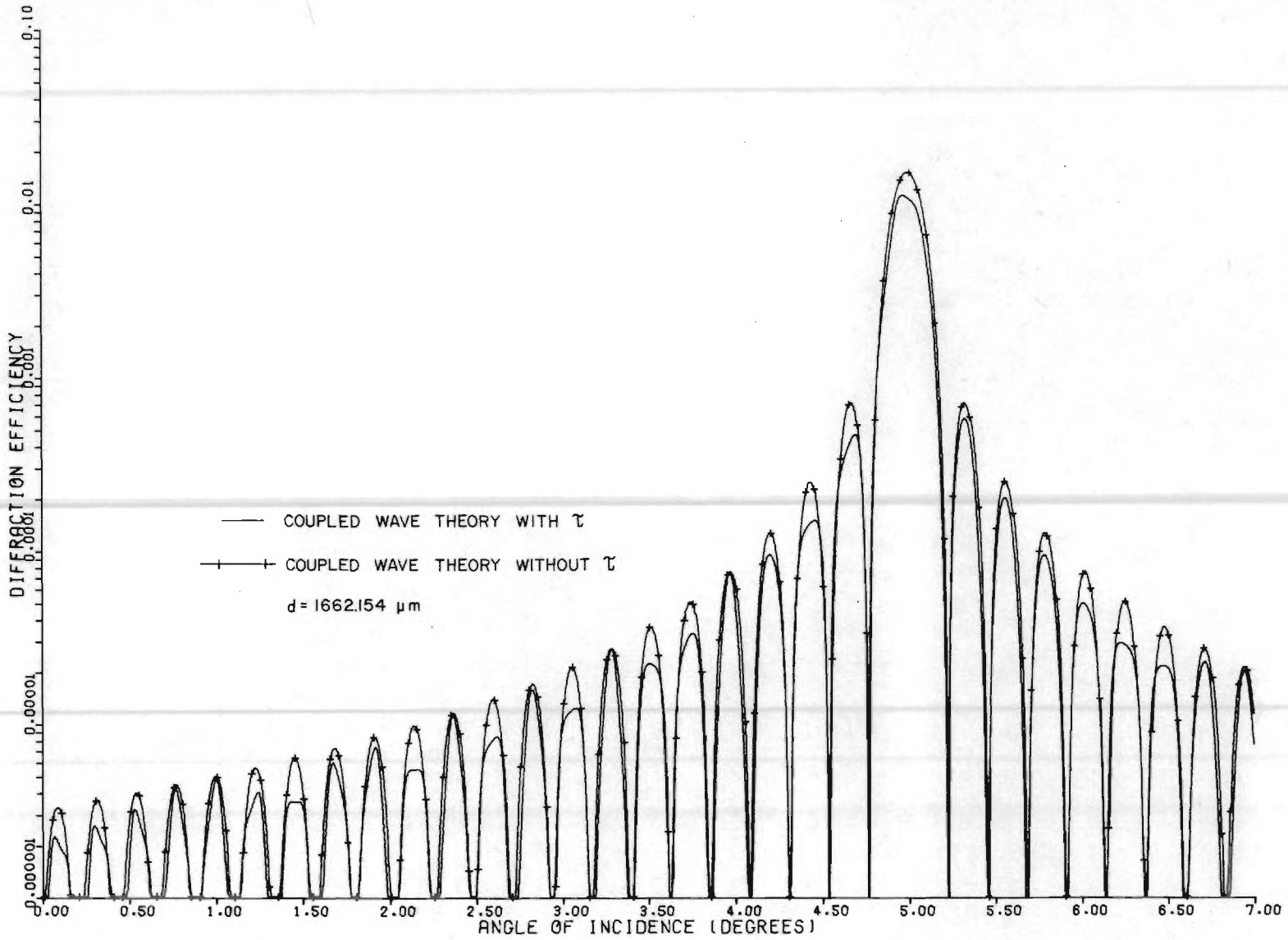

FIGURE 5. EFFECT OF THE TRANSMITTANCE FACTOR ON ANGULAR SELECTIVITY.

IV. BEAM DIVERGENCE EFFECTS

The effect of writing beam divergence was studied. First, a hologram was written with a frequency doubled Nd:YAG laser (λ = 530nm) with a beam divergence of 0.143^{o}. Second, a hologram was written with an argon laser (λ = 514.5nm) with a beam divergence of 0.035^{o}. The angular selectivities of these holograms were then measured with a He-Ne laser. The half-power angular width in both cases was found to be within 10% of the theoretical value derived in our paper [2]. Thus, it was concluded that writing beam divergence has little effect on the final read-out process.

V. RECORDING SENSITIVITY

Recording materials must possess a number of important characteristics to achieve the high storage capacities that have been predicted for optical memories. These requirements on the optical recording material include: 1. High sensitivity—It is desirable that only a small amount of optical energy per unit area be needed to record the hologram of a data page. Table 3 in Ref. 6 (reproduced later in this report) lists the necessary writing energy densities for a number of recording materials. For a practical system an energy density of about 1 millijoule/cm^2 or less will be needed. 2. Large diffraction efficiency—Diffraction efficiency is the fraction of the reading light (reference beam) that is diffracted into the reconstructed data beam. It must be possible to record a single hologram with a large diffraction efficiency, so that in practice many holograms may be recorded at a single location, each with an equal share of the total maximum diffraction efficiency. Therefore, it is desirable to have the maximum diffraction efficiency as close to 100% as possible. 3. Erasable and rewritable—For a rapid cycle read-write-erase memory system, it must be possible to continuously alter the stored data in the memory without encountering any degradation in the material characteristics. 4. Long lifetime of stored information—Stored data should persist for long periods of time before having to be refreshed. Ideally, storage should be permanent. 5. Non-volatile storage—Data should remain recorded in the memory in the absence of system power. 6. Nondestructive readout—It should be possible to perform an essentially unlimited number of read operations without degrading or altering the stored data. 7. Three dimensional storage—To achieve very high capacity storage, the information should be stored in thick (volume) holograms. Together with the requirement of high diffraction efficiency, this means that the hologram

should be a thick phase (nonabsorbing) hologram. 8. High resolution— The storage material obviously must be capable of recording the very fine (wavelength size) variations of the interference pattern produced by the intersection of the object and reference beams.

Considering all of the above material requirements, the photorefractive materials (optically induced changes in index of refraction) appear to be especially promising. These materials, often ferroelectric crystals such as lithium niobate and strontium barium niobate (SBN), have been considerably developed and improved. For example, in the first use of lithium niobate as a recording material in 1968 a writing energy density of approximately 100 joules/cm^2 was required [7]. Less than six years later, doped versions of lithium niobate have now been shown in this work to exhibit writing energy densities of 2 millijoules/cm^2! We have announced this improvement in sensitivity of almost 5 orders of magnitude in Applied Physics Letters [8]. This article is reproduced here for completeness. Fig. 6 depicts this recent jump in sensitivity with respect to other potential recording materials. In addition, recent work by von der Linde et al. [9] indicates that even higher sensitivities are possible in lithium niobate!

Volume holographic recording and storage in Fe-doped $LiNbO_3$ using optical pulses*

Pradeep Shah, T. A. Rabson, and F. K. Tittel
Department of Electrical Engineering, Rice University, Houston, Texas 77001

T. K. Gaylord
School of Electrical Engineering, Georgia Institute of Technology, Atlanta, Georgia 30332

(Received 4 June 1973)

Volume holographic recording and storage in Fe-doped $LiNbO_3$ using single 30–75-nsec duration optical pulses at 694.3 and 531 nm from Q-switched ruby and frequency-doubled Nd:glass lasers, respectively, is reported. The recording sensitivity for a pulsed writing source is found to be better than that estimated for a cw source. A sensitivity of 2 mJ/cm^2 at 476 nm and 2.5 mJ/cm^2 at 488 nm to record a hologram of 1% diffraction efficiency is the best sensitivity figure yet reported. The orders of magnitude of improvement in sensitivity is attributed to higher fractional concentration of Fe^{2+}.

Ferroelectric materials have recently become the subject of considerable interest on account of their potential use in optical storage and information processing. Such a ferroelectric storage medium must meet certain system requirements, which include high bit density storage capability, high sensitivity and speeds of recording, and high readout efficiency. In this work we discuss two of these parameters, speed and sensitivity of iron-doped $LiNbO_3$, which make it a most interesting storage medium in addition to strontium barium niobate (SBN). The results of the experiments conducted demonstrate the feasibility of volume holographic recording, storage, and retrieval of information by means of single optical pulses of nanosecond duration using the photoinduced index of refraction changes in lithium niobate. Here we report the best recording sensitivities yet published—an order-of-magnitude improvement over recent reported sensitivities of SBN[1] and almost two-orders-of-magnitude improvement in Fe-doped $LiNbO_3$.[2] These sensitivities are for the experiment conducted without any external electric field across the crystal. Further improvements in sensitivity are expected with external bias fields. Furthermore, our experiments indicate that the charge generation and transport processes occur with time constants considerably faster than 10^{-8} sec since no difficulty in recording and reconstructing was experienced using pulses from Q-switched lasers. The recording sensitivity for a pulsed source is slightly better than that estimated for a cw source.

Volume holograms in the form of interference fringes of two plane waves were recorded in two iron-doped $LiNbO_3$ crystals. Both these crystals were cut from the same boule grown by Crystal Technology, Inc. and contained 0.05 mole% concentration of iron. One of these crystals was annealed in pure oxygen atmosphere at 700 °C to increase the transmission in the shorter-wavelength region of the visible spectrum. The absorption spectra of both these crystals (1 mm thick) are shown in Fig. 1. In the same figure an absorption spectrum corrected for comparable crystal thickness from previously reported data[2] is plotted. The writing sources included single pulses from a Q-switched frequency-doubled Nd:glass laser capable of an output of 0.005 J at 531 nm with pulse duration of ~75 nsec, a ruby laser with 0.05 J energy at 694.3 nm with pulse duration of 30 nsec, and in addition a continuous wave argon laser using output at 476.5, 488, 496.5, and 514.5 nm and a He-Ne laser (632.8 nm). All these sources were made to operate in a single transverse mode. The recording of the hologram and the reconstruction was accomplished using an experimental set-up shown in schematic form in Fig. 2. The recording beam is split into a reference and an object beam of approximately equal intensity using a beam splitter and is lightly focused using a 125-cm-focal-length lens. These beams intersect in the storage medium at an angle of 12°. The writing beams are polarized perpendicular to the c axis of the crystal and the plane of the writing beams. The diffraction efficiency and the writing curve are measured using the reference beam with the object beam shuttered intermittently during the recording process and also by a He-Ne laser polarized parallel to the c axis of the $LiNbO_3$ crystal. The diffraction efficiency in the pulsed mode is measured by simultaneously monitoring the transmitted and diffracted reference beams. Optimum reconstruction is observed when the reading beam is polarized parallel to the c axis which is in agreement with the previously reported observations.[3] The recording sensitivity defined in terms of the total required exposure in J/cm^2 to construct a hologram with 1% diffraction efficiency[4] is plotted in Fig. 3 for various recording wavelengths available from the various pulsed and cw sources for both untreated and annealed crystals. The results and conclusions obtained from the experimental data are as follows:

(i) Volume holographic information recording, stor-

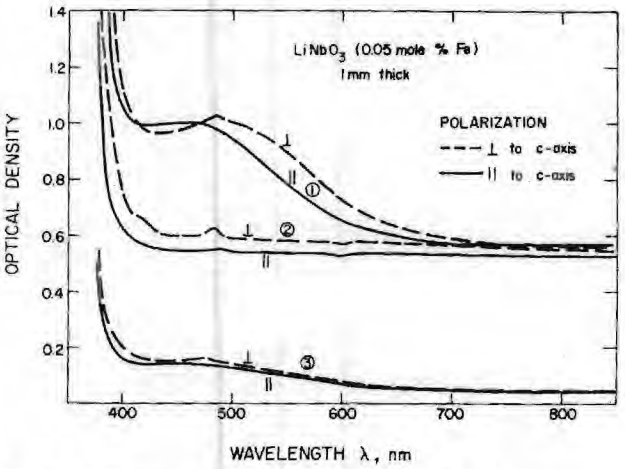

FIG. 1. Absorption spectra of 0.05 mole% iron-doped $LiNbO_3$ for (1) 1-mm-thick unannealed crystal and (2) 1-mm-thick annealed crystal. Curve (3) shows previously reported RCA spectral data corrected to a 1-mm-thick crystal for comparison.

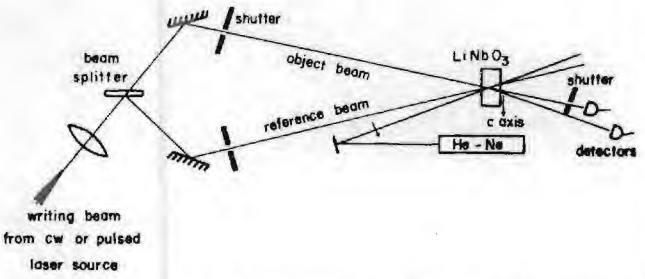

FIG. 2. Experimental arrangement for volume holographic storage. The writing beams used were from a cw argon laser (476.5, 488, 496.5, 514.5 nm), He-Ne laser (632.8 nm), and from a Q-switched frequency-doubled Nd:glass and ruby laser at 531 and 694.3 nm, respectively.

age, and retrieval has been accomplished in photorefractive crystals such as $LiNbO_3$ in times of 30 nsec, only limited by the duration of the optical source.

(ii) The recording sensitivities obtained for a pulsed writing source are slightly higher than the values estimated from sensitivity as a function of wavelength using cw sources at the other wavelengths.

(iii) The 1-mm-thick 0.05 mole% iron-doped $LiNbO_3$ crystal (not annealed) with a significant absorption band near the band edge had a recording sensitivity of 2.0 $mJ/cm^2/\%\eta$ at 476 nm and 2.5 $mJ/cm^2/\%\eta$ at 488 nm. These figures show that the crystal is at least 4 times more sensitive than the most sensitive strontium barium niobate crystal[1] and 60 times more sensitive than the previously reported most sensitive Fe-doped $LiNbO_3$.[2] In fact these sensitivities are even more significant if one considers the smaller interaction lengths of the crystal used in our experiments.

(iv) The storage with 10^{-8}-sec duration pulses indicates that the over-all time constant of recording process contributed by photoionization charge transport and retrapping is much shorter than the pulse duration times. Shorter pulses—such as picosecond duration—must be used to try to determine the dynamic response characteristics and ultimate speed limitations on the recording process.

(v) Increased sensitivity of the medium at longer wavelengths 632.8 nm and even at 694.3 nm is of considerable practical value since such storage material can be used with inexpensive low-power optical sources such as He-Ne lasers.

(vi) Comparison of the recording sensitivities and the absorption spectra of the two crystals cut from the same boule and heat treated after the growth conclusively indicates that the absorbing Fe^{+2} impurities play an important role in the recording sensitivity of the medium. The improvement in sensitivity for the unannealed crystal is by a factor of 100 over that of the annealed crystal characterized by the lower absorption. The unannealed crystal is also considerably more sensitive than the previously reported iron-doped $LiNbO_3$ of comparable doping concentration.[2] The improvement over the annealed crystal and the other reported

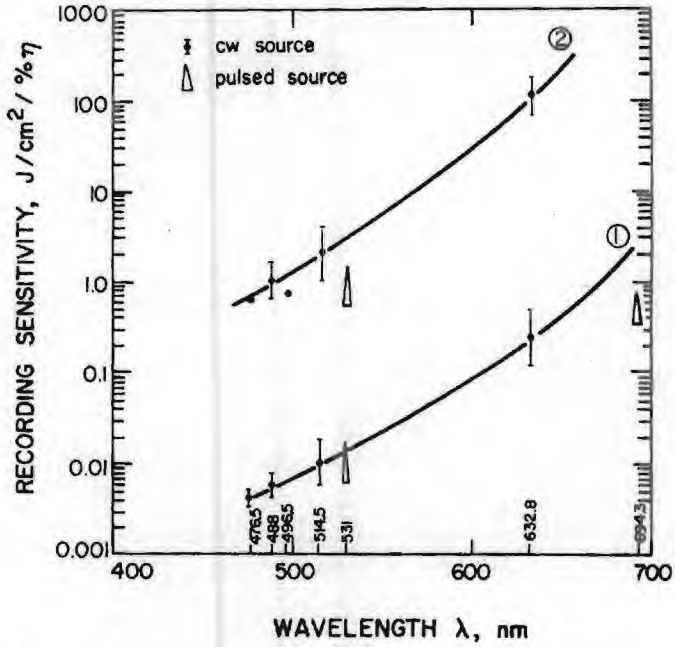

FIG. 3. Recording sensitivity measured in terms of energy required to write holograms capable of diffracting 1% of transmitted beam at 632.8 nm as a function of recording wavelength plotted for 0.05 mole% Fe-doped crystals; curve (1), 1-mm-thick unannealed and curve (2), 1-mm-thick but annealed. The required recording exposure (open triangles) for pulsed writing source is also plotted for these crystals.

results is significantly more than can be explained by only the increased absorption at writing wavelengths. Other processes in addition to photoionization, such as charge transport and retrapping, must play an additional role in determining the sensitivity. It is hypothesized that in addition to the above-mentioned effect the photoexcited carriers must be retrapped selectively to produce a space charge. This indicates that in addition to the absolute concentration of Fe^{+2} ions, the concentration of Fe^{+3} accepter ions and the relative concentration of the two ions must play a significant role in the improvement of the sensitivity. This point is also supported by the fact that the sensitivity data in Fig. 3. show that the ratio of the sensitivities of the two crystals seems relatively constant over the range of the studies.

*Work supported by the National Aeronautics and Space Administration.

[1]J. B. Thaxter and M. Kestigian, OSA Topical meeting on Optical Storage of Digital Data, Aspen, Colorado (unpublished).

[2]W. Phillips, J. J. Amodei, and D. L. Stabler, RCA Rev. 33, 94 (1972).

[3]F. S. Chen, J. T. La Macchia, and D. B. Frazer, Appl. Phys. Lett. 13, 223 (1968).

[4]The diffraction efficiency η is defined in terms of a fraction of transmitted light that is diffracted reconstructing the original information and is a function of interaction length L, change in index of refraction Δn, reading wavelength λ, and angle of incidence θ. All the diffraction efficiencies are either measured or corrected for a reading beam of wavelength $\lambda = 632.8$ nm using $\eta_\lambda = \sin^2(\pi \Delta n L/\lambda \cos\theta)$.

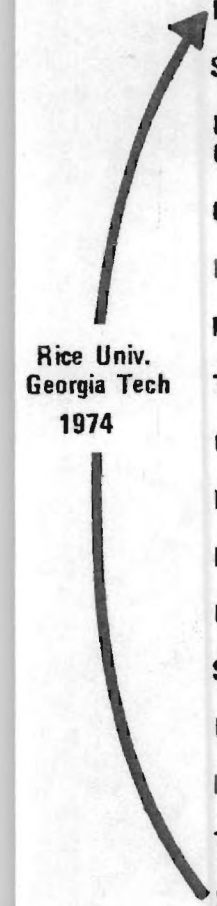

Material	Type of Material	Writing Energy Density (joules/cm^2)
$Bi_{12}Si\ O_{20}$	Ferroelectric–Photoconductive	1×10^{-5}
Malachite Green: Sucrose Benzoate	Thermoplastic	2×10^{-5}
Agfa 8E70	Photographic	2×10^{-5}
Kodak 649F	Photographic	7×10^{-5}
$Bi_4Ti_3O_{12}$–ZnSe	Ferroelectric–Photoconductive	1×10^{-3}
$LiNbO_3$:Fe	Photorefractive	2×10^{-3}
$Sr_{0.75}Ba_{0.25}Nb_2O_6$	Photorefractive	6×10^{-3}
Dichromated Gelatin	Photochemical	9×10^{-3}
Ca F_2: Ce	Photochromic	1×10^{-2}
KCL:Na	Photochromic	1×10^{-2}
Mn Bi	Magnetooptic	3×10^{-2}
$Te_{88}Ge_7As_5$	Amorphous Semiconductor	5×10^{-2}
Gd I G	Magnetooptic	9×10^{-2}
Eu O	Magnetooptic	9×10^{-2}
Na F	Photochromic	9×10^{-2}
Co–P–Ni–Fe	Magnetooptic	1×10^{-1}
$SrTiO_3$:Ni:Mo	Photochromic	2×10^{-1}
Ba Ti O_3	Photorefractive	2×10^{-1}
Mn Al Ge	Magnetooptic	3×10^{-1}
$Te_{81}Ge_{15}Sb_2S_2$	Amorphous Semiconductor	5×10^{-1}
$LiNbO_3$:Fe	Photorefractive	8×10^{-1}
KBr	Photochromic	1
$Cu_2Hg\ I_4$	Thermoplastic	3
$BaNaNb_5O_{15}$	Photorefractive	5
$Bi_4Ti_3O_{12}$	Photorefractive	10
$Sr_{0.75}Ba_{0.25}Nb_2O_6$	Photorefractive	14
$LiNbO_3$	Photorefractive	100

FIGURE 6. REQUIRED WRITING ENERGY DENSITY FOR VARIOUS OPTICAL RECORDING MATERIALS.

VI. SCATTERED LIGHT EFFECTS

Scattered light during hologram reconstruction has been recognized as a problem for high capacity storage in lithium niobate [10].

We have reported [11] the presence of cones of diffracted light upon illumination of previously laser-exposed crystals of lithium niobate. These diffraction cones are shown to result from the internally recorded interference pattern (hologram) resulting from the interference of the original incident laser beam with light scattered from material inhomogeneities. Diffraction cones are observed in iron-doped lithium niobate crystals that were exposed to a single laser beam and in crystals that were exposed to two superposed laser beams (i.e., during conventional holographic recording). In the two beam case, the diffraction cones are present in addition to the first order diffracted beam when the conventional two beam thick hologram is reconstructed. The diffracted cones produce the impression of scattered light during hologram reconstruction, an effect that has previously been reported in transition metal doped lithium niobate [10].

The diffraction cones, which have their apex in the exposed region of the crystal, are observed as rings (referred to as "scattering" rings, or diffraction rings) when a screen or a piece of film intersects the cone of light. Figure 1 in Reference 11 shows two typical diffraction ring patterns. For the single beam case, the observed results in lithium niobate are effectively the same as the experimental observations of Moran and Kaminow [12] for polymethyl methacrylate (PMMA), which had been exposed to ultraviolet laser light.

The presence of diffracted cones of light represents a possible limitation of heavily iron doped lithium niobate for data storage applications

because optical power is lost into the scattering induced diffraction cones that could otherwise be used to increase the diffraction efficiency and thus the total bit capacity of the two beam grating hologram. However, it has already been shown by Phillips, Amodei, and Staebler [10] that the "scattered" light may be erased 1) by illumination with uniform incoherent light or 2) by writing additional superposed holograms at new angles. In the latter case, "scattered" light from the previous holograms tends to be erased.

Our Ref. 11 is reproduced here for completeness.

Reprinted from APPLIED OPTICS, Vol. 13, page 1545, July 1974

Laser Scattering Induced Holograms in Lithium Niobate

R. Magnusson and T. K. Gaylord

School of Electrical Engineering, Georgia Institute of Technology, Atlanta, Georgia 30332.
Received 6 March 1974.

The presence of cones of diffracted light on illumination of previously laser-exposed crystals of lithium niobate is reported here. These diffraction cones are shown to result from the internally recorded interference pattern (hologram) resulting from the interference of the original incident laser beam with light scattered from material inhomogeneities. Diffraction cones are observed in iron-doped lithium niobate crystals that were exposed to a single laser beam and in crystals that were exposed to two superposed laser beams (i.e., during conventional holographic recording). In the two-beam case, the diffraction cones are present in addition to the first order diffracted beam when the conventional two-beam thick hologram is reconstructed. The diffraction cones produce the impression of scattered light during hologram reconstruction, an effect that has previously been reported in transition metal-doped lithium niobate[1] and photopolymers.[2]

The diffraction cones, which have their apex in the ex-

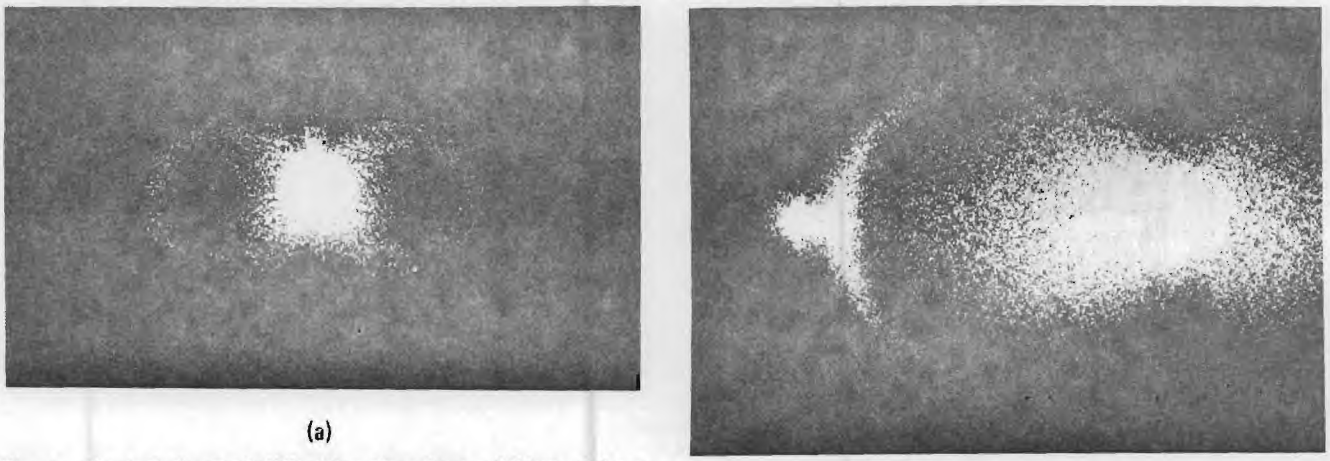

(a) (b)

Fig. 1. Typical observed diffraction rings from a lithium niobate crystal in which a plane holographic grating has been recorded. The original writing beams had a wavelength λ_w = 515 nm, and the subsequent probing beam for the above photographs was λ_r = 633 nm and had an angle of incidence in (a) of $\alpha = 0°$, resulting in cone angles of $\Phi_1 = 5.7°$ and $\Phi_2 = -5.7°$, and an angle of incidence in (b) of $\alpha = 4.5°$, resulting in a cone angle $\Phi_1 = 10.6°$. Note in (b) the first order diffracted beam just to the left of the diffraction ring.

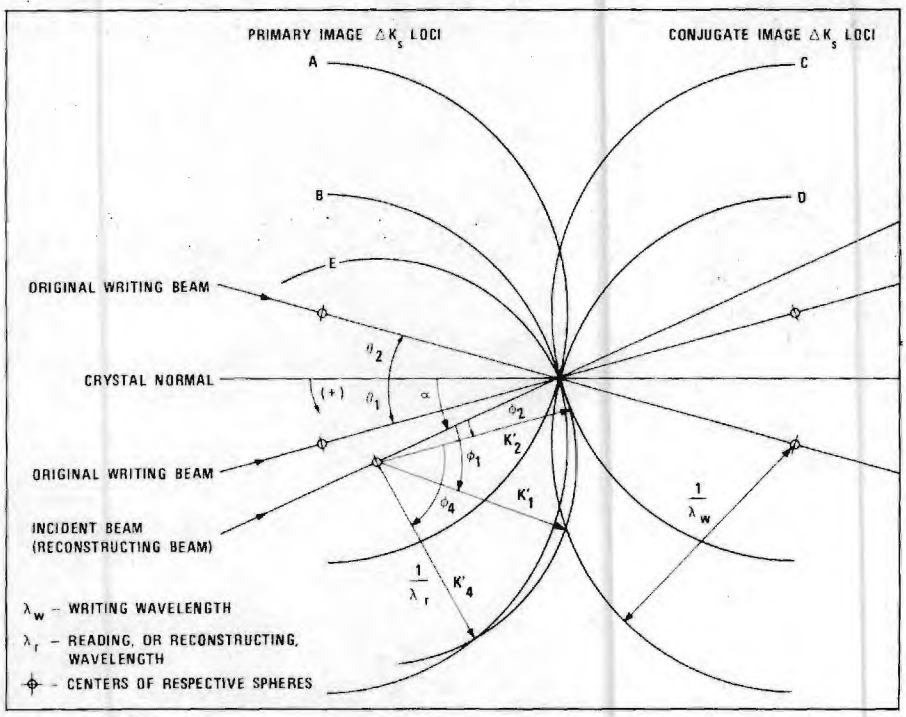

Fig. 2. Ewald sphere construction used in deriving the relationship between the diffraction cone angles, Φ, and the angle of incidence, α.

posed region of the crystal, are observed as rings (referred to as scattering rings, or diffraction rings) when a screen or a piece of film intersects the cone of light. Figure 1 shows two typical diffraction ring patterns. For the single-beam case, the observed results in lithium niobate are effectively the same as the experimental observations of Moran and Kaminow[3] for polymethyl methacrylate (PMMA), which had been exposed to ultraviolet laser light. The cones of diffracted light for this case of a single original exposing beam have been explained by Forshaw[2,4] using the Ewald sphere construction from diffraction theory (see, e.g., Ref. 5). This method is extended here to describe the diffraction cones that result when there are two intersecting exposing beams as in conventional holographic recording.

The Bragg diffraction condition $\Delta\bar{K}_G = \bar{K}' - \bar{K}$, where K' and $\bar{K}$ are the diffracted and incident beam wave vectors, respectively, and $\Delta\bar{K}_G$ is the fundamental holographic grating vector, predicts the direction of the well-defined first order diffracted beam. Another diffraction pattern is also produced that is described by $\Delta\bar{K}_s = \bar{K}_s - \bar{K}_i$, where $\bar{K}_s$ is any one of the wave vectors of the scattered wavelets of the original writing beam, and $\bar{K}_i$ is the wavevector of the original incident writing beam. The scattered light within the crystal interferes with the original beam, and this interference pattern is written into the crystal in the

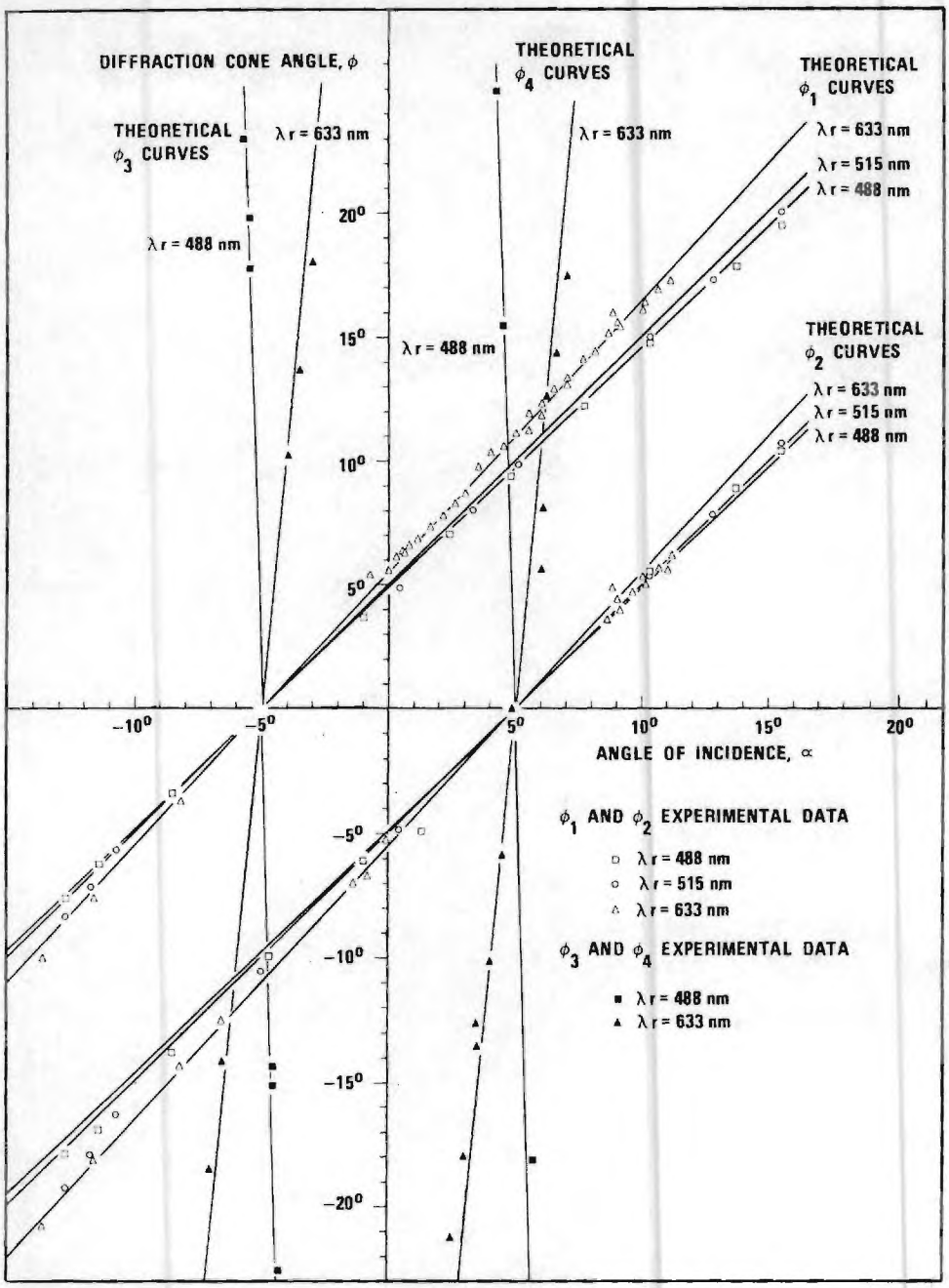

Fig. 3. Comparison of theoretical and experimental results for a $LiNbO_3$ crystal originally exposed to two intersecting laser beams of λ_w = 515 nm having angles of incidence equal to +5° and −5° and subsequently probed with a single low power laser beam of λ_r = 488 nm, 515 nm, and 633 nm. The theoretical curves are the same as those in Fig. 4, the patterns having been displaced by $\Delta\alpha = \pm 5°$.

same manner as the basic holographic grating is recorded in the crystal. Figure 2 illustrates the Ewald sphere construction necessary to analyze the diffraction cones that result for the case of two intersecting exposing beams. The surfaces A and B are the primary image loci for the $\Delta\bar{K}_s$ pattern, and the surfaces C and D are the corresponding conjugate image loci. That is, the vectors $+\Delta\bar{K}_s$ and $-\Delta\bar{K}_s$, if originating at the intersection of the original writing beams, terminate on the primary and conjugate spheres, respectively. All of these spheres have radii $1/\lambda_w$ where λ_w is the writing wavelength. The surface E is the reconstructing sphere with radius $1/\lambda_r$ where λ_r is the reading wavelength. $\bar{K}_1'$, $\bar{K}_2'$, and $\bar{K}_4'$ are the reconstruction wave vectors, and Φ_1, Φ_2, and Φ_4 are the corresponding diffraction cone angles. The intersection of the surface E with each of the other spheres describes a circle.

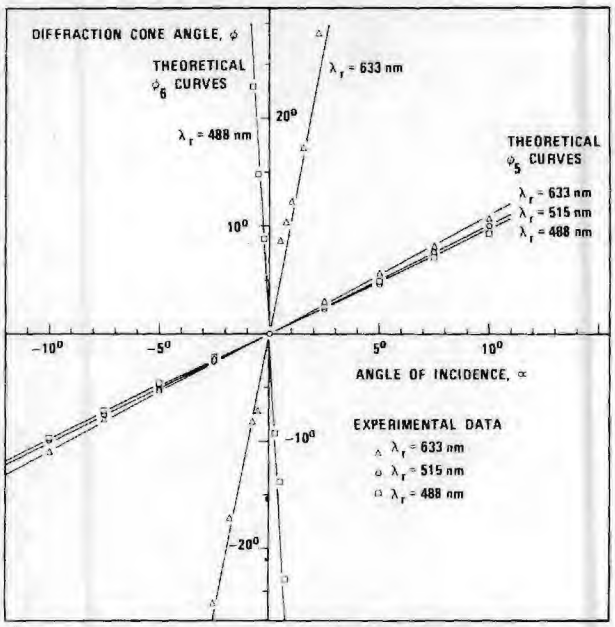

Fig. 4. Comparison of theoretical and experimental results for a $LiNbO_3$ crystal originally exposed to a single laser beam of λ_w = 515 nm at normal incidence and subsequently probed with a laser beam of λ_r = 488 nm, 515 nm, and 633 nm.

Wave vectors drawn from the center of E to these intersection circles represent the diffraction cones. By trigonometry it can be shown that

$$\phi_1,\phi_2 = 2\tan^{-1}\{[\sin(\alpha - \theta_2,\theta_1)]/[\cos(\alpha - \theta_2,\theta_1) + \lambda_w/\lambda_r]\}, \quad (1)$$

$$\phi_3,\phi_4 = 2\tan^{-1}\{[\sin(\alpha - \theta_2,\theta_1)]/[\cos(\alpha - \theta_2,\theta_1) - \lambda_w/\lambda_r]\}, \quad (2)$$

where Φ_1 and Φ_3 are the diffraction cone angles associated with the original writing beam that was at angle Θ_2. Likewise, Φ_2 and Φ_4 are associated with the writing beam that was at Θ_1. Angle Φ_3 is not shown in Fig. 2 because the intersection to which it corresponds (of reconstructing sphere E and primary sphere A) is not pictured. The diffraction cone angles, Φ_5 and Φ_6, for the normal incidence single writing beam case are obtained by setting Θ_1 and Θ_2 equal to zero in the above equations.

$$\phi_5 = \phi_1|_{\theta_2=0} = \phi_2|_{\theta_1=0} = 2\tan^{-1}[(\sin\alpha)/(\cos\alpha + \lambda_w/\lambda_r)], \quad (3)$$

$$\phi_6 = \phi_3|_{\theta_2=0} = \phi_4|_{\theta_1=0} = 2\tan^{-1}[(\sin\alpha)/(\cos\alpha - \lambda_w/\lambda_r)]. \quad (4)$$

These equations can be shown to be mathematically identical to Eqs. (3) and (4) in Ref. 2 on appropriate redefinition of angles.

Equations (1) and (2) are plotted in Fig. 3 as functions of the angle of incidence, α, for $\Theta_1 = +5°$, $\Theta_2 = -5°$, λ_w = 515 nm, and λ_r = 488 nm, 515 nm, and 633 nm. Experimentally measured values of the cone angle Φ are also plotted in Fig. 3. These are found to be in agreement with the theoretical predictions. It is seen from Fig. 3 that two rings are visible at all times. These represent the diffraction cones (of angles Φ_1 and Φ_2) generated by the intersection of the reconstructing surface with the conjugate writing surfaces. The angles Φ_3 and Φ_4 are found to be very sensitive to changes in α. Consequently, the corresponding rings are seen only for a very narrow angular range about $\alpha = \Theta_1, \Theta_2$ at our experimental wavelengths. This may also be seen from Fig. 2. (Imagine α varies and observe Φ_4.)

Equations (3) and (4) for the single exposing beam case at normal incidence ($\Theta_1 = 0$ or $\Theta_2 = 0$) are plotted as functions of the angle of incidence, α, in Fig. 4 for λ_w = 515 nm and λ_r = 488 nm, 515 nm, and 633 nm. Experimental data for the diffraction cone angle Φ are also included in Fig. 4. The data are seen to conform very closely to the theoretically predicted values.

The material used in these experiments was a 3.0-mm thick poled single crystal of lithium niobate doped with 0.1 mole% iron (in the melt). This heavily doped material, which was initially reddish, was oxygen annealed to make it transparent (presumably changing Fe^{2+} to Fe^{3+}). Laser scattering induced holograms were written with a single beam and with two intersecting beams of an argon ion laser operating at λ_w = 515 nm. Writing exposures to produce a readily observable diffraction cone pattern were typically 1 J. In the intersecting beam case the plane-wave grating holograms produced had a diffraction efficiency of approximately 20%.

The presence of diffracted cones of light represents a possible limitation of heavily iron-doped lithium niobate for data storage applications because optical power is lost into the scattering induced diffraction cones that could otherwise be used to increase the diffraction efficiency and thus the total bit capacity of the two-beam grating hologram. However, it has already been shown by Phillips, Amodei, and Staebler[1] that the scattered light may be erased (1) by illumination with uniform incoherent light or (2) by writing additional superposed holograms at new angles. In the latter case, scattered light from the previous holograms tends to be erased.

In addition, the reconstruction of laser scattering induced holograms in a material is potentially useful as a diagnostic tool to determine the nature of the scattering centers in the material. The above analysis has shown the *geometrical* relationships that exist for the diffraction cones. An analysis of the *distribution* of diffracted light within these cones is expected to yield detailed information about the scatterers.

This work was supported by the National Science Foundation and by the National Aeronautics and Space Administration.

References

1. W. Phillips, J. J. Amodei, and D. L. Staebler, RCA Rev. 33, 94 (1972).
2. M. R. B. Forshaw, Appl. Opt. 13, 2 (1974).
3. J. M. Moran and I. P. Kaminow, Appl. Opt. 12, 1964 (1973).
4. M. R. B. Forshaw, Opt. Commun. 8, 201 (1973).
5. V. V. Aristov and V. Sh. Shekhtman, Sov. Phys. Usp. 14, 263 (1971).

VII. MULTIPLE HOLOGRAM STORAGE

In the last four sections, problems associated with multiple hologram storage have been discussed. The experimental results presented have been obtained using the basic experimental configuration shown in Fig. 1. Basic diagnostic experiments were performed by storing both single holograms and by storing multiple holograms [13] at a single location. The theoretical storage density of two dimensional (thin) holograms is 4×10^8 bits/cm^2 (one bit per square area one wavelength on a side) whereas in three dimensional volume (thick) holograms the theoretical storage density is 8×10^{12} bits/cm^3 (one bit per cube volume wavelength on a side) [14]. Obviously for truly high capacity storage, thick holograms (such as in optical crystals) need to be used instead of thin holograms (such as in photographic emulsions or metal films). Holographic memory systems have been described that utilize three-dimensional storage [15]. These systems superpose many holograms at a single location inside the thick recording medium by using a different reference beam angle for each hologram. The superposition of multiple holograms at a single volume location introduces the additional problem of writing new holograms in that volume without affecting those already there. When lithium niobate is used as the three dimensional storage material, this problem may be solved by the application of an external electric field [16], [17]. This greatly increases the sensitivity for writing while the sensitivity for erasure remains unchanged at a much lower value. Thus, as a new hologram is written, the other holograms at that location are only slightly erased. Work is presently underway in our laboratory to duplicate these electric field effects.

VIII. RECORDED HOLOGRAM ANALYSIS

A method for analyzing the diffraction efficiency of thick, lossless transmission holograms in lithium niobate was developed. In lithium niobate and similar ferroelectrics, the literature assumes the induced changes in index of refraction are sinusoidal in nature, like the two beam plane wave interference pattern. The diffraction efficiency can be predicted for the sinusoidal case [1]. In actual fact, the index of refraction variation is probably not sinusoidal due to the obviously nonlinear writing characteristic (diffraction efficiency versus exposure), which is experimentally observed.

We have developed [3] a method for calculating arbitrary-order diffraction efficiencies of thick, lossless transmission gratings with arbitrary periodic grating shapes. For illustration, numerical values of the diffraction efficiencies at the first three Bragg angles were calculated for sinusoidal, square wave, triangular, and sawtooth gratings. The complete details of this method are expounded in Ref. 3, which is duplicated in this report. Also a comparison of our method to an extension of the Burckhardt matrix method [18] is presented in Fig. 7. Our method was determined to be 20 times faster on the computer!

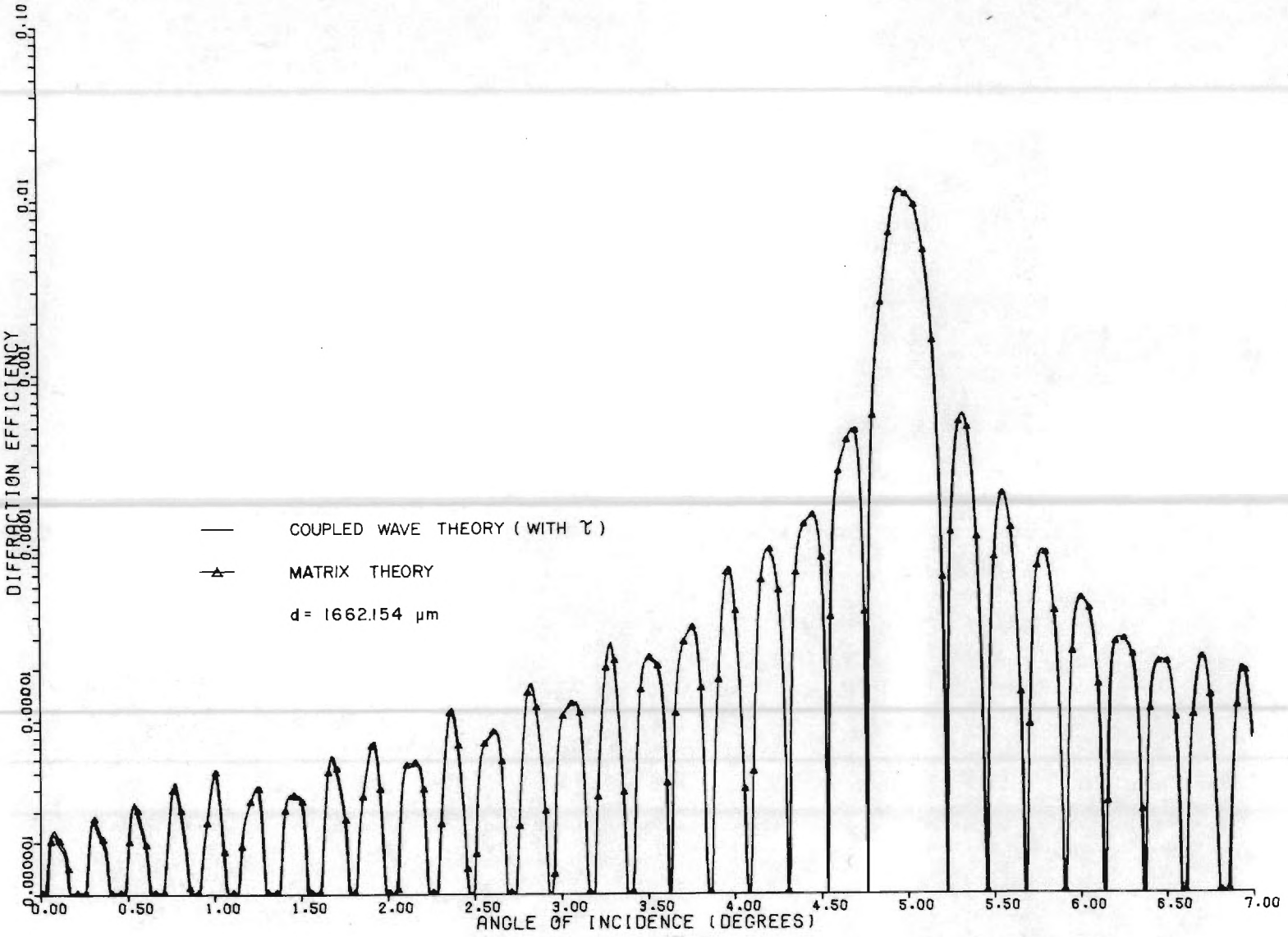

FIGURE 7. COMPARISON OF COUPLED-WAVE AND MATRIX THEORIES. The plot actually consists of two curves, but the difference is not discernible.

Journal of the Optical Society of America, vol. 65, no. 1, January 1975.

Calculation of arbitrary-order diffraction efficiencies of thick gratings with arbitrary grating shape*

S. F. Su and T. K. Gaylord

hool of Electrical Engineering, Georgia Institute of Technology, Atlanta, Georgia 30332

(Received 18 July 1974, revision received September 1974)

A method for calculating arbitrary-order diffraction efficiencies of thick, lossless transmission gratings with arbitrary periodic grating shapes has been developed. This represents an extension of previous work to nonsinusoidal gratings and to higher-order Bragg angles. A Fourier-series representation of the grating is employed, along with a coupled-mode theory of diffraction. For illustration, numerical values of the diffraction efficiencies at the first three Bragg angles are calculated for sinusoidal, square-wave, triangular, and saw-tooth gratings. Numerical results for the same grating shapes with the same parameters are also calculated for comparison, by extending Burckhardt's numerical method for analyzing thick sinusoidal gratings. The comparison shows that the coupled-mode theory provides results with relative computational ease and results that are in agreement with calculations obtained by extending the more-rigorous Burckhardt theory to nonsinusoidal grating shapes and to higher-order Bragg angles.

Index Headings: Gratings, Diffraction.

It is well known that thick dielectric diffraction gratings differ from thin gratings in a number of important ways. Among these are the capability of high diffraction efficiency,[1] wavelength selectivity,[1] angular selectivity,[1] and reduced noise.[2] These give rise to the use of thick gratings as highly efficient diffraction gratings, narrow-band spectral filters,[3] thick-grating optical components, such as lenses,[4] and imaging systems capable of spectral resolution of extended objects.[2] In the field of integrated optics, thick gratings may be used as diffraction gratings for surface guiding of waves,[5] for thin-film distributed-feedback lasers,[6] for frequency-selective grating reflectors in thin-film lasers,[7] for grating couplers for launching single-mode light waves into thin-film waveguides,[8,9] and for electro-optic grating deflectors and modulators.[10]

In addition, thick (volume) holograms may be regarded as recordings of an infinite number of thick gratings. Thick holograms have attracted a great deal of interest by their use in high-capacity information storage,[11] in color holography,[12] and in white-light reconstruction of holograms.[13]

The diffraction of a plane wave by a thick sinusoidal grating at or near Bragg incidence has been considered by Burckhardt[14] and by Kogelnik.[1] Burckhardt has treated this case by solving the exact electromagnetic boundary-value problem and has obtained numerical results with a digital computer to determine the eigenvalues of a matrix and to solve the resulting set of linear algebraic equations. Kogelnik has obtained a closed-form expression for the diffraction efficiency at the first-order Bragg angle, by employing a coupled-wave theory. Coupled-wave theories also have been used successfully in the treatment of light diffraction by acoustic waves.[15,16] Recently, Chu and Tamir[17] treated this problem by using a guided-wave

technique. They assumed sinusoidal modulation of the relative permittivity by the sound wave. Their treatment was based on a rigorous modal approach, utilizing the interrelationships between the characteristic mode and the coupled-mode representations. With their method, not only the diffraction efficiency at the first order but also that of any higher order can be obtained.

In this paper, Chu and Tamir's approach is extended to examine the first- and higher-order diffraction efficiencies of thick, arbitrary-shape gratings. Because of the periodicity of the grating, a Fourier-series representation of the grating is employed. The gratings are assumed to be lossless. The reflections at surfaces of the gratings are at first neglected in the derivation, because, in practice, these can be eliminated by antireflection coatings. When surface and internal reflections are present, the results are corrected by a multiplicative transmittance factor.[18] For illustration, numerical values of the diffraction efficiencies at the first three Bragg angles are calculated for sinusoidal, square-wave, triangular, and saw-tooth gratings. For comparison, numerical results for the same grating shapes with the same parameters are also calculated by extending Burckhardt's numerical method. The comparison shows that the results from these two methods are in close agreement and that the present method is computationally simpler and more efficient.

THEORETICAL ANALYSIS

The model for a thick periodic grating can be described by Fig. 1. The x axis is chosen in the plane of incidence and parallel to the surfaces of the medium, the z axis is perpendicular to the surfaces of the medium, and the y axis is perpendicular to the page. For convenience, the fringe planes of the grating are assumed to be perpendicular to the surfaces of the medium and to the plane of incidence. The grating vector $\bar{K}$ is, therefore, parallel to the x axis. Thus, for lossless periodic gratings, the fringes of the grating can be represented by a spatial modulation of the relative dielectric constant,

$$\epsilon_r(x) = \epsilon(x)/\epsilon_o = \epsilon_{ro} + \sum_{h=1}^{\infty} [\epsilon_{ch}\cos(hKx) + \epsilon_{sh}\sin(hKx)], \qquad (1)$$

where $K = 2\pi/L$, L is the period of the grating, ϵ_{ro} is the average value of ϵ_r, and ϵ_{ch} and ϵ_{sh} are the spatial modulations of ϵ_r, the subscripts c, s and h denoting the quantities connected with the cosine gratings, the sine gratings and the h th-harmonic grating, respectively. Corresponding to the distribution of the relative dielectric constant, the distribution of the refractive index of the medium is

$$n(x) = n_o + \sum_{h=1}^{\infty} [n_{ch}\cos(hKx) + n_{sh}\sin(hKx)], \qquad (2)$$

where n_o is the average refractive index of the medium, and n_{ch} and n_{sh} are the spatial modulations of n.

The electric field of the incident wave is assumed to be polarized perpendicular to the plane of incidence (H mode) and is of the form

$\exp[j(\eta_o x + \xi_o z - \omega_o t)]$. The wave propagation in the grating can be described by the scalar wave equation

$$[\nabla^2 + k^2 \varepsilon_r(x)]\, E(x,z) = 0, \tag{3}$$

where $k = 2\pi/\lambda$, λ is the free-space wavelength of the incident plane wave, and $E(x,z)$ is the complex amplitude of the y component of the electric field, which is independent of y.

Eq. (3) has been solved by Burckhardt,[14] using separation of variables, an infinite-series solution for the x-dependent equation, and a matrix method to solve the eigenvalue problem associated with a truncated set of the resulting infinite system of equations. This approach has been used to obtain numerical results for sinusoidal gratings. Kaspar[19] has extended Burckhardt's method to find the diffraction efficiency for nonsinusoidal absorption gratings. He has pointed out that when the absorption is strong, the phase-grating contribution to the diffraction efficiency is very small.

Chu and Tamir[17] have shown that the field inside the grating can be described in terms of coupled modes if the modulations of the relative dielectric constant are very small. In general, in addition to the zeroth mode, many higher-order modes are excited, because of the presence of the grating. For an incident wave (zero-order mode) of wavelength λ, and at an angle θ_o, the fundamental grating will diffract this wave if the Bragg condition, $m\lambda = 2L \sin\theta_o$, is satisfied or nearly satisfied. For this particular wavelength and angle, the harmonic gratings may or may not produce diffraction, depending on whether or not their corresponding Bragg conditions are satisfied or nearly satisfied. These diffracted modes of the fundamental and the harmonic gratings propagate in the same direction.

The dimensionless quantities

$$q_{ch} = 2\left(\frac{L}{h\lambda}\right)^2 \epsilon_{ch}, \qquad h = 1, 2, 3, \ldots \tag{4}$$

$$q_{sh} = 2\left(\frac{L}{h\lambda}\right)^2 \epsilon_{sh}, \qquad h = 1, 2, 3, \ldots \tag{5}$$

are called the effective-modulation indices.[17,20] Because ϵ_{ch} and ϵ_{sh} would typically be 10^{-4} or smaller, q_{ch} and q_{sh} are small even if L is many times as large as λ. For example, if $\theta_o = 5^o$ and $\epsilon_{c1} = 10^{-4}$, then $q_{c1} = 0.0066$. When q is very small compared to unity, it can be shown[17,21] that two coupled-wave equations and therefore two modes are sufficient to describe the coupling effects when the incident angle is equal to or near the Bragg angle. Therefore, for an incident wave of wavelength λ and at an angle θ_o, the electric field inside the grating can be written as the sum of the fundamental mode and an arbitrary mode

$$\tilde{E}(x,z) = \tilde{S}_o(z) \exp(j\tilde{\eta}_o x) + \tilde{S}_m(z) \exp(j\tilde{\eta}_m x), \tag{6}$$

where $\tilde{\eta}_o$ and $\tilde{\eta}_m$ are the zeroth-mode and the m th-mode (with respect to the fundamental grating) transverse wave numbers, respectively. The continuity of the electric field at z = 0 and the Floquet theorem require that $\tilde{\eta}_o = \eta_o = k \sin\theta_o$ and $\tilde{\eta}_m = \eta_m = \eta_o - 2m\pi/L$. The tilde ~ will henceforth be used to denote the quantities in the dielectric medium when the gratings are present. The integer subscript m represents the m th-order diffraction. The integer h represents the h th-harmonic grating. Diffraction occurs when the h th-harmonic grating satisfies or nearly satisfies the Bragg condition $m_h \lambda = 2(L/h) \sin\theta_o$, where m_h represents the m_h th mode (with respect to the h th-harmonic grating) excited due to the h th-harmonic grating. Exact-Bragg conditions occur when m_h is equal to m/h where h divides evenly into m. Near-Bragg conditions occur for the wavelength λ 1) when the angle of

incidence is near, but not equal to θ_o, and/or 2) when the value of m is large, and h divides nearly evenly into m, so that m/h is almost an integer. Thus, $\tilde{S}_m(z)$ in Eq. (6) represents the total amplitude, together with the propagation factor in the z direction, of the diffracted mode due to all of the gratings that satisfy or nearly satisfy the foregoing Bragg condition. At the boundary z = d, $\tilde{S}_o$ propagates at the angle θ_o, whereas $\tilde{S}_m$ propagates at an angle θ_m, which is determined by

$$\theta_m = -\sin^{-1}\left(\frac{\eta_m}{k}\right) = -\sin^{-1}\left(\sin\theta_o - \frac{m\lambda}{L}\right) \tag{7}$$

The diffracted modes due to the gratings that are far from obeying the Bragg condition are assumed to be negligibly small compared with $\tilde{S}_o$ and $\tilde{S}_m$. Therefore, the interaction between $\tilde{S}_o$ and $\tilde{S}_m$ can be characterized by the coupled-mode equations[22]

$$\frac{d\tilde{S}_o}{dz} - j\bar{\xi}_o\tilde{S}_o - j\left[\sum_h^m (C_{chm_h} + jC_{shm_h})\right]\tilde{S}_m = 0, \tag{8}$$

$$\frac{d\tilde{S}_m}{dz} - j\bar{\xi}_m\tilde{S}_m - j\left[\sum_h^m (C_{chm_h} - jC_{shm_h})\right]\tilde{S}_o = 0, \tag{9}$$

where $\bar{\xi}_o$ and $\bar{\xi}_m$ are the longitudinal wave numbers inside the medium when the gratings are absent. They are given by $\bar{\xi}_o = k(\epsilon_{ro})^{\frac{1}{2}}\cos\varphi$ and $\bar{\xi}_m = \{k^2\epsilon_{ro} - [k(\epsilon_{ro})^{\frac{1}{2}}\sin\varphi - (2m\pi/L)]^2\}^{\frac{1}{2}}$, where φ, the refraction angle in the medium, is given by $\varphi = \sin^{-1}[(\sin\theta_o)/(\epsilon_{ro})^{\frac{1}{2}}]$. The bar notation will henceforth be used to denote the quantities inside the medium when the gratings are absent. For a given value of the integer m, the subscript h may be any integer that divides evenly or nearly evenly into m, provided the corresponding h th-harmonic

grating exists. The symbol $\sum_{h}^{m}$ denotes the summation over all of these possible values of h. The coupling coefficients in Eqs. (8) and (9) are given by[17,21]

$$C_{chm_h} \cong \frac{1}{\bar{\xi}_o + \bar{\xi}_m} \left[\frac{1}{(2)^{(m_h-1)}(m_h-1)!}\right]^2 \left(\frac{\pi}{L/h}\right)^2 (q_{ch})^{m_h}, \tag{10}$$

$$C_{shm_h} \cong \frac{1}{\bar{\xi}_o + \bar{\xi}_m} \left[\frac{1}{(2)^{(m_h-1)}(m_h-1)!}\right]^2 \left(\frac{\pi}{L/h}\right)^2 (q_{sh})^{m_h}. \tag{11}$$

If the grating does not exist, $C_{chm_h} = C_{shm_h} = 0$, there is no coupling between $\bar{S}_o$ and $\bar{S}_m$ and therefore no diffraction. Under this condition, only Eq. (8) has physical significance. It represents the propagation of the fundamental mode (incident wave) inside the medium.

The solutions of Eqs. (8) and (9) are of the form

$$\tilde{S}_o(z) = A_o \exp(j\tilde{\xi}_o z) + B_o \exp(j\tilde{\xi}_m z), \tag{12}$$

$$\tilde{S}_m(z) = A_m \exp(j\tilde{\xi}_o z) + B_m \exp(j\tilde{\xi}_m z). \tag{13}$$

The wave numbers $\tilde{\xi}_o$ and $\tilde{\xi}_m$ can be found directly by substituting Eqs. (12) and (13) into Eqs. (8) and (9). They are

$$\tilde{\xi}_{o,m} = \frac{\bar{\xi}_o + \bar{\xi}_m}{2} \pm \left[\left(\frac{\bar{\xi}_o - \bar{\xi}_m}{2}\right)^2 + \left(\sum_{h}^{m} C_{chm_h}\right)^2 + \left(\sum_{h}^{m} C_{shm_h}\right)^2\right]^{\frac{1}{2}}, \tag{14}$$

where the + sign corresponds to $\tilde{\xi}_o$ and the - sign to $\tilde{\xi}_m$. The constants A_o, B_o, A_m, and B_m are determined by the boundary conditions and

$$\left[\sum_{h}^{m} (C_{chm_h} - jC_{shm_h})\right] A_o - (\tilde{\xi}_o - \bar{\xi}_m) A_m = 0, \tag{15}$$

$$\left[\sum_{h}^{m} (C_{chm_h} - jC_{shm_h})\right]B_o - (\tilde{\xi}_m - \bar{\xi}_m)B_m = 0, \tag{16}$$

which are obtained from Eqs. (9), (12), and (13). To specify the boundary conditions, the amplitude of the incident wave is assumed to be unity at z=0 so that, from Eq. (12),

$$\tilde{S}_o(0) = A_o + B_o = 1. \tag{17}$$

Initially, the amplitude of the diffracted wave is zero. Therefore, evaluating Eq. (13) at z = 0 gives

$$\tilde{S}_m(0) = A_m + B_m = 0. \tag{18}$$

Solving Eqs. (15), (16), (17), and (18) for A_o, B_o, A_m, and B_m gives

$$A_o = \frac{\tilde{\xi}_o - \bar{\xi}_m}{\tilde{\xi}_o - \tilde{\xi}_m}$$

$$= \frac{1}{2}\,\frac{(\bar{\xi}_o - \bar{\xi}_m) + \left\{(\bar{\xi}_o - \bar{\xi}_m)^2 + 4\left[\left(\sum_{h}^{m} C_{chm_h}\right)^2 + \left(\sum_{h}^{m} C_{shm_h}\right)^2\right]\right\}^{\frac{1}{2}}}{\left\{(\bar{\xi}_o - \bar{\xi}_m)^2 + 4\left[\left(\sum_{h}^{m} C_{chm_h}\right)^2 + \left(\sum_{h}^{m} C_{shm_h}\right)^2\right]\right\}^{\frac{1}{2}}}, \tag{19}$$

$$B_o = \frac{\bar{\xi}_m - \tilde{\xi}_m}{\tilde{\xi}_o - \tilde{\xi}_m}$$

$$= \frac{1}{2}\,\frac{(\bar{\xi}_m - \bar{\xi}_o) + \left\{(\bar{\xi}_o - \bar{\xi}_m)^2 + 4\left[\left(\sum_{h}^{m} C_{chm_h}\right)^2 + \left(\sum_{h}^{m} C_{shm_h}\right)^2\right]\right\}^{\frac{1}{2}}}{\left\{(\bar{\xi}_o - \bar{\xi}_m)^2 + 4\left[\left(\sum_{h}^{m} C_{chm_h}\right)^2 + \left(\sum_{h}^{m} C_{shm_h}\right)^2\right]\right\}^{\frac{1}{2}}}, \tag{20}$$

$$A_m = -B_m = \frac{\left(\sum_{h}^{m} C_{chm_h}\right) - j\left(\sum_{h}^{m} C_{shm_h}\right)}{\left\{(\bar{\xi}_o - \bar{\xi}_m)^2 + 4\left[\left(\sum_{h}^{m} C_{chm_h}\right)^2 + \left(\sum_{h}^{m} C_{shm_h}\right)^2\right]\right\}^{\frac{1}{2}}}. \tag{21}$$

For the exact-Bragg condition, $\bar{\xi}_m = \bar{\xi}_o$ and $\theta_m = \theta_o$. Hence, Eqs. (14), (19), (20), and (21) become

$$\tilde{\xi}_{o,m} = \bar{\xi}_o \pm [(\sum_h^m C_{chm_h})^2 + (\sum_h^m C_{shm_h})^2]^{\frac{1}{2}}, \tag{22}$$

$$A_o = 1/2 = B_o, \tag{23}$$

$$A_m = -B_m = \frac{1}{2} \frac{(\sum_h^m C_{chm_h}) - j(\sum_h^m C_{shm_h})}{[(\sum_h^m C_{chm_h})^2 + (\sum_h^m C_{shm_h})^2]^{\frac{1}{2}}}. \tag{24}$$

Thus, the transmitted and the diffracted modes are

$$\tilde{S}_o(z) = \exp(j\bar{\xi}_o z) \cos\{[(\sum_h^m C_{chm_h})^2 + (\sum_h^m C_{shm_h})^2]^{\frac{1}{2}} z\}, \tag{25}$$

$$\tilde{S}_m(z) = j2A_m \exp(j\bar{\xi}_o z) \sin\{[(\sum_h^m C_{chm_h})^2 + (\sum_h^m C_{shm_h})^2]^{\frac{1}{2}} z\}, \tag{26}$$

where C_{chm_h} and C_{shm_h} are given by Eqs. (10) and (11) with $\bar{\xi}_m = \bar{\xi}_o$, and A_m is given by Eq. (24). Eq. (26) is the general formula for the m th-diffracted mode due to any periodic grating when the incident angle of the zeroth mode satisfies the Bragg condition $m\lambda = 2L \sin\theta_o$. The diffraction efficiency for the m th order of diffraction is defined as

$$DE_m \triangleq \frac{\tilde{S}_m(d)\, \tilde{S}_m^*(d)}{\tilde{S}_o(0)\, \tilde{S}_o^*(0)}, \tag{27}$$

and thus for exact-Bragg conditions

$$DE_m = \sin^2\{[(\sum_h^m C_{chm_h})^2 + (\sum_h^m C_{shm_h})^2]^{\frac{1}{2}} d\}, \tag{28}$$

where the asterisk * denotes complex conjugate. Upon substituting Eqs. (10)

and (11), with $\bar{\xi}_m = \bar{\xi}_o$, into Eq. (28) and performing some algebraic manipulations, we find that

$$DE_m = \sin^2\left[\left(\left\{\sum_h^m \frac{1}{(2)^{m_h}}\left[\frac{1}{(m_h-1)!\,(h)^{(m_h-1)}}\right]^2 \frac{L^{2(m_h-1)}}{\lambda^{(2m_h-1)}} \frac{\pi(\epsilon_{ch})^{m_h}}{(\epsilon_{ro})^{\frac{1}{2}}\cos\varphi}\right\}^2\right.$$

$$\left.+\left\{\sum_h^m \frac{1}{(2)^{m_h}}\left[\frac{1}{(m_h-1)!\,(h)^{(m_h-1)}}\right]^2 \frac{L^{2(m_h-1)}}{\lambda^{(2m_h-1)}} \frac{\pi(\epsilon_{sh})^{m_h}}{(\epsilon_{ro})^{\frac{1}{2}}\cos\varphi}\right\}^2\right)^{\frac{1}{2}} d\Bigg]. \qquad (29)$$

Eq. (29) is the general expression for the diffraction efficiency at the m th-order Bragg angle for a periodic grating of arbitrary grating shape. For example, the first-, second-, and third-order diffraction efficiencies for a grating, whose dielectric constant profile can be expressed as a Fourier sine series, are

$$DE_1 = \sin^2\left[\frac{\epsilon_{s1}\pi d}{2\lambda(\epsilon_{ro})^{\frac{1}{2}}\cos\varphi}\right], \qquad (30)$$

$$DE_2 = \sin^2\left\{\left[\frac{L^2(\epsilon_{s1})^2}{2\lambda^2} + \epsilon_{s2}\right]\frac{\pi d}{2\lambda(\epsilon_{ro})^{\frac{1}{2}}\cos\varphi}\right\}, \qquad (31)$$

and

$$DE_3 = \sin^2\left\{\left[\frac{L^4(\epsilon_{s1})^3}{16\lambda^4} + \epsilon_{s3}\right]\frac{\pi d}{2\lambda(\epsilon_{ro})^{\frac{1}{2}}\cos\varphi}\right\}. \qquad (32)$$

In Eqs. (30), (31), and (32), only the Fourier grating components ϵ_{s1}, ϵ_{s2}, and ϵ_{s3} are required to evaluate the diffraction efficiencies DE_1, DE_2, and DE_3. Table I gives these Fourier components, normalized to the amplitude of the fundamental grating, ϵ_{s1}, for gratings having sinusoidal, square-wave, triangular, and saw-tooth dielectric constant profiles. Note that the sinusoidal, square-

wave, and triangular grating shapes can each be represented by a Fourier cosine series also. In this case, the resultant diffraction efficiency expressions contain only ϵ_{c1}, ϵ_{c2}, and ϵ_{c3}. If $n_{ch} \ll n_o$ and $n_{sh} \ll n_o$, which are true in most cases[1], it can be shown that $\epsilon_{ch} = 2n_o n_{ch}$ and $\epsilon_{sh} = 2n_o n_{sh}$. Therefore, with $(\epsilon_{ro})^{\frac{1}{2}} = n_o$, Eq. (29) becomes

$$DE_m = \sin^2 \left\{ \left(\left\{ \sum_h^m \left[\frac{1}{(m_h-1)!\,(h)^{(m_h-1)}} \right]^2 \frac{L}{\lambda}^{2(m_h-1)} \frac{\pi (n_o)^{(m_h-1)} (n_{ch})^{m_h}}{(2m_h-1)\cos\varphi} \right\}^2 \right.\right.$$

$$\left.\left. + \left\{ \sum_h^m \left[\frac{1}{(m_h-1)!\,(h)^{(m_h-1)}} \right]^2 \frac{L}{\lambda}^{2(m_h-1)} \frac{\pi (n_o)^{(m_h-1)} (n_{sh})^{m_h}}{(2m_h-1)\cos\varphi} \right\}^2 \right)^{\frac{1}{2}} d \right\}. \qquad (33)$$

The results calculated with Eqs. (30), (31), and (32) do not agree with those calculated by use of Burckhardt's matrix method. This is because Burckhardt takes the boundary reflections into account, whereas they are not included in the foregoing derivation. Our results may be corrected to include boundary reflections by multiplying the diffraction efficiency by the transmittance factor,

$$\tau_m = \frac{(1-R)^2 \left[1+2R\cos(2\beta d)+R^2\right]}{(1-R^2)^2 + 4R^2\left[\cos^2(2\nu_m d)+\cos^2(2\beta d)\right] - 4R(1+R^2)\cos(2\nu_m d)\cos(2\beta d)}, \qquad (34)$$

where $R = \sin^2(\theta_o - \varphi)/\sin^2(\theta_o + \varphi)$, $\beta = 2\pi(\epsilon_{ro})^{\frac{1}{2}}(\cos\varphi)/\lambda$, and $\nu_m = \left[\left(\sum_h^m C_{chm_h} \right)^2 + \left(\sum_h^m C_{shm_h} \right)^2 \right]^{\frac{1}{2}}$ evaluated with $\bar{\xi}_m = \bar{\xi}_o$ for exact-Bragg conditions. This factor is the same as the transmittance factor derived by Kogelnik and given as Eq. (8) in Ref. 18, but with νd in that equation replaced by the argument of the sine function in Eq. (28) of this paper. This allows generalization to higher diffraction orders and nonsinusoidal gratings.

RESULTS AND DISCUSSION

The coupled-wave analysis in the preceding section was numerically implemented on a UNIVAC 1108 computer and calculations were performed for gratings having sinusoidal, square-wave, triangular, and saw-tooth distributions of the dielectric constant. Table II gives numerical values for the diffraction efficiencies at the first-, second-, and third-order Bragg angles for these gratings. These results represent $DE_1\ \tau_1$, $DE_2\ \tau_2$, and $DE_3\ \tau_3$ as obtained from Eqs. (30), (31), (32), and (34) with $\epsilon_{ro} = 2.3225$ (value used in Refs. 14 and 18) and $\epsilon_{s1} = 10^{-4}\epsilon_{ro}$. The fundamental spacing of these gratings is L = 3.630 μm (resulting from recording with two beams of $\lambda = 632.8$ nm at $\theta_o = \pm 5.0^o$). For comparison, the results obtained by extending Burckhardt's numerical method (matrix method) to nonsinusoidal gratings are also shown in Table II. These results were calculated by programming Burckhardt's method on a UNIVAC 1108 computer and using the UNIVAC Math Pack subroutines to solve the eigenvalue problem and the set of linear algebraic equations. Table II shows that the results of these two methods are in close agreement; the deviation between these two methods does not exceed 2.8% for diffraction efficiencies larger than $5\text{x}10^{-6}$%. Diffraction efficiencies smaller than $5\text{x}10^{-6}$% are less significant physically because the corresponding low-level diffracted intensities are difficult to measure. Diffraction efficiencies of less than $5\text{x}10^{-8}$% have been listed as zero in Table II. In addition to the results in Table II, we have performed calculations for other grating thicknesses (15μm, 50μm, 1500μm, and 2000μm) and other fundamental grating spacings (1.222μm and 1.822μm). We found that the deviation between the coupled-wave analysis and the matrix analysis does not exceed 6.7% for any case with a diffraction efficiency larger than

5×10^{-6}%. Typically, the percentage deviation is a few tenths of one percent.

Although Burckhardt's numerical approach is rigorous, a number of mathematical problems such as truncation of the matrix and discarding of large positive eigenvalues must be overcome. A discussion of these is included in Ref. 14. In addition, another mathematical difficulty associated with the Burckhardt method, encountered in the present work, is a singularity that arises in the process of solving a set of linear algebraic equations. For pure phase gratings, Eq. (9) in Ref. 14 is real and symmetric. When the incident wave is at the Bragg angle, pairs of equal elements are introduced on the principal diagonal of the matrix in that equation. Thus, when the modulation amplitude is small, pairs of equal eigenvalues are usually induced. This results in a singularity in the matrix in Eq. (34) in Ref. 14; therefore, the equation is nonsolvable. For the parameters in the particular examples of Ref. 14, this problem does not occur because the modulation amplitude is large ($0.0035\ \epsilon_{ro}$). However, the modulation amplitude may, in practice, be very small (of the order 10^{-4} or smaller) and the singularity problem must, therefore, be overcome. A way to avoid the singularity is by shifting the incident angle by a negligible amount away from the Bragg angle. Physically, because the shift is negligibly small (10^{-5} degrees was used here), the incident wave can still be regarded as being incident at the Bragg angle. In the present method, a closed-form expression for the diffraction efficiency is obtained, and no mathematical difficulties arise in the process of calculation. The computer time needed in the present method is only about 1/20 of that needed with the extended Burckhardt method to perform the same calculations.

From the results, we found that boundary reflections produced by the surfaces

can considerably change the diffraction efficiency. The change can be an increase or a decrease depending on whether the transmittance factor is greater or less than unity. This effect has been studied by Cohen and Gordon.[23] For the grating parameters used here, τ is typically in the range 0.70 to 1.20. In practice, the boundary reflections can be eliminated by antireflection coatings on the surfaces of the gratings. We also found that the diffraction efficiency of a given higher order is mainly contributed by the corresponding higher-order Fourier component of the grating. The difference between the diffraction efficiencies for sinusoidal and nonsinusoidal gratings (having the same average and fundamental grating amplitudes) appears only in the higher-order diffractions. The higher-order diffraction efficiencies, however, very strongly depend on the grating shape. Also, for small grating modulations, the diffraction efficiencies at any order are very dependent on grating thickness; they increase with increasing thickness. Marcuse[24] has suggested that, for small-amplitude thick nonsinusoidal phase gratings, the higher-order diffraction efficiencies might be estimated from the relative amplitudes of the spatial harmonics, consistent with the assumption of perturbation theory that only one Fourier component can satisfy the Bragg condition for a given wavelength incident wave. Our calculations show that this is true except when the amplitude of the harmonic grating ($h = m$) is very small compared to the amplitude of the fundamental and the lower-order contributing harmonic gratings. In this case, the contributions from higher-order diffractions ($h < m$) are significant. In addition, we found that the agreement between the coupled-wave method and the matrix method is better when the $h = m$ term is dominant over $h < m$ terms. Rigrod[25] has shown that for reflection gratings there is no correlation between higher-order diffraction efficiencies and the corresponding harmonics of the index profile. The present results show that

this is not true for transmission gratings.

The present method can be used to analyze the diffraction efficiency of any thick periodic grating regardless of the dielectric constant profile (grating shape). The examples analyzed here have had even or odd symmetry. However, the method does not require any symmetry to exist, but only that the grating be periodic. From the gratings analyzed, different grating shapes have shown different distributions of higher-order diffraction efficiencies. This indicates the possibility that this type of analysis might be used in reverse to determine the grating shapes of thick hologram gratings such as those recorded in ferroelectric crystals.[26] Due to nonlinearities in these materials, a sinusoidal exposure does not necessarily produce a sinusoidal change in index of refraction. Depending on which of the possible physical mechanisms is operative in a given situation (such as drift of charge carriers or diffusion of carriers) different grating shapes are generated.[27]

Further, the derivations in the preceding section have assumed that the grating medium is lossless, that the gratings are unslanted with respect to the grating boundaries (grating vector parallel to surfaces of medium), and that the incident wave is H mode polarized. If the medium is lossy, the results still apply except that the coupling coefficients are complex, and therefore the attenuation factors are implicitly contained in the expressions for the transmitted wave and the diffracted wave. The method presented here can also be straightforwardly applied to the analysis of slanted gratings and to E mode polarization of the incident wave.

CONCLUSIONS

A simple method of calculating arbitrary-order diffraction efficiencies of thick transmission gratings with arbitrary periodic grating shapes has been presented. The analysis uses a coupled-mode theory to obtain a closed-form expression for the diffraction efficiency of an arbitrary order. This method provides results with relative computational ease and results that are in close agreement with those obtained by extending Burckhardt's numerical method.

ACKNOWLEDGEMENT

The authors are indebted to Frank G. Kaspar for his helpful comments on this work.

REFERENCES

*This work was supported by the National Science Foundation under Grant No. GK-37453 and by the National Aeronautics and Space Administration under Contract No. NAS8-30246.

[1]H. Kogelnik, Bell Syst. Tech. J. 48, 2909 (1969).

[2]M. R. B. Forshaw, Opt. and Laser Technol. 6, 28 (1974).

[3]B. H. Crawford, J. Sci. Instr. 31, 333 (1954).

[4]J. N. Latta and R. C. Fairchild, J. Opt. Soc. Am. 63, 487 (1973).

[5]R. Shubert and J. H. Harris, J. Opt. Soc. Am. 61, 154 (1971).

[6]H. Kogelnik and C. V. Shank, Appl. Phys. Lett. 18, 152 (1971).

[7]I. P. Kaminow, H. P. Weber, and E. A. Chandross, Appl. Phys. Lett. 18, 497 (1971).

[8]H. Kogelnik and T. P. Sosnowski, Bell Syst. Tech. J. 49, 1602 (1970).

[9]M. L. Dakss, L. Kuhn, P. F. Heidrich, and B. A. Scott, Appl. Phys. Lett. 16, 523 (1970).

[10]J. M. Hammer, Appl. Phys. Lett. 18, 147 (1971).

[11]P. J. van Heerden, Appl. Opt. 2, 393 (1963).

[12]K. S. Pennington and L. H. Lin, Appl. Phys. Lett. 7, 56 (1965).

[13]G. W. Stroke and A. E. Labeyrie, Phys. Lett. 20, 368 (1966).

[14]C. B. Burckhardt, J. Opt. Soc. Am. 56, 1502 (1966).

[15]P. Phariseau, Proc. Indian Acad. Sci. 44A, 165 (1956).

[16]C. F. Quate, C. D. W. Wilkinson and D. K. Winslow, Proc. IEEE 53, 1604 (1965).

[17]R. S. Chu and T. Tamir, IEEE Tran. Micro. Thry. Tech. 18, 486 (1970).

[18]H. Kogelnik, J. Opt. Soc. Am. 57, 431 (1967).

[19]F. G. Kaspar, J. Opt. Soc. Am. 63, 37 (1973).

[20]T. Tamir and H. C. Wang, Can. J. Phys. 44, 2073 (1966).

[21]T. Tamir, Can. J. Phys. 44, 2461 (1966).

[22]D. A. Watkins, Topics in Electromagnetic Theory (Wiley, New York, 1958).

[23]M. G. Cohen and E. I. Gordon, Bell Syst. Tech. J. 45, 945 (1966).

[24]D. Marcuse, Light Transmission Optics (Van Nostrand Reinhold, N. Y., 1972), p. 71.

[25]W. W. Rigrod, J. Opt. Soc. Am. 64, 97 (1974) and erratum, J. Opt. Soc. Am. 64, 895 (1974).

[26]F. S. Chen, J. T. LaMacchia and D. B. Fraser, Appl. Phys. Lett. 13, 223 (1968).

[27]J. J. Amodei, RCA Rev. 32, 185 (1971).

FIGURE CAPTION

Figure 1. Geometry of a thick grating with unslanted fringes. The spatial modulation of ε is indicated by the line pattern.

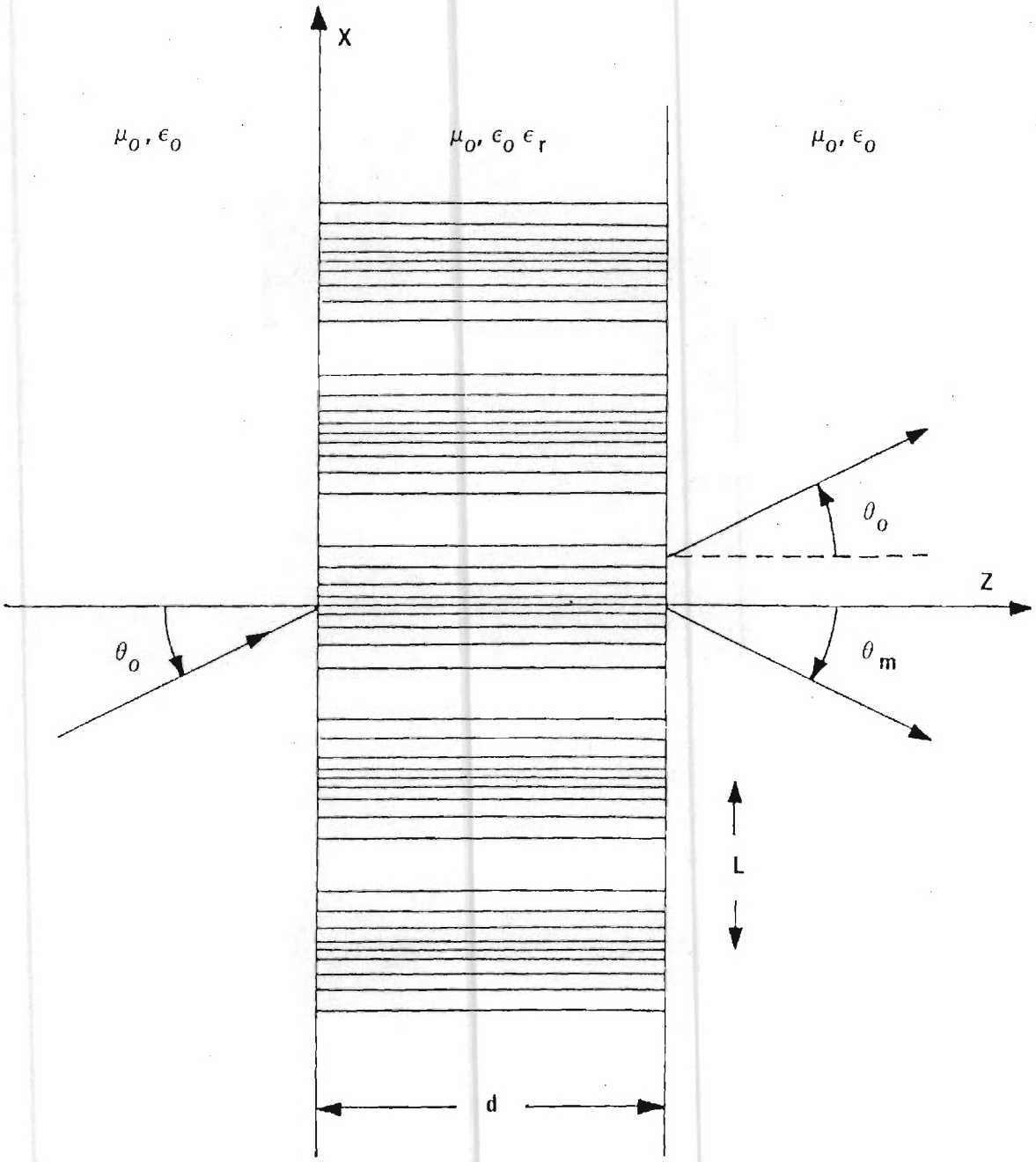
X
μ_o, ϵ_o
$\mu_o, \epsilon_o \epsilon_r$
μ_o, ϵ_o
θ_o
Z
θ_o
θ_m
L
d

Fig. 1

TABLE I. First three Fourier components for various relative dielectric constant profiles (grating shapes). Components are normalized to the amplitude of the fundamental grating, ϵ_{s1} .

Grating Component	Sinusoidal grating	Square-wave grating	Triangular grating	Saw-tooth grating
$\epsilon_{s1}/\epsilon_{s1}$	1	1	1	1
$\epsilon_{s2}/\epsilon_{s1}$	0	0	0	-1/2
$\epsilon_{s3}/\epsilon_{s1}$	0	1/3	-1/9	1/3

TABLE II. Comparison of diffraction efficiency in percent at the first-, second-, and third-order Bragg angles for transmission gratings with boundary reflections and with the same average and fundamental Fourier grating components. The grating parameters are $\epsilon_{ro} = 2.3225$ (value used in Refs. 14 and 18), $\epsilon_{s1} = 10^{-4}\epsilon_{ro}$, $L = 3.6303\,\mu m$, and the wavelength $\lambda = 0.6328\,\mu m$. Diffraction efficiencies of less than $5 \times 10^{-8}\%$ are listed as 0.00(-5).

Grating thickness (microns)	Diffraction order	Diffraction Efficiency (in % with power of ten in parentheses)							
		Sinusoidal grating		Square-wave grating		Triangular grating		Saw-tooth grating	
		Coupled-wave	Matrix	Coupled-wave	Matrix	Coupled-wave	Matrix	Coupled-wave	Matrix
10	1	1.64(-3)	1.64(-3)	1.64(-3)	1.64(-3)	1.64(-3)	1.64(-3)	1.64(-3)	1.64(-3)
	2	0.00(-5)	0.00(-5)	0.00(-5)	0.00(-5)	0.00(-5)	0.00(-5)	3.81(-4)	3.87(-4)
	3	0.00(-5)	0.00(-5)	1.14(-4)	1.14(-4)	1.26(-5)	1.25(-5)	1.14(-4)	1.13(-4)
100	1	1.57(-1)	1.57(-1)	1.57(-1)	1.57(-1)	1.57(-1)	1.57(-1)	1.57(-1)	1.57(-1)
	2	0.15(-5)	0.13(-5)	0.15(-5)	0.14(-5)	0.15(-5)	0.13(-5)	2.49(-2)	2.56(-2)
	3	0.00(-5)	0.00(-5)	1.12(-2)	1.12(-2)	1.25(-3)	1.23(-3)	1.12(-2)	1.12(-2)
1000	1	1.21(+1)	1.21(+1)	1.21(+1)	1.21(+1)	1.21(+1)	1.21(+1)	1.21(+1)	1.21(+1)
	2	2.53(-4)	2.46(-4)	2.53(-4)	2.46(-4)	2.53(-4)	2.46(-4)	4.16(+0)	4.26(+0)
	3	0.00(-5)	0.00(-5)	1.64(+0)	1.64(+0)	1.83(-1)	1.84(-1)	1.64(+0)	1.66(+0)

IX. SYSTEMS CONSIDERATIONS

A three-dimensional lithium niobate recording and storage system is shown schematically in Fig. 8. The systems aspects of such an optical recording scheme were thoroughly reviewed in this study. One of the results of this review was the publication of a state-of-the-art review [6]. This article is reproduced in this report and is a self-contained review. Another result of this review was a change in our experimental reading system. An angular accessing system was developed and it is illustrated in Fig. 9. This system allows accurate and simple angular beam positioning without the need to rotate the crystal.

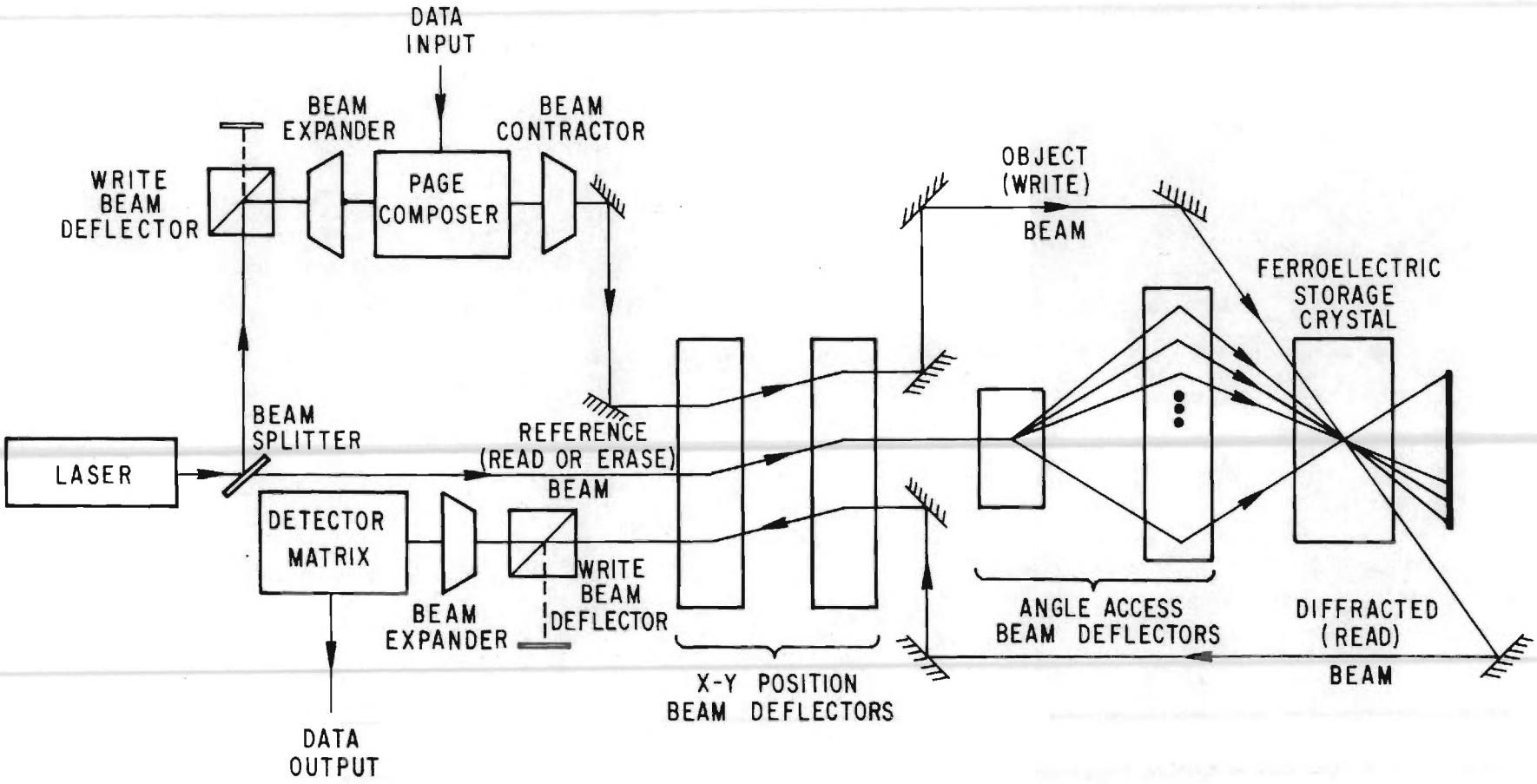

FIGURE 8. SCHEMATIC OF A READ-WRITE-ERASE OPTICAL HOLOGRAPHIC COMPUTER MEMORY.

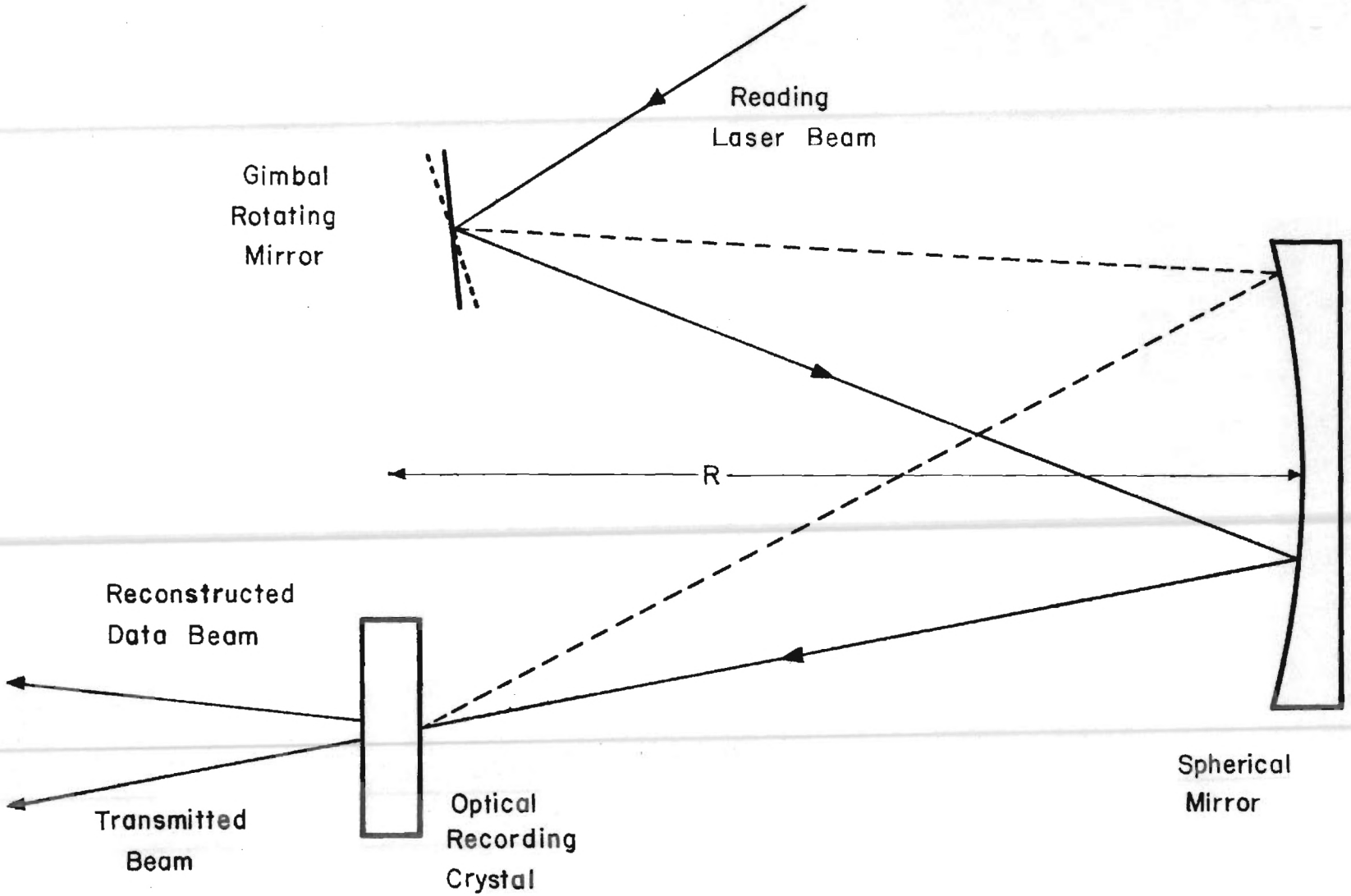

FIGURE 9. ANGULAR ACCESS SCANNER FOR READING MULTIPLE HOLOGRAMS STORED AT A SINGLE LOCATION.

OPTICAL MEMORIES:

Filling the storage gap

by Thomas K. Gaylord

THAT GAP BETWEEN THE MEMORY system needed and existing memories has only increased. Already the need for large-capacity rapid-access storage has raced ahead of existing technology. And the need is steadily growing.

Have your cake . . .

There has been what seems to be an inherent tradeoff between memory capacity and access time. Rapidly developing optical memory technology, however, promises to avoid the tradeoff and fill the gap. Figure 1 graphically represents the state of existing memories, and the expected performance of optical memories.

From slow and steady

The need for mass storage may be divided into several categories. Perhaps the least demanding of these categories is archival storage or record access. In this category large amounts of data need to be stored in a central memory and occasionally accessed. Examples include libraries, insurance data, medical data, seismic data, criminal data, tax information, patent records, national defense data, telephone numbers, stock market information, computer software packages, etc. Numerous governmental and private organizations currently have magnetic tape libraries containing over 200,000 reels of magnetic tape. Information stored in this manner is both expensive and very slowly accessible. This category of storage primarily requires a read-only memory, as changing the data occurs infrequently by computer standards.

To a burst of data

A second category requires high data rate recording and temporary storage. An example would be high bit rate optical communications systems. In optical communications efficient use of turbulent channels will require very high capacity, very fast, reusable mass storage for recording during temporary interruptions of these channels. Another example is data recording during a space probe fly-by. Here a very large amount of data is gathered during a brief period of time. If this information could be stored, it could later be transmitted at a low bit rate to minimize transmission errors in the data.

And replacing the hierarchy

A third category for high capacity storage is in computer memories. Present day computing systems utilize a complex hierarchy of storage devices. Some of the more important of these memories are magnetic tape, disks, drums, cores, and semiconductors. The access times and storage capacities of these devices are given in Fig. 1. Modern computers use a combination of the large and slow along with small and fast memories in a hierarchical structure to realize efficient computing. The optical memory, due to its very high capacity and fast random access, offers the potential of replacing a large portion of the existing memory hierarchy. This is probably the most obvious application of high capacity, rapid access optical memories.

Or changing it

The development of new computer architectures is another area where optical memories will prove useful. This represents a new area based largely on the multi-port capability of optical memories [2] and will be discussed in more detail in a later section.

A long way to go

Today several high capacity memories using nonoptical technology are available [3]. These include the Ampex Terabit System (TBM) and the Grumman Masstape System. These memory systems are shown in Fig. 1 to have access times of about 10 seconds. The maximum storage capacities for these memories are 8.8×10^{11} bits for the Grumman Mosstape and 2.9×10^{12} bits for the Ampex Terabit System. While this amount of storage is certainly adequate, the long access times make these systems unusable as rapid random access memories.

Down to basics

Design of an optical memory system has received much analysis (see e.g. refs. 1, 4-8). Among the fundamental design decisions are:

INFORMATION SHOULD BE STORED IN HOLOGRAPHIC FORM AS OPPOSED TO DIRECT IMAGE STORAGE. In the typical configuration, the hologram will be the recording of the interference pattern between the Fourier transform of the bit pattern and a plane wave reference beam. Due to the distributed nature of the information, the storage of data in holographic form provides protection from localized loss of data due to material imperfections or dust.

INFORMATION SHOULD BE STORED IN A PAGE ORGANIZED FORMAT AS OPPOSED TO A THREE DIMENSIONAL ISOMETRIC VIEW. The ability of holography to provide three dimensional views of objects is of no particular value in mass data storage. The reconstructed data will simply be in the form of two dimensional pages.

INFORMATION SHOULD BE STORED IN A BINARY CODE AS OPPOSED TO A PICTORIAL REPRESENTATION. A page of binary data would appear as a series of bright and dark spots representing the 1's and 0's of the digital data. Pictoral representations, such as a printed page, a drawing, a map or a photograph, are also usable. However, for very high information densities, constraints on the page composer and the detector matrix favor the use of binary code.

INFORMATION SHOULD BE STORED IN THICK HOLOGRAMS AS OPPOSED TO THIN HOLOGRAMS. The theoretical storage density of two dimensional (thin) holograms is 4×10^8 bits/cm^2 (one bit per square area one wavelength on a side) whereas in three dimensional volume (thick) holograms the theoretical storage density is 8×10^{12} bits/cm^3 (one bit per cube volume wavelength on a side) [9]. Obviously for truly high capacity storage, thick holograms (such as in optical crystals) need to be used instead of thin holograms (such as in photographic

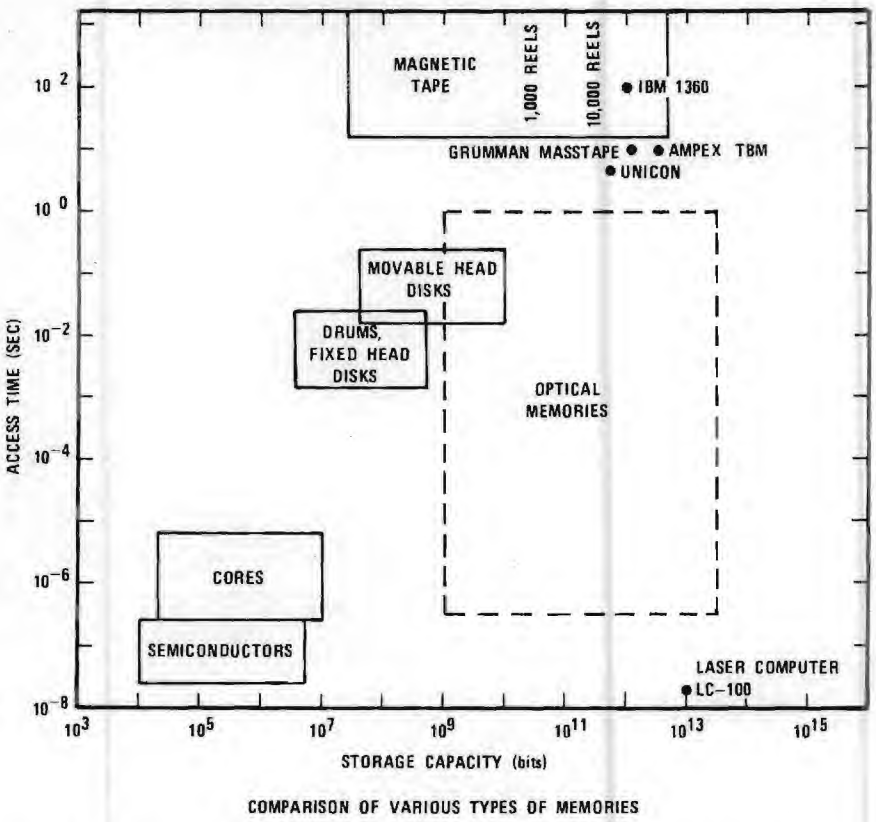

Figure 1. A graphic view of present and future memory performance.

emulsions or metal films). Holographic memory systems have been described which utilize three-dimensional storage [10, 11]. These systems superpose many holograms at a single location inside the thick recording medium by using a different reference beam angle for each hologram. Because of their volume nature, these holograms exhibit very strong angular selectivity [12, 13]. That is, in order to read a hologram, the reference beam must illuminate the hologram within a narrow angular corridor about the Bragg angle for that hologram. Illumination outside of this angular corridor produces a rapidly decreasing intensity of reconstructed data. In addition, the thicker the hologram is, the narrower the angular corridor for reconstruction becomes. The superposition of multiple holograms at a single volume location introduces the additional problem of writing new holograms in that volume without affecting those already there. When lithium niobate is used as the three dimensional storage material, this problem may be solved by the application of an external electric field [14, 15]. This greatly increases the sensitivity for writing while the sensitivity for erasure remains unchanged at a much lower value. Thus as a new hologram is written, the other holograms at that location are only slightly erased.

THE OPTICAL MEMORY SYSTEM SHOULD CONTAIN NO MOVING PARTS. This is necessary to achieve realistic operating speeds that are consistent with computer requirements. In addition, mechanical movements in a complex memory system may well reduce the reliability to an unacceptable level.

Memory building blocks

To construct an optical memory five basic components are needed: an optical source, beam defelectors, a page composer, the recording material, and a detector matrix. These components are then interfaced with each other using conventional optics and electronics. The technologies associated with page composers, beam deflectors, and recording materials, overlap each other to a large extent. Specifically, it is conceivable that lithium niobate may be used in all three components.

OPTICAL SOURCE A laser is needed to produce the coherent, collimated light required in an optical memory system. The laser must be gated or pulsed so as to operate at about 10^6 pulses per second. Additionally, an average optical power of about one watt will be needed. These requirements as well as requirements on the reliability, amplitude stability, and frequency stability can all be met with existing lasers. Completely satisfactory, argon ion lasers are available. The drawbacks of this laser are its high cost (about $20,000) and its low efficiency of conversion of electrical power to optical power (about 0.1%).

BEAM DEFLECTORS An optical memory system must utilize a number of beam deflectors to accurately position the laser beams for the reading, writing, and erasing operations. This positioning process must be both quick and accurate.

As shown in Table 1, there are three basic types of deflectors: galvonometers, acousto-optic deflectors, and electro-optic deflectors. A number of examples in each of these categories are also listed in the Table. The performance of a deflector may be quantified by the resolution and the random access time. Resolution may be defined as the maximum deflection angle divided by the diffraction limited angle. This ratio gives the total number of resolvable spots or total number of resolvable angular positions. Random access time is the time required to deflect the laser beam to a new angular position.

An extensive comparison of light beam deflectors has been performed by Zook [16]. Mechanical galvonometer deflectors are too slow for fast access memory applications (which require an access time of approximately one microsecond). Acousto-optic and electro-optic deflectors, on the other hand, can be constructed to achieve the necessary access times. These devices, however, lack the resolution attainable in galvonometers and must frequently be cascaded to achieve the number of resolvable locations needed. For example, an electro-optic deflector has been built capable of resolving a two dimensional array of 1024 × 1024 spots using twenty stages of deflection with an access time of 0.8 microseconds [17].

PAGE COMPOSER The input device for the optical memory is a page composer (block data composer), which converts digital electrical signals directly into a two dimensional optical array of bits. The page composer will be located in the object beam of the two beam holographic configuration. Reconstruction of the recorded data will duplicate the array of 1's and 0's (bright and dark spots) generated by the page composer.

There are a number of characteristics that the page composer must possess. These requirements include: 1. High frame speed — It must be possible to rapidly change the data page in the page composer. The change time ideally must be in the microsecond range. 2. High resolution — The size of each bit in the page composer needs to be small. Sizes in the range 10 to 100 microns would be suitable. 3. Large aperture — The total area of the page composer transverse to the laser beam needs to be large enough to accommodate the number of bits per page desired. For many applications the bit array size should be in the range 64 × 64 elements to 1024 × 1024 elements. 4. High contrast ratio — The achievement of a high contrast ratio relaxes the subsequent requirements on the recording material and the detector matrix. A contrast ratio of 100 to 1 or greater is desirable and this has been achieved in a number of page composer type devices. 5. Stability — The characteristics of page composer materials must not be degraded by exposure to high intensity light (the object beam). 6. Uniformity — Material nonuniformities in the block data composer must be below the minimum level associated with the onset of readout errors in the memory system.

A wide variety of approaches exist for the construction of page composers. A number of these approaches are listed in Table 2. Obviously, a large number of physical effects and a large number of materials are potentially usable in page composers. Liquid crystal block data composers (see Ref. 18 and Ref. 19) appear to be very useful. RCA has constructed a 1024 bit liquid crystal page composer [8]. A major problem with liquid crystal page composers has been their relatively slow frame speed (on the order of 100 ms). Lead lanthanum zirconate titanate (PLZT) block data composers [20] also appear to be very promising. These page composers, which do not suffer from a slow frame rate, have four basic modes of operation: strain biased mode, scattering mode, edge effect mode, and differential phase mode [21]. This last mode of operation eliminates the detrimental effects of background nonuniformities in the PLZT, but requires a double hologram exposure through the data mask. Two recently developed approaches to block data composers utilize a thin, deformable, membrane mirror array [22] and the thermally induced shift in the optical absorption band edge in CdS [23].

Table 1
Types of Beam Deflectors

Galvonometers
Moving iron galvonometer
Moving coil galvonometer

Acousto-Optic
Alpha-iodic acid (α - HIO_3)
Lead molybdate ($PbMoO_4$)
Tellurite glass
Tl_3AsS_4
H_2O
As_2S_3 glass
TeO_2

Electro-Optic
Lithium niobate ($LiNbO_3$)
Strontium barium niobate ($Sr_{0.75}Ba_{0.25}Nb_2O_6$)
Nitrobenzene
Potassium tantalum niobate (KTN)

RECORDING MATERIAL The central element of the optical memory is the recording material. This piece of material, often rather small in size, provides the entire storage capacity of the optical memory system. Recording materials must possess a number of important characteristics to achieve the high storage capacities that have been predicted for optical memories. These requirements on the optical recording material include: 1. High sensitivity — It is desirable that only a small amount of optical energy per unit area be needed to record the hologram of a data page. Table 3 lists the necessary writing energy densities for a number of recording materials. For a practical system an energy density of about 1 millijoule/cm² or less will be needed. 2. Large diffraction efficiency — Diffraction efficiency is the fraction of the reading light (reference beam) that is diffracted into the reconstructed data beam. It must be possible to record a single hologram with a large diffraction efficiency, so that in practice many holograms may be recorded at a single location, each with an equal share of the total maximum diffraction efficiency. Therefore it is desirable to have the maximum diffraction efficiency as close to 100% as possible. 3. Erasable and rewritable — For a rapid cycle read-write-erase memory system, it must be possible to continuously alter the stored data in the memory without encountering any degradation in the material characteristics. 4. Long lifetime of stored information — Stored data should persist for long periods of time before having to be refreshed. Ideally, storage should be permanent. 5. Nonvolatile storage — Data should remain recorded in the memory in the absence of system power. 6. Nondestructive readout — It should be possible to perform an essentially unlimited number of read operations without degrading or altering the stored data. 7. Three dimensional storage — To achieve very high capacity storage, the information should be stored in thick (volume) holograms. Together with the requirement of high diffraction efficiency, this means that the hologram should be a thick phase (nonabsorbing) hologram. 8. High resolution — The storage material obviously must be capable of recording the very fine (wavelength size) variations of the interference pattern produced by the intersection of the object and reference beams.

Research and development on optical recording materials for optical memories has produced remarkable advances in the past few years. Many different types of materials, as indicated in Table 2, are contenders for recording applications. Considering all of the above material requirements, the photorefractive materials (optically induced changes in index of refraction) appear to be especially promising. These materials, often ferroelectric crystals such as lithium niobate and strontium barium niobate (SBN), have been considerably developed and improved. For example, in the first use of lithium niobate as a recording material in 1968 a writing energy density of approximately 100 joules/cm² was required [24]. Less than six years later, doped versions of lithium niobate were shown to exhibit writing energy densities of 2 millijoules/cm² [25]. This is an improvement in sensitivity of almost 5 orders of magnitude. Similar sensitivity improvements have been reported for SBN [26]. The other needed material characteristics have all been reported in the photorefractive ferroelectrics — large diffraction efficiency [24, 27], optical erasing and rewriting [14, 15, 28], long lifetime of stored data [29], three dimensional storage [13, 24], etc. At the present time these very favorable material characteristics have not been simultaneously observed in a single sample. Further, it is still not clear that all of the desired characteristics can coexist in a single doped ferroelectric material. Trade-offs that have not been discovered may exist between the various desired properties. Clearly,

Table 2
Types of Page Composers*

Page Composer Concept	Materials	Addressing Techniques
Polarization rotation by induced birefringence (electrooptic effects)	PLZT (ceramic), $Bi_4Ti_3O_{12}$ KDP, KD*P, ADP	Electrode matrix, Electron beam, Light beam (with photoconductor)
Phase changes by formation of surface relief pattern	Thermoplastics, Photoplastics, Thin metalized membranes	Electron beam, Electrode matrix plus charge
Phase disturbances by piezoelectric excitation of reflecting surfaces	Mirrored piezoelectric crystals	Individual switches to an rf driver
Optical density change by induced absorption	Photochromics, Cathodochromics	Light beam (uv) plus flood illumination for erase, Electron beam plus flood illumination for erase
Optical scattering change by electrical agitation	Liquid crystals	Electrode matrix, Light beam (with photoconductor)
Polarization rotation by magnetooptic effects	MnBi, EuO:Fe, Ni-Fe $FeBO_3$, FeF_3	Light beam (absorption), Conductor matrix
Traveling phase changes by acoustooptic interaction (Debye-Sears and Bragg effects)	Water (and other liquids), Fused quartz (and other amorphous solids), $PbMoO_4$ (and other crystals)	Transverse interaction of coherent light and traveling acoustic waves
Thermally induced shift in absorption band edge	CdS, CdSe, As_2S_3	Electrode matrix for heating and heat sink substrate for cooling
Optical scattering by poled and unpoled regions of a ferroelectric	PLZT (ceramic)	Electrode matrix
Phase changes by variation of optical path length	Electrostrictive materials, PLZT (ceramic)	Electrode matrix, Double hologram recording method
Reflection changes from thin, deformable membrane mirror elements	Metal films over a substrate support structure	Electrode feedthrough from transistor on back of substrate

*adapted from H. N. Roberts, Applied Optics, vol. 11, pp. 397-404, February 1972.

more basic research on optical recording materials is required to resolve the many remaining questions. If a single material can reliably and reproducibly be made with all of the above required properties, it is certain that read-write-erase optical memories will become commercially available.

DETECTOR MATRIX An array of photodetectors is needed to convert the optical holographically reconstructed data into an electrical signal. This photosensitive readout array would have one photodiode or phototransistor for each bit of data in the reconstructed page. Each sensor in the array would function as a threshold detector indicating the presence or absence of light (a binary 1 or 0). All stored holograms would be read out with the same detector matrix (for a single port memory).

The photodetectors ideally must exhibit a low threshold detection power. Noise associated with the operation of the photodetector determines the lower limit of optical power needed for threshold detection. For a signal-to-noise ratio of about 10, an optical power in the range of 0.1 to 1.0 microwatts per bit will be required. Already readout arrays operating at 0.3 microwatts per bit have been constructed [30].

The second basic requirement on the detector matrix is that a large defect free array be constructable with existing technology. Modern semiconductor technology has fulfilled this requirement. Bell Laboratories has constructed a silicon-diode-array camera tube that consists of 525,000 individual photodiodes on a single silicon slice [31]. An LSI phototransistor array with 51,200 silicon phototransistors has been built [32] using multilayer interconnection techniques so that any bit can be read out in about a microsecond. Continuing advances in semiconductor technology assure the availability of high quality photodetector arrays.

Where we are now

Optical mass memories currently in existence include the IBM 1360 memory, introduced in 1966 but no longer in production. This Photo Digital Mass Storage System uses electron beams for recording and is read out optically. As shown in Fig. 1 its trillion bits are only very slowly accessible. Precision Instrument's Unicon laser mass memory system is an optical mass memory that now is commercially available. It uses an argon laser to perform bit-by-bit recording by vaporizing small holes in a metallized polyester belt. This read-only nonholographic memory has a storage capacity of 7×10^{11} bits and an average access time of somewhat less than 10 seconds.

The Laser Computer Corporation has aroused a great deal of discussion by its

announcement of a 10^{13} bit memory having a 20 nanosecond access time. As shown in Fig. 1 this would place their memory beyond the predicted future limits associated with optical memories. Unfortunately, very few details are available about this system.

Table 3
Required Writing Energy Density for Various Optical Recording Materials

Material	Type of Material	Writing Energy Density (joules/cm²)
$Bi_{12}SiO_{20}$	Ferroelectric-Photoconductive	1×10^{-6}
Malachite Green:		
Sucrose Benzoate	Thermoplastic	2×10^{-6}
Agfa 8E70	Photographic	2×10^{-6}
Kodak 649F	Photographic	7×10^{-6}
$Bi_4Ti_3O_{12}$-ZnSe	Ferroelectric-Photoconductive	1×10^{-3}
$LiNbO_3$:Fe	Photorefractive	2×10^{-3}
$Sr_{0.75}Ba_{0.25}Nb_2O_6$	Photorefractive	6×10^{-3}
Dichromated Geletin	Photochemical	1×10^{-2}
CaF_2:Ce	Photochromic	1×10^{-2}
PLZT	Ferroelectric-Photoconductive	1×10^{-2}
KCL:Na	Photochromic	1×10^{-2}
MnBi	Magnetooptic	3×10^{-2}
$Te_{88}Ge_7As_5$	Amorphous Semiconductor	5×10^{-2}
GdIG	Magnetooptic	9×10^{-2}
EuO	Magnetooptic	9×10^{-2}
NaF	Photochromic	9×10^{-2}
CoPniFe	Magnetooptic	1×10^{-1}
$SrTiO_3$:Ni:Mo	Photochromic	2×10^{-1}
$BaTiO_3$	Photorefractive	2×10^{-1}
MnAlGe	Magnetooptic	3×10^{-1}
$Te_{81}Ge_{15}Sb_2S_2$	Amorphous Semiconductor	5×10^{-1}
PMMA (Q-doped)	Photopolymer	1
KBr	Photochromic	1
Cu_2HgI_4	Thermoplastic	3
$BaNaNb_5O_{15}$	Photorefractive	5
$As_{16}S_{85}$	Amorphous Semiconductor	5
$Bi_4Ti_3O_{12}$	Photorefractive	10
$LiNbO_3$ (undoped)	Photorefractive	100
PMMA (undoped)	Photopolymer	100

A design revolution

Optical memories, in addition to increasing the capabilities of existing computers, promise to spur the development of new computer architectures [2]. It is conceptually simple to construct an optical memory in which any of the data pages may be accessed by multiple users simultaneously. This feature, not available in conventional memories, allows access to the memory through any of its multiple ports.

Speed, capacity, and cost relationships have determined a basic computer architecture that utilizes a hierarchical memory structure. A common way of inplementing this structure has been to provide for page swaps between a local memory and the mass store, and for word (or character) swaps between the local store and the central processing unit. Such a structure has inevitably led to problems of addressing, replacing pages, multiple contention for pages and memory allocation. The contention problem can be relieved by building a mass memory with multiple access ports. If such a memory has simultaneous read/write capability, then each user demanding use of mass memory appears to have complete control. Problems of write protection, memory allocation and paging still remain, but the speed of the mass memory has been effectively increased by having multi-port capability.

Speed can be further enhanced by utilizing a mass memory which accesses a single page in one access cycle. This differs from mass memory devices such as a disk where the page is accessed sequentially making the access time proportional to page size. A parallel transfer of a single page between the mass memory and an individual memory port coupled with the idea of multi-port simultaneous page access can provide a distinctly new storage device for parallel computation. Current methods in parallel computation utilize multiple processors and multiple memories and require many memory to memory swaps to perform array type computations. A mass memory with multi-port access capability would reduce the word exchanges and could enhance parallel computation.

Three typical applications for a multiport memory as shown in Fig. 2 are: 1. Record access — As previously discussed, many applications exist that require the storage and retrieval of large blocks of information. This can be realized very efficiently with a multi-port memory. In these systems, data would be stored in page format in the multiport memory. In these systems, data would be stored in page format in the multi-port memory. Access to any page would be via a terminal through one of the memory access ports. The data requirement of each terminal is, in some applications, low enough to have one memory port support several terminals through a multiplexer. Normally these terminals are used in a read access mode and would not be allowed to perform write operations to the memory. 2. Simultaneously shared memory computing — In this application the user performs transformations on the data accessed. This adds arithmetic logic units to the architecture as shown. 3. Parallel processing — There are many scientific problems requiring enormous numbers of computations. One approach to this problem has been a multiprocessor parallel computation technique. Essentially all processors are dedicated to solving one step and then after a transfer to the appropriate processor, repeating the step-wise computation. Problems arise from synchronization and system reliability when the parallelism is carried as far as that in Illiac IV. A possible structure for parallel processing is also shown in Fig. 2. Each processor is connected to the multi-port memory through a port. Transfers between processors can be made on an outer bus connecting each processor.

Summary

There has been a great deal of activity in recent years related to optical memories. Research and development has produced advances in optical memory components and the materials used in these components. In the area

of recording materials, more basic research clearly is required. The other components for the optical memory are either available or can be with additional engineering effort.

In the realm of system configurations for optical memories, there has been a sizeable effort to develop prototype memory systems. Holographic optical memories have been built by RCA Labs, Harris-Intertype, Bell Labs, Thomson-CSF, Nippon Corp., and others. For the most part these are limited versions of the full scale high capacity read-write-erase memory system of the future. In additon, new computer architectures are being identified to take advantage of and efficiently use the unique capabilities that are possible in optical memories. □

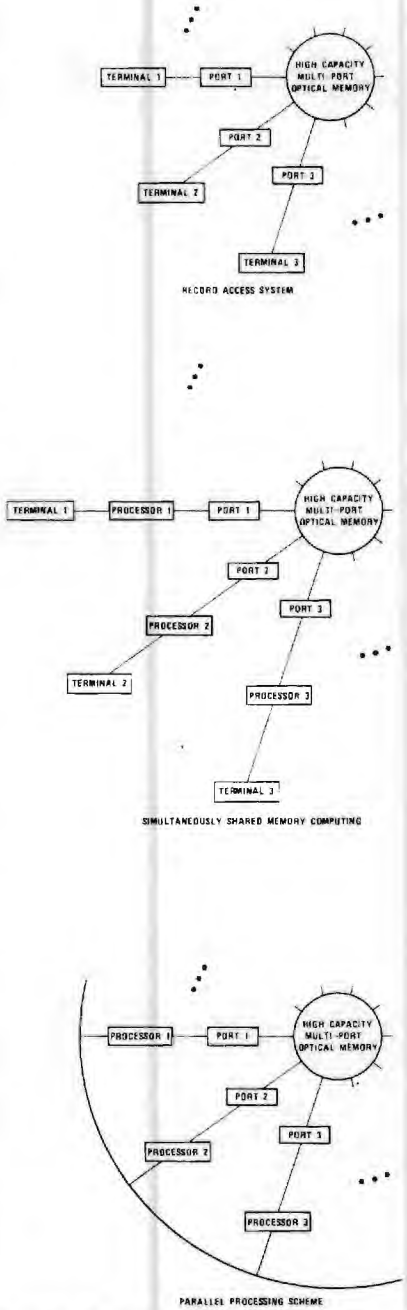

Figure 2. Possible schemes for new computer architectures using optical memories.

References

1. Rajchman, J. A., "Promise of optical memories," J. Appl. Phys., vol. 41, pp. 1376-1383, March 1, 1970.
2. Alford, C. O. and Gaylord, T. K., "Applications and implementation of a multi-port laser optical memory," NSF Proposal, April 1974.
3. Houston, G. B., "Trillion bit memories," Datamation, vol. 19, pp. 52-58, October 1973.
4. Vander Lugt, A., "Design relationships for holographic memories," Appl. Optics, vol. 12, pp. 1675-1685, July 1973.
5. Anderson, L. K., "Application of holographic optical techniques to bulk memory," IEEE Trans. Magnetics, vol. MAG-7, pp. 601-605, Sept. 1971.
6. Graf, P. and Lang, M., "Geometrical aspects of consistent holographic memory design," Appl. Optics, vol. 11, pp. 1382-1388, June 1972.
7. Hill, B., "Some aspects of a large capacity holographic memory," Appl. Optics, vol. 11, pp. 182-191, January 1972.
8. Stewart, W. C., Mezrich, R. S., Cosentino, L. S., Nagle, E. M., Wendt, F. S., and Lohman, R. D., "An experimental read-write holographic memory," RCA Review, vol. 34, pp. 3-44, March 1973.
9. van Heerden, P. J., "Theory of optical information storage in solids," Appl Optics, vol. 2, pp. 393-400, April 1963.
10. Gaylord, T. K., "The high capacity storage problem: Is optical holography the answer?" Optical Spectra, vol. 6, 25-37, November 1972.
11. d'Auria, L., Huignard, J. P., Slezak, C., and Spitz, E., "Experimental holographic read-write memory using 3-D storage," Appl. Optics, vol. 13, no. 4, pp. 808-818, April 1974.
12. Kogelnik, H., "Coupled wave theory for thick hologram gratings," Bell Sys. Tech. J., vol. 48, pp. 2909-2947, November 1969.
13. Gaylord, T. K. and Tittel, F. K., "Angular selectivity of lithium niobate volume holograms," J. Appl. Phys., vol. 44, pp. 4771-4773, October 1973.
14. Amodei, J. J. and Staebler, D. L., "Holographic recording in lithium niobate," RCA Review, vol. 33, pp. 71-93, March 1972.
15. Staebler, D. L., and Phillips, W., "Fe-doped $LiNbO_3$ for read-write applications," Appl. Optics, vol. 13, pp 788-794, April 1974.
16. Zook, J. D., "Light beam deflector performance: a comparative analysis," Applied Optics, vol. 13, pp. 875-887, April 1974.
17. Meyer, H., Riekmann, D., Schmidt, K.P., Schmidt, U.J., Rahlff, M., Schröeder, E., and Thust, W., "Design and performance of a 20-stage digital light beam deflector," Applied Optics, vol. 11, pp. 1732-1736, August 1972.
18. White, D. L. and Feldman, M., "Liquid crystal light valves," Electronics Letters, vol. 6, pp. 837-840, December 1970.
19. Special Issue of Display Devices, IEEE Trans. on Electron Devices, vol. ED-20, November 1973.
20. Roberts, H. N., "Strain-biased PLZT input devices (page composers) for holographic memories and optical data processing," Appl. Optics, vol. 11, pp. 397-404, February 1972.
21. Drake, M. D., "PLZT matrix-type block data composers," Applied Optics, vol. 13, pp. 45-79, March 1973.
23. Hill, B. and Schmidt, K. P., "New page composer for holographic data storage," Applied Optics, vol. 12, pp. 1193-1198, June 1973.
24. Chen, F. S., LaMacchia, J. T., and Fraser, D. B., "Holographic storage in lithium niobate," Appl. Phys. Letters, vol. 13, pp. 223-225, October 1, 1968.
25. Shah, P., Rabson, T. A., Tittel, F. K., and Gaylord, T. K., "Volume holographic recording and storage in Fe-doped $LiNbO_3$ using optical pulses," Appl. Phys. Letters, vol. 24, pp. 130-131, February 1974.
26. Thaxter, J. B., and Kestigian, M., "Unique properties of SBN and their use in a layered optical memory," Appl. Optics, vol. 13, pp. 913-924, April 1974.
27. Amodei, J. J., Phillips, W., and Staebler, D. L., "Improved electro optic materials and fixing techniques for holographic recording," Appl. Optics, vol. 11, pp. 390-396, February 1972.
28. Gaylord, T. K., Rabson, T. A., and Tittel, F. K., "Optically erasable and rewritable solid-state holograms," Appl. Phys. Letters, vol. 20, pp. 47-49, January 1, 1972.
29. Amodei, J. J. and Staebler, D. L., "Holographic pattern fixing in electro-optic crystals," Appl. Phys. Letters, vol. 18, pp. 540-542, June 15, 1971.
30. Assour, J. M. and Lohman, R. D., "A photodector array for holographic optical memories," RCA Review, vol. 30, pp. 557-566, December 1969.
31. Crowell, M. H. and Labuda, E. F., "The silicon diode array camera tube," Bell Sys. Tech. J., vol. 48, pp. 1481-1528, May-June 1969.
32. Mend, W. G., McCoy, E. E., and Anders, R. A., "Microminiature solid-state imaging system utilizing hybrid LSI techniques," IEEE J. Solid-State Circuits, vol. SC-5, pp. 254-260, October 1970.

Meet the author

Thomas K. Gaylord received his B.S. degree in physics and his M.S. degree in electrical engineering from the University of Missouri-Rolla. He earned his Ph.D. degree in electrical engineering from Rice University in 1970. He is currently on the faculty of the School of Electrical Engineering of Georgia Institute of Technology. Dr. Gaylord was recently named to the Editorial Advisory Board of The Optical Publishing Company.

REFERENCES

[1] H. Kogelnik, "Coupled wave theory for thick hologram gratings," Bell System Tech. J., Vol. 48, No. 4, pp. 2902-2947, November 1969.

[2] T. K. Gaylord and F. K. Tittel, "Angular selectivity of lithium niobate holograms," J. Appl. Phys., Vol. 44, No. 9, September 1973.

[3] S. F. Su and T. K. Gaylord, "Calculation of arbitrary-order diffraction efficiencies of thick gratings with arbitrary grating shape," J. Optical Soc. of Am. (to be published).

[4] H. Kogelnik, "Bragg diffraction in hologram gratings with multiple internal reflections," J. Optical Soc. of Am., Vol. 57, pp. 431-433, March 1967.

[5] M. G. Cohen and E. I. Gordon, "Acoustic scattering of light in Fabry-Perot resonator," Bell System Tech. J., Vol. 45, pp. 945-966, July-August 1966.

[6] T. K. Gaylord, "Optical memories," Optical Spectra, Vol. 8, No. 6, pp. 29-34, June 1974.

[7] F. S. Chen, J. T. LaMacchia, and D. B. Fraser, "Holographic storage in lithium niobate," Appl. Phys. Letters, Vol. 13, pp. 223-225, October 1, 1968.

[8] P. Shah, T. A. Rabson, F. K. Tittel, and T. K. Gaylord, "Volume holographic recording and storage in Fe-doped $LiNbO_3$ using optical pulses," Appl. Phys. Letters, Vol. 24, No. 3, pp. 130-131, February 1974.

[9] D. von der Linde, A. M. Glass, and K. F. Rogers, "Multiphoton photorefractive processes for optical storage in $LiNbO_3$," Appl. Phys. Letters, Vol. 25, No. 3, pp. 155-157, August 1, 1974.

[10] W. Phillips, J. J. Amodei, and D. L. Staebler, "Optical and holographic storage properties of transition metal doped lithium niobate," RCA Review, Vol. 33, No. 1, pp. 94-109, March 1972.

[11] R. Magnusson and T. K. Gaylord, "Laser scattering induced holograms in lithium niobate," Appl. Optics, Vol. 13, No. 7, pp. 1545-1548, July 1974.

[12] J. M. Moran and I. P. Kaminow, "Properties of holographic gratings photo-induced in polymethyl methacrylate," Applied Optics, Vol. 12, pp. 1964-1970, August 1973.

[13] D. L. Staebler, J. J. Amodei, and W. Phillips, "Multiple storage of thick phase holograms in $LiNbO_3$," Digest of Technical Papers, 1972 International Quantum Electronics Conference, p. 93, May 8-17, 1972.

[14] P. J. van Heerden, "Theory of optical information storage in solids," Appl. Optics, Vol. 2, No. 4, pp. 393-400, April 1963.

[15] L. d'Auria, J. P. Huignard, C. Siezak, and E. Spitz, "Experimental holographic read-write memory using 3-D storage," Applied Optics, Vol. 13, No. 4, pp. 808-818, April 1974.

[16] J. J. Amodei and D. L. Staebler, "Holographic recording in lithium niobate," RCA Review, Vol. 33, No. 1, pp. 71-93, March 1972.

[17] D. L. Staebler and W. Phillips, "Fe-doped $LiNbO_3$ for read-write applications," Appl. Optics, Vol. 13, No. 4, pp. 788-794, April 1974.

[18] C. B. Burckhardt, "Diffraction of a plane wave at a sinusoidally stratified dielectric grating," J. Optical Soc. Am., Vol. 56, pp. 1502-1509, November 1966.

CONTRACT NAS8-30246

STUDY OF MULTIPLE HOLOGRAM RECORDING IN LITHIUM NIOBATE

T. K. Gaylord and W. R. Callen
School of Electrical Engineering
Georgia Institute of Technology
Atlanta, Georgia 30332

January 1976

FINAL REPORT PERIOD 1 OCTOBER 1973 – 1 JANUARY 1976

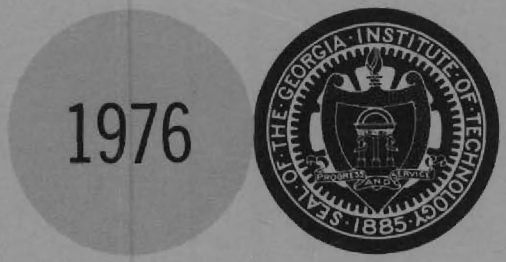

Performed for

National Aeronautics and Space Administration
George C. Marshall Space Flight Center
Marshall Space Flight Center, Alabama 35812

SCHOOL OF ELECTRICAL ENGINEERING
Georgia Institute of Technology
Atlanta, Georgia 30332

FINAL REPORT

PROJECT NO. E-21-633

STUDY OF MULTIPLE HOLOGRAM RECORDING IN LITHIUM NIOBATE

by

T. K. Gaylord and W. R. Callen

RESEARCH CONTRACT NAS8-30246

1 October 1973 to 1 January 1976

Performed for

NATIONAL AERONAUTICS AND SPACE ADMINISTRATION
George C. Marshall Space Flight Center
Marshall Space Flight Center, Alabama 35812

ABSTRACT

The results of a number of theoretical and experimental studies relating to multiple hologram recording in lithium niobate are reported. The analysis of holographic gratings stored in lithium niobate has been extended to cover a more realistic range of physical situations. A new successful dynamic (feedback) theory for describing recording, non-destructive reading, erasure, enhancement, and angular sensitivity has been developed. In addition, the possible architectures of mass data storage systems have been studied.

TABLE OF CONTENTS

I. INTRODUCTION

The possibility of high capacity, fast, random access storage by using three-dimensional optical holographic techniques has been known for more than five years now. This goal, however, has proved to be somewhat elusive and not as straightforward as originally anticipated. Full scale, full capability systems have not been built because of a number of problems. These problems are being investigated at Georgia Tech to determine 1) if fundamental, inherent limitations exist that were previously unknown and 2) what constitutes a sufficiently complete understanding of volume holography in ferroelectrics to allow routine engineering development of workable systems.

It is a pleasure to report that no inherent limiting factors have been found to date. This is of paramount importance. Indeed, the second aspect--that of developing a sufficient understanding of three dimensional holography has shown itself to be an area where additional basic scientific research is needed. Research is being pursued to provide this needed understanding. This final report covers this aspect of our work for the last nine months.

II. ANALYSIS OF HOLOGRAMS STORED IN LITHIUM NIOBATE

The description of the formation of phase holograms in ferroelectric crystals is strongly dependent on the internal electric field. Amodei has derived expressions [1] for the electric field patterns generated through diffusion and through drift respectively, for plane-wave holograms for the cases of the initial and the steady-state stages of holographic recording. We have greatly extended this model to cover the entire range of exposures in the formation of plane wave holograms. This is accomplished by a numerical approach, with both diffusion and drift of charge carriers included. The results of this approach reduce to the existing analytic expressions [1] for the electric field for the limiting cases of the initial and the final steady-state stages of hologram formation. Since analytic expressions for the electric field pattern, in general, cannot be obtained in the intermediate stages of holographic recording, the numerical approach permits the establishment of the limits of validity for the analytic expressions in terms of exposures and material parameters.

A corresponding problem is the determination of the refractive index profile of thick phase gratings in linear electro-optic crystals. In these materials, a sinusoidal light intensity pattern does not necessarily produce a sinusoidal change in the index of refraction or a change that is in phase with the recording intensity pattern. Depending on the crystals, the details of exposure, and the physical mechanisms in the process of hologram recording, different grating

profiles and different spatial phase shifts may be generated. Therefore, in the study of microscopic physical processes in these optically-induced phase gratings, a knowledge of the resulting gratings is of fundamental importance.

We have developed a method for determining the grating profile of thick gratings in linear electro-optic crystals. This method also determines the effective photovoltaic field and the relative contributions of diffusion and drift during hologram recording. The method requires only a knowledge of the modulation ratio during hologram recording and the fundamental and the higher-order diffraction efficiencies of the grating. Thus, simple external measurements reveal the microscopic internal properties.

Complete details of the work on the formation of phase holograms in ferroelectric crystals and on the determination of refractive index profile and physical processes can be found in References [2], [3], and [4], which are reproduced here for completeness.

Unified approach to the formation of phase holograms in ferroelectric crystals*

S. F. Su and T. K. Gaylord

School of Electrical Engineering, Georgia Institute of Technology, Atlanta, Georgia 30332
(Received 16 June 1975; in final form 2 September 1975)

The description of the formation of thick-phase holograms over the entire range of exposures has been accomplished using numerical methods. The internal electric field distributions (and thus the refractive-index profiles for linear electro-optic crystals) generated through diffusion and through drift of charge carriers are calculated. The treatment allows for the presence of an effective electric field due to the photovoltaic effect and an externally applied electric field. The results of this approach reduce to the existing analytic expressions for the limiting cases of the initial and the steady-state stages of hologram formation. This approach establishes the limits of validity for the analytic expressions in terms of exposure and material parameters.

PACS numbers: 42.30.N, 42.40.K, 78.20.J

I. INTRODUCTION

The recording of thick-phase holograms in ferroelectric crystals was first shown in lithium niobate by Chen *et al.*[1] The grating patterns of the holograms were optically induced refractive-index changes in the bulk material. Their work stimulated study of the theory of hologram formation in ferroelectrics. Three different models of the physical mechanisms have been proposed[2–4] to explain the phenomenon of this optically induced refractive-index change. Chen[2] explained the refractive-index change by drift of photoexcited carriers under the influence of an internal electric field. He assumed that there are electron traps in the material. Initially, some of the traps are filled (neutral charge state) and they provide electrons upon photoexcitation. The others are empty and they capture electrons. In addition, he assumed that there is an internal electric field in the direction opposite to that of the spontaneous polarization. The photoexcited electrons drift toward the positive side of the field (or the spontaneous polarization) leaving behind positive charges of ionized trap centers. The photoexcited charges will be retrapped and reexcited out of the traps until they finally drift out of the illuminated region and are trapped. Therefore, a space-charge field is created between the positive ionized centers and the trapped negative charges. This space-charge field causes the spatial variation of the refractive index via the linear electro-optic effect of the sample. The need for an internal field in Chen's model was removed by Glass *et al.*[5] by introducing the concept of a high-field photoeffect. They found that the current inside the crystal is due to a bulk photovoltaic effect and not due to internal fields.

Johnston[3] proposed a light-generated polarization pattern to explain the variation of the refractive index. In his model, an extremely high density of free electrons are required to generate the large field necessary to account for the variation of the refractive index.

Another model has been proposed by Amodei.[4] He has pointed out that charge migration by diffusion is an important factor in holographic recording for sufficiently small grating periods. He has shown that even in the absence of an internal field or an externally applied field, the photoexcited electrons still can migrate out of the illuminated region by thermal processes. Further, he has derived[6] expressions for the electric field patterns generated through diffusion and through drift, respectively, for plane-wave holograms for the cases of the initial and the steady-state stages of holographic recording.

Young *et al.*[7] have generalized Amodei's formulation by removing the assumption that the diffusion length is small compared to a grating period. This treatment applies only to the initial stage of hologram formation.

In this paper, Amodei's model is extended to cover the entire range of exposures in the formation of plane-wave holograms. This is accomplished by a numerical approach and both the diffusion and the drift of charge carriers are included. The electric field distributions generated through these two mechanisms are obtained. The results of this approach reduce to the existing analytic expressions[6] for the limiting cases of the initial and the final steady-state stages of hologram formation. Since analytic expressions for the electric field pattern, in general, cannot be obtained in the intermediate stages of holographic recording, the numerical approach permits the establishment of the limits of validity for the analytic expressions in terms of exposures and material parameters.

II. THEORY

Two plane waves of wavelength λ having angles of incidence upon the medium of $+\theta$ and $-\theta$ produce an interference pattern inside the medium of intensity $I(x)=I_0(1+m\cos Kx)$, where I_0 is the sum of the intensities (power per unit area transverse to the direction of energy flow) of the two waves, m is the modulation ratio $(0<m\leq 1)$, x is the direction perpendicular to the bisector of the angle between the beams, and $K=2\pi/L$, where $L=\lambda/2\sin\theta$. Staebler and Amodei[8] have shown for lithium niobate that the electric field patterns, which cause the spatial variation of the refractive index, are generated through both diffusion and drift of photogenerated free electrons (as opposed to holes). Thus the charge carriers will be assumed to be electrons. The method is equally applicable to holes, however. Assuming that the concentration of trapped electrons is sufficiently large so that its variation due to migration

is negligibly small and that the generation rate and trapping time are essentially unchanged during recording, then the concentration of free electrons excited to the conduction band is given by[6]

$$n(x) = \tau g_0(1 + m\cos Kx), \tag{1}$$

where τ is the lifetime of charge carriers and g_0, the generation rate, is given by[6]

$$g_0 = I_0\alpha/hf, \tag{2}$$

where α is the optical absorption coefficient, h is Planck's constant, and f is the light frequency. For an isotropic material (or if the x direction is along one of the crystallographic axes for an anisotropic material), the spatial distribution of the current density at any time is given by

$$J(x,t) = eD_n\frac{dn}{dx} + e\mu_n n[E_0' + E_{sc}(x,t)] + \kappa_1\alpha I, \tag{3}$$

where e is the magnitude of the electronic charge, D_n is the diffusion coefficient for electrons, μ_n is the mobility for electrons, E_0' is the externally applied field (if any), $E_{sc}(x,t)$ is the space-charge field, and κ_1 is a constant depending on the nature of the absorption center and wavelength.[5] The third term on the right-hand side of Eq. (3) represents the photovoltaic effect.[5] Using Eq. (1) and the definition of I, Eq. (3) can be rewritten as

$$J(x,t) = eD_n\frac{dn}{dx} + e\mu_n n[E_0 + E_{sc}(x,t)], \tag{4}$$

where

$$E_0 \equiv E_0' + \frac{\kappa_1\alpha I_0}{e\mu_n\tau g_0}. \tag{5}$$

The last term in Eq. (5) may be regarded as an effective field due to the photovoltaic effect. Using the Einstein relation, $\mu_n/D_n = e/kT$, where k is the Boltzmann constant and T is the absolute temperature, the current density, Eq. (4), can be rewritten as

$$J(x,t) = e\mu_n\left(\frac{kT}{e}\frac{dn}{dx} + n[E_0 + E_{sc}(x,t)]\right). \tag{6}$$

The accumulation rate of the space-charge density ρ at any point and at any time is given by the one-dimensional continuity equation,

$$\frac{\partial\rho(x,t)}{\partial t} = -\frac{\partial J(x,t)}{\partial x}. \tag{7}$$

Combining this with Poisson's equation gives

$$\frac{\partial E_{sc}(x,t)}{\partial x} = \frac{\rho(x,t)}{\epsilon} = -\frac{1}{\epsilon}\int_0^t \frac{\partial J(x,t')}{\partial x}\,dt', \tag{8}$$

where ϵ is the permittivity of the material. Equation (8) cannot be solved analytically except in the limiting case of the initial stage of hologram formation in which $E_{sc}(x,t)$ is neglected in the transport equation. Therefore, a numerical approach was employed to reveal the behavior of $E_{sc}(x,t)$ for the exposures in which $E_{sc}(x,t)$ cannot be neglected in the transport equation. The total space-charge field is $E_{sc}(x,t) \equiv E_{sc}'(x,t) + E_{sc}''(x,t)$, where $E_{sc}'(x,t)$ and $E_{sc}''(x,t)$ are the space-charge fields due to diffusion and drift, respectively. In order to obtain a better insight into the relative importance of diffusion and drift, these two mechanisms are considered separately as follows.

A. Diffusion only (no internal or externally applied field)

In this case, $E_0 = 0$ and $E_{sc}(x,t) = E_{sc}'(x,t)$, therefore Eq. (6) becomes

$$J(x,t) = e\mu_n\tau g_0 \times [-(kT/e)mK\sin Kx + (1 + m\cos Kx)E_{sc}'(x,t)]. \tag{9}$$

The exposure time t is set equal to $p\Delta t$, where p is any positive integer and Δt is a constant increment of the exposure time that is sufficiently small so that the variation of dJ/dx is negligible over the time interval Δt. Then, Eq. (8) reduces to a difference-differential equation,

$$\frac{dE_{sc}(x,p\Delta t)}{dx} = \frac{dE_{sc}(x,(p-1)\Delta t)}{dx} - \frac{1}{\epsilon}\frac{dJ(x,(p-1)\Delta t)}{dx}\Delta t. \tag{10}$$

Substituting Eq. (9) into Eq. (10) with E_{sc} replaced by E_{sc}', we obtain

$$\frac{dE_{sc}'(x,p\Delta t)}{dx} = \frac{dE_{sc}'(x,(p-1)\Delta t)}{dx} + \left(\frac{e\mu_n\tau g_0}{\epsilon}\right) \times\left[\left(\frac{kT}{e}\right)mK^2\cos Kx - (1 + m\cos Kx) \times\frac{dE_{sc}'(x,(p-1)\Delta t)}{dx} + mK\sin(Kx) \times E_{sc}'(x,(p-1)\Delta t)\right]\Delta t. \tag{11}$$

From Eq. (11), together with the boundary condition $E_{sc}'(0,t) = 0$ and the initial condition $\partial E_{sc}'(x,0)/\partial x = 0$, the space-charge field, $E_{sc}'(x,t)$, can be obtained by numerical integration.

B. Drift only (with large dc field)

In this case, there is a dc field that is sufficiently large so that the diffusion component of the current can be neglected compared with the drift component. Therefore, Eq. (6) becomes

$$J(x,t) = e\mu_n\tau g_0(1 + m\cos Kx)[E_0 + E_{sc}''(x,t)]. \tag{12}$$

Letting the exposure time t be equal to $p\Delta t$ and substituting Eq. (12) into Eq. (10) with E_{sc} replaced by E_{sc}'' gives

$$\frac{dE_{sc}''(x,p\Delta t)}{dx} = \frac{dE_{sc}''(x,(p-1)\Delta t)}{dx} + \left(\frac{e\mu_n\tau g_0}{\epsilon}\right) \times\left(mK\sin(Kx)[E_0 + E_{sc}''(x,(p-1)\Delta t)] - (1 + m\cos Kx)\frac{dE_{sc}''(x,(p-1)\Delta t)}{dx}\right)\Delta t. \tag{13}$$

Equation (13) is the difference-differential equation for drift. It can also be solved numerically for $E_0 + E_{sc}''$, provided that the boundary and the initial conditions are specified.

C. Diffusion and drift

When the electric field, E_0 (externally applied field plus effective photovoltaic field), is small such that

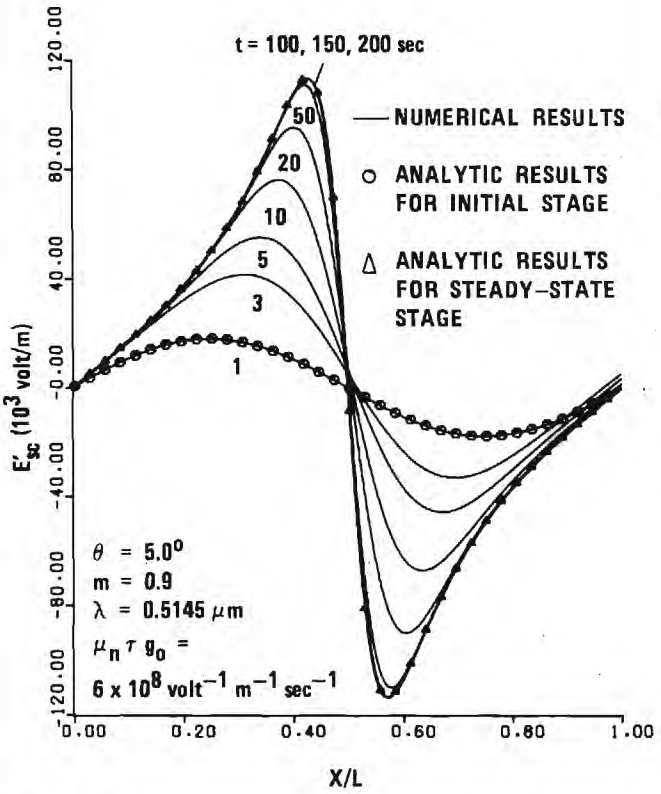

FIG. 1. One grating period of the calculated space-charge field, $E'_{sc}(x,t)$, produced by diffusion.

both the diffusion and drift components are present, the space-charge field is the superposition of the fields due to these two components. That is, $E_{sc}=E'_{sc}+E''_{sc}$. Usually, when the electric field E_0 is several hundred thousand volts per meter, the space-charge field due to diffusion is very small compared with the space-charge field due to drift.

III. RESULTS AND DISCUSSION

Equations (11) and (13) were numerically solved by use of the Runge-Kutta method. As can be seen from these equations the controlling material parameter is $\mu_n\tau g_0/\epsilon$. The low-frequency permittivity ϵ is known for most ferroelectrics as a function of temperature and crystallographic direction. For lithium niobate at room temperature, a typical value is $\epsilon=30\epsilon_0$, where ϵ_0 is the permittivity of free space. Values for the parameters μ_n and τ are not accurately known. Photoconductivity data for doped lithium niobate[5] imply that the product $\mu_n\tau\approx 10^{-13}$ m^2/V (using $e\mu_n\tau\alpha/hf=1.4\times10^{-10}$ m/V^2 and $\alpha=3.8\times10^3$ m^{-1} from Ref. 5). The generation rate g_0 can vary over an extremely wide range depending on the doping and treatment of the sample as well as the intensity of the laser beams. A typical value of $g_0=6\times10^{22}$ m^{-3} sec^{-1} is chosen here and thus $\mu_n\tau g_0=6\times10^8$ V^{-1} m^{-1} sec^{-1} in this work. The exposure time increment Δt was 1 sec. The space-charge field distribution for diffusion is shown in Fig. 1. Figure 1 shows that for the initial stage of hologram formation (after a 1-sec exposure time in this case), the field distribution is sinusoidal. As the exposure increases, the amplitude of the space-charge field increases and the field distribution becomes nonsinusoidal, and the positions at which the field extrema occur are shifted. However, the field pattern retains odd symmetry at all stages of hologram formation. When the steady-state stage of hologram formation is reached (after about a 100-sec exposure), the amplitude and the distribution of the space-charge field pattern remain fixed and do not change with further exposure. For comparison, the results of the analytic solutions for the initial and the final steady-state stages of hologram formation are also shown in Fig. 1. The circles in Fig. 1 represent the results for the initial stage of hologram formation as obtained from the analytic expression[6]

$$E'_{sc}(x,t)=(1/\epsilon)kT\mu_n\tau g_0 mKt\sin Kx, \tag{14}$$

evaluated for an exposure time of 1 sec with $\mu_n\tau g_0=6\times10^8$ V^{-1} m^{-1} sec^{-1}. The triangles in Fig. 1 represent the results for the steady-state stage of hologram formation as obtained from the analytic expression[6]

$$E'_{sc}(x)=(kT/e)(mK\sin Kx)(1+m\cos Kx)^{-1}, \tag{15}$$

evaluated at room temperature. The comparison shows that the numerical results correctly reduce to the analytic results for the limiting cases. In addition, the limits of validity for Eqs. (14) and (15) are established by the numerical approach in terms of exposure and material parameters. For example, from Fig. 1, it is seen that Eq. (14) is valid when $t\leq 1$ sec and that Eq. (15) is valid when t is near or greater than 100 sec for the parameters used here. Figure 2 presents the behavior of the amplitude of the space-charge field as a function of exposure. The amplitude increases rapidly in the early stages of hologram formation. For $\mu_n\tau g_0$

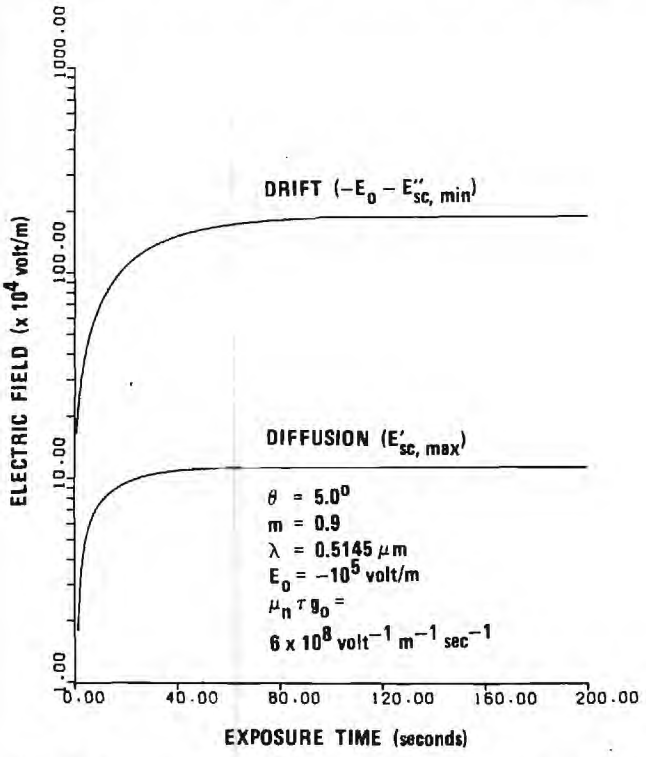

FIG. 2. Calculated values of the space-charge field amplitude produced by diffusion and by drift as a function of exposure time.

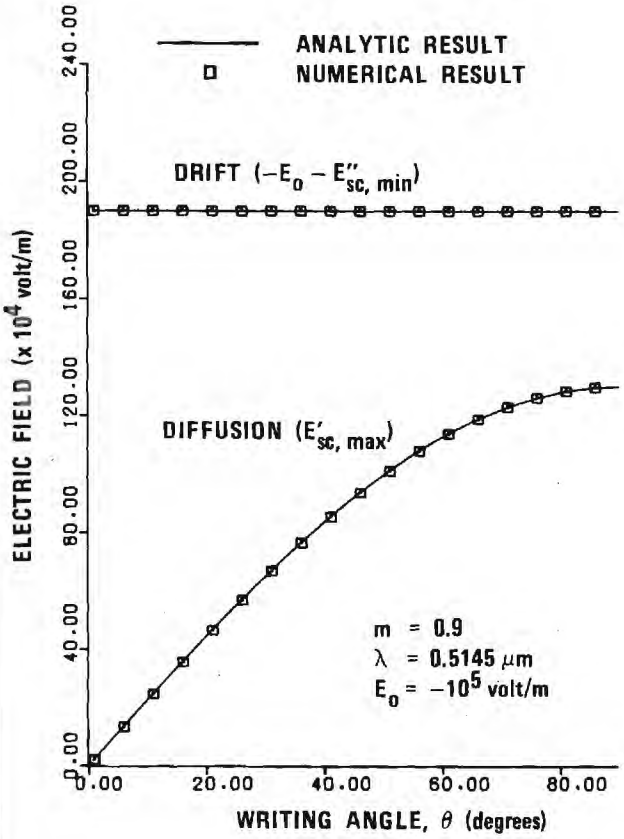

FIG. 3. Calculated steady-state final amplitude of the space-charge field produced by diffusion and by drift as a function of writing angle.

$= 6\times10^8$ $V^{-1}\,m^{-1}\,sec^{-1}$, the amplitude begins to saturate near 40 sec of exposure and finally remains unchanged after about 100 sec of exposure. Since the value of g_0 is proportional to I_0 as given by Eq. (2), the limits of validity of Eqs. (14) and (15) depend on I_0 for a given set of material parameters. Larger values of I_0 result in larger values of g_0 and, therefore, shorter exposure times are needed to reach any given exposure. In other words, the amplitude of the field saturates more rapidly for larger values of g_0. Equation (14), for the case of the initial stage of hologram formation, is valid as long as the space-charge field is negligible in the transport equation. Strictly speaking, the space-charge field cannot be neglected at any time except at the very beginning of hologram formation. In the numerical approach, the space-charge field is neglected in the transport equation only for an exposure time of Δt in duration from the beginning of hologram formation. In the calculation of the results here, Δt was chosen to be 1 sec. In fact, other values of Δt can be used, provided that the values of Δt are small enough to assure that there is no appreciable variation in dJ/dx over the time interval Δt. In addition to $\Delta t = 1.0$ sec, the calculations have been performed with $\Delta t = 0.5$ sec and the same resultant electric field patterns are obtained. In general, in order to maintain the same level of numerical accuracy, a smaller value of Δt must be used for a larger value of g_0 for given material parameters, writing angle, and beam modulation ratio.

Figure 3 presents the amplitude of the space-charge field as a function of writing angle in the steady-state stage of hologram formation. The squares in Fig. 3 represent the numerical results, while the solid curve represents the analytic solution. The field amplitude for diffusion increases as writing angle increases (grating period decreases). This is true for all stages of hologram formation though only the steady-state case is shown in Fig. 3. The space-charge field amplitude as a function of the modulation ratio m for the steady-state case is shown in Fig. 4. Again, the results of the numerical method and the analytic solution are represented by the squares and the solid curve, respectively. The field amplitude increases as the modulation ratio increases. This is also true for all other stages of hologram formation.

In the case of drift, the electric field at the boundary is not zero. It depends on the charge density at the surface and the applied voltage across the sample. The electric field at the boundary is assumed to be equal to the dc field E_0 at all times. The shape of the electric field pattern produced is independent of the value of the dc field E_0. The amplitude of the pattern, however, is dependent upon E_0, increasing with increasing E_0. The initial condition for drift is $\partial E''_{sc}(x, 0)/\partial x = 0$. Figure 5 shows the total electric field distribution when drift is dominant. The dc field E_0 is assumed to be -1.0×10^5 V/m. As for the diffusion case, the field distribution is sinusoidal at the initial stage of hologram formation. As exposure increases, the amplitude increases and the field distribution becomes nonsinusoidal and sharply

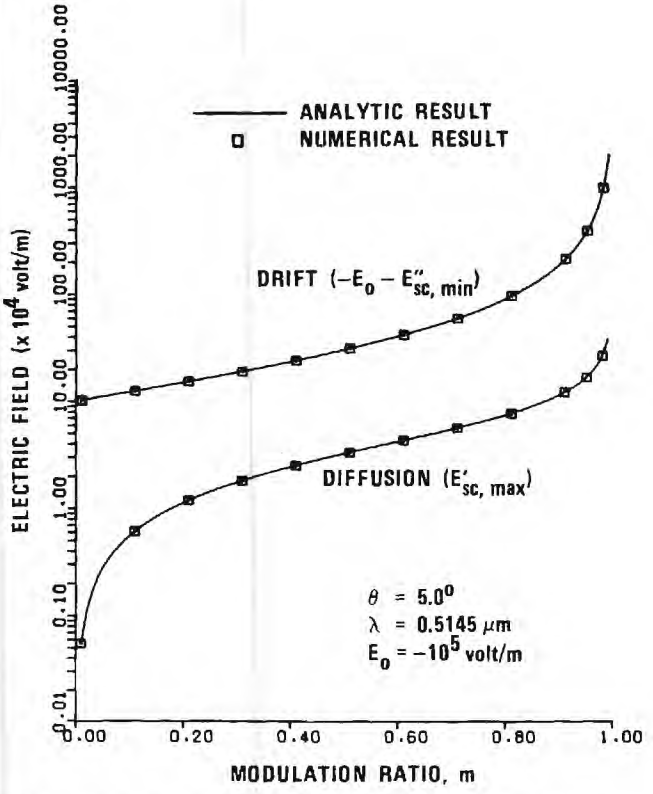

FIG. 4. Calculated steady-state final amplitude of the space-charge field produced by diffusion and by drift as a function of beam modulation ratio.

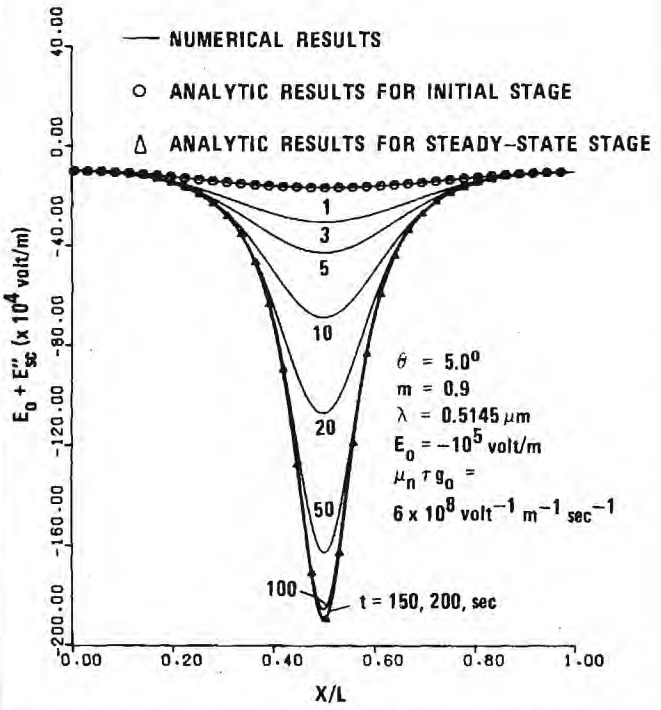

FIG. 5. One grating period of the calculated total electric field, $E(x,t) = E_0 + E''_{sc}(x,t)$, produced by drift.

peaked. However, the positions at which the field extrema occur do not shift with exposure. In addition, the field pattern has even symmetry at all times. Also shown in Fig. 5 are the analytic solutions for the electric field distribution at the initial and the steady-state stages of hologram formation. The same value for the electric field at the boundary has been used in these analytic solutions. The circles in Fig. 5 represent the results of the initial stage solution (proportional to $\cos Kx$). The triangles represent the steady-state solution [proportional to $(1+m)/(1+m\cos Kx)$]. The numerical results again correctly reduce to the analytic solutions in these limiting cases of the initial and the steady-state stages of hologram formation. From Fig. 5, it is observed that, for $\mu_n \tau g_0 = 6\times 10^8\ \mathrm{V^{-1}\,m^{-1}\,sec^{-1}}$, the analytic solutions are valid when t is equal to or less than 1 sec for the initial stage of hologram recording and when t is near or greater than 150 sec for the steady-state case. The behavior of the drift electric field amplitude as a function of exposure is also plotted in Fig. 2. The saturation time is about 150 sec for $\mu_n \tau g_0 = 6\times 10^8\ \mathrm{V^{-1}\,m^{-1}\,sec^{-1}}$, which is somewhat longer than that for the diffusion case. Figure 3 contains the steady-state drift electric field amplitude as a function of writing angle. It is observed that the amplitude does not change with the writing angle (and therefore grating period). This is also true for all other stages of hologram formation as well. In Fig. 4, the steady-state drift electric field amplitude as a function of the beam modulation ratio is plotted. It shows that only when the beam modulation ratio is greater than about 0.8 will an appreciable amplitude of the electric field be produced.

These results indicate the following distinctions between the electric field pattern produced by the diffusion mechanism and that produced by the drift mechanism:

(i) The electric field pattern due to diffusion has odd symmetry at all times, whereas the field pattern due to drift has even symmetry at all times.

(ii) For diffusion, the field amplitude increases as writing angle increases (decreasing grating period). For drift, the field amplitude is independent of the writing angle (and grating period).

(iii) The exposure time needed to reach steady state is somewhat longer for drift than for diffusion. In other words, the field due to diffusion saturates more rapidly than the field due to drift.

(iv) In the case of diffusion, the position for the maximum (and minimum) value of the electric field is a function of exposure. In the case of drift, the position for the field maximum (and minimum) remains fixed for all exposures.

(v) There is a 90.0° phase difference between the fundamental Fourier component of the electric field patterns for diffusion and drift for all exposures.

The analysis of this paper is applicable if holes instead of electrons were the charge carriers. For the case of hole charge carriers, the electric field pattern due to diffusion is the same as that produced by electrons except that it is reflected about the $x=0$ axis [$E'_{sc}(x,t)$ becomes $E'_{sc}(-x,t)$]. The electric field patterns due to drift are independent of the type of charge carriers.

The electric field (due to diffusion and/or drift) in ferroelectric lithium niobate causes a spatial modulation of the refractive index via the electro-optic effect. For lithium niobate, the electro-optic effect is linear (Pockels effect). Thus, the amplitude of the modulation of the refractive index is proportional to the magnitude of the electric field. Therefore, the refractive-index pattern caused by the electric field via the electro-optic effect is the same as the electric field pattern calculated here. It follows that the spatial distribution of the refractive index (grating shape) resulting from diffusion is different from that resulting from drift. Since different grating shapes produce different distributions of the higher-order diffraction efficiencies,[9] these higher-order diffraction efficiencies of a hologram grating produced by diffusion are different from those of a hologram grating produced by drift. This indicates the possibility that the physical mechanisms (diffusion and/or drift) that occur during the hologram formation may be determined by measuring the higher-order diffraction efficiencies of a hologram.

IV. CONCLUSIONS

The internal electric field patterns generated by diffusion and drift during hologram recording in ferroelectric crystals were obtained by numerically solving the appropriate difference-differential equations. Unlike previous analytic solutions, this method is applicable for all exposure times. These numerical results reduce to existing analytic results for the limiting cases of the initial and the final steady-state stages of hologram formation. For a given set of material parameters, the

limits of validity of the analytic solutions as well as further distinctions between diffusion and drift have been revealed.

Note added in proof. Calculations of the internal electric field distributions for all stages of hologram development have recently been made using analytical methods. A closed-form solution has been presented by G. A. Alphonse, R. C. Alig, D. L. Staebler, and W. Phillips [RCA Rev. **36**, 213 (1975)] using the assumption that their function G is equal to $e\mu_n \tau g_0 E_0/\epsilon$. Analytical results have also been obtained assuming $E_{sc}(0,t) = 0$ (as in the present work) by W. D. Cornish, M. G. Moharam, and L. Young (unpublished).

*Work supported by the National Science Foundation and by the National Aeronautics and Space Administration.

[1]F. S. Chen, J. T. LaMacchia, and D. B. Fraser, Appl. Phys. Lett. **13**, 223 (1968).
[2]F. S. Chen, J. Appl. Phys. **40**, 3389 (1969).
[3]W. D. Johnston, Jr., J. Appl. Phys. **41**, 3279 (1970).
[4]J. J. Amodei, Appl. Phys. Lett. **18**, 22 (1971).
[5]A. M. Glass, D. von der Linde, and T. J. Negran, Appl. Phys. Lett. **25**, 233 (1974).
[6]J. J. Amodei, RCA Rev. **32**, 185 (1971).
[7]L. Young, W. K. Y. Wong, M. L. W. Thewalt, and W. D. Cornish, Appl. Phys. Lett. **24**, 264 (1974).
[8]D. L. Staebler and J. J. Amodei, J. Appl. Phys. **43**, 1042 (1972).
[9]S. F. Su and T. K. Gaylord, J. Opt. Soc. Am. **65**, 59 (1975).

Determination of physical parameters and processes in hologram formation in ferroelectrics*

S. F. Su and T. K. Gaylord

School of Electrical Engineering, Georgia Institute of Technology, Atlanta, Georgia 30332
(Received 29 January 1976)

The material parameters and physical processes during hologram formation in ferroelectric crystals have previously been identified. Some methods (based largely on new diagnostic techniques) for evaluating these critical parameters and for quantifying the physical processes are summarized here.

PACS numbers: 42.40.Kw, 42.30.Nt, 78.20.Jq

A multitude of applications exist for volume (thick) holograms and gratings. The use of ferroelectric crystals such as lithium niobate for volume holographic recording was established by Chen, LaMacchia, and Fraser.[1] Since then there has been considerable experimentation and analysis involving these materials. The holographic diffraction efficiency has been shown to be very sensitive to the material parameters and the physical processes that are operative in these linear electro-optic materials. The physical processes, in turn, are largely dependent on the recording conditions. Some methods for evaluating the material parameters and quantifying the physical processes are summarized here.

The physical processes occurring during hologram recording are known to be diffusion and drift of electrons.[2,3] The resultant space-charge electric field modulates the index of refraction via the linear electro-optic effect. There may be an effective electric field due to the bulk photovoltaic effect[4] and/or an externally applied electric field during recording. A charge transport analysis[2,5-7] of the holographic recording process in these electro-optic crystals indicates that the controlling parameter is $e\mu_n\tau g_0 t/\epsilon$, where e is the magnitude of the electronic charge, μ_n is the electron mobility, τ is the electron lifetime, g_0 is the electron photogeneration rate, t is the exposure time, and ϵ is the low-frequency dielectric permittivity. The permittivity (a tensor) is well known for any given direction in most crystals. The exposure time t is externally controlled and is thus known. The unknown (and highly variable) factor is therefore $\mu_n\tau g_0$.

The product $\mu_n\tau g_0$ may be calculated via several methods. One method is by evaluation of the exposure parameter u. The exposure parameter, which is defined as $u \equiv \mu_n\tau g_0 t$, may be evaluated from a knowledge of the beam modulation ratio m during recording, the measured fundamental diffraction efficiency DE_1, and the higher-order diffraction efficiencies, DE_2, DE_3, etc. A detailed procedure for determining u is given in Ref. 8. Since the exposure duration t is known, the product $\mu_n\tau g_0$ is then determined by u/t. A second method to obtain the product $\mu_n\tau g_0$ is via a single-beam erasure experiment. The normal decay of the diffraction efficiency η of any hologram from its initial value η_0 under uniform illumination can be shown[5] to be

$$\sin^{-1}(\eta^{1/2})/\sin^{-1}(\eta_0^{1/2}) = \exp(-e\mu_n\tau g_0 t/\epsilon). \quad (1)$$

From measurements of η and η_0, the product $\mu_n\tau g_0$ may be obtained for known t. For small diffraction efficiencies, Eq. (1) reduces to $\eta = \eta_0 \exp(-2e\mu_n\tau g_0 t/\epsilon)$ as given in Ref. 5. A third method to evaluate $\mu_n\tau g_0$ is by measurement of the photoconductivity σ, since $\sigma = e\mu_n n = e\mu_n\tau g_0$, where n is the photogenerated electron concentration.

The photogeneration rate g_0 is proportional to the total intensity I_0 and the optical absorption coefficient α of the crystal. It is given by $g_0 = \alpha I_0/hf$, where h is Planck's constant and f is the optical frequency. Thus, g_0 may be determined from I_0, α, and f. It is difficult to evaluate μ_n and τ separately. The product $\mu_n\tau$ is frequently treated as a single parameter. If g_0 has been obtained, the product $\mu_n\tau$ may be determined using any one of the three methods mentioned previously.

The physical processes of diffusion and drift during hologram recording are conveniently quantified by giving the effective diffusion electric field E_D and the effective internal drift electric field E_0. The field E_D is given by $(kT/e)K$, where k is Boltzmann's constant, T is the absolute temperature during recording, and $K = 2\pi/L$, where L is the grating period. The field E_0 is the sum of an effective bulk photovoltaic field and the applied field (if any). The relative magnitudes of the effective fields are a measure of the relative contributions of diffusion and drift. Thus,

$$\%\ \text{diffusion} = [E_D/(E_D + |E_0|)] \times 100\%, \quad (2)$$

and

$$\%\ \text{drift} = [E_0/(E_D + |E_0|)] \times 100\%. \quad (3)$$

Usually K and T are known and, therefore, E_D can be easily calculated.

The value of E_0 may be evaluated several ways. From a knowledge of the beam modulation ratio during recording and the measured fundamental and higher-order diffraction efficiencies, the field E_0 can be determined.[8] The procedure involves first determining the exposure parameter u and then determining the Fourier components of the refractive-index profile. These Fourier components determine the grating profile. By a best fit of the analytical expression for the space-charge field, which is a function of u and E_0, to the grating profile, the value of E_0 may be determined.

The value of E_0 may also be evaluated via photocurrent measurements. It has been shown[4] that the effective photovoltaic electric field is given by

$$E_0 = \kappa_1 hf / e\mu_n \tau, \quad (4)$$

where κ_1 is a constant that is proportional to the induced photocurrent and is dependent on the impurity centers involved. For example, for iron-doped lithium niobate, Glass *et al.*[4] have found a value of κ_1 to be about 3.0×10^{-11} A m/W. From Eq. (4), E_0 may be evaluated from a knowledge of κ_1, f, and the product $\mu_n \tau$.

A third method for determining E_0 is by direct experimentation. The magnitude of an externally applied electric field (along the c axis) may be varied until the electric field is found that produces the minimum writing sensitivity. In this situation, it is assumed that the external electric field is cancelling the effective internal field E_0, and thus E_0 is equal in magnitude and opposite in direction to the applied field that yields minium sensitivity.

For small exposures which produce sinusoidal or nearly sinusoidal refractive index gratings, the physical processes of diffusion and drift may be quantified by evaluating the parameter ϕ_n, which is the spatial phase difference between the hologram-forming light interference pattern and the resulting refractive-index profile. The range of values for ϕ_n is from 0° (pure drift) to 90° (pure diffusion).[3] For a light interference pattern with a maximum at the coordinate system origin, diffusion contributes sine grating components and drift contributes cosine grating components. The value of the parameter ϕ_n is determined by the relative amplitudes of the fundamental sine grating and the fundamental cosine grating. Specifically, $\phi_n = |\tan^{-1}(n_{s_1}/n_{c_1})|$, where n_{s_1} and n_{c_1} are the fundamental sine and cosine components, respectively. These two quantities may be determined from m, DE_1, DE_2, etc.[8] Therefore, ϕ_n may also be quantified.

For illustration, a hologram was recorded in a 2.12-mm-thick 0.02-mole% iron-doped lithium-niobate crystal possessing an absorption coefficient of 0.37 m^{-1}. The hologram was written with a wavelength of 514.5 nm, a total intensity of 8.77 mW/mm^2, external angles of incidence of $\pm 5.00°$, a recording time of 187 sec, polarization in the plane of incidence, a modulation ratio of 0.994, and no applied electric field. For this case, it was determined by the methods summarized in this letter that $u = 4.74 \times 10^8$ V^{-1} m^{-1} (using $\epsilon = 30\epsilon_0$, where ϵ_0 is the permittivity for free space), $g_0 = 8.39 \times 10^{21}$ m^{-3} sec^{-1}, $\mu_n \tau = 3.04 \times 10^{-16}$ V^{-1} m^2, $E_D = 5.50 \times 10^4$ V m^{-1}, $E_0 = -1.06 \times 10^5$ V m^{-1}, $\phi_n = 27.3°$, % diffusion = 34%, and % drift = 66%. An external electric field during recording applied in the $+c$ or $-c$ directions was found, respectively, to subtract or to add to E_0. This changes the relative contributions of diffusion and drift. In addition, the diffraction efficiencies, the Fourier grating components, and ϕ_n also are changed by the application of an electric field during recording.

*Work supported by the National Science Foundation and by the National Aeronautics and Space Administration.

[1]F. S. Chen, J. T. LaMacchia, and D. B. Fraser, Appl. Phys. Lett. **13**, 223 (1968).
[2]J. J. Amodei, RCA Rev. **32**, 185 (1971).
[3]D. L. Staebler and J. J. Amodei, J. Appl. Phys. **43**, 1042 (1972).
[4]A. M. Glass, D. von der Linde, and T. J. Negran, Appl. Phys. Lett. **25**, 233 (1974).
[5]G. A. Alphonse, R. C. Alig, D. L. Staebler, and W. Phillips, RCA Rev. **36**, 213 (1975).
[6]W. D. Cornish, M. G. Moharam, and L. Young, J. Appl. Phys. (to be published).
[7]S. F. Su and T. K. Gaylord, J. Appl. Phys. **46**, 5208 (1975).
[8]S. F. Su and T. K. Gaylord, Appl. Opt. (to be published).

Applied Optics, vol. 15, no. 8, August 1976.

Refractive-Index Profile and Physical Process Determination in Thick Gratings in Electro-Optic Crystals*

S. F. Su and T. K. Gaylord

A method for determining the refractive index profile of thick phase gratings in linear electro-optic crystals is presented. This method also determines the effective photovoltaic electric field and the relative contributions of diffusion and drift during hologram recording. The method requires only a knowledge of the modulation ratio during hologram recording and the fundamental and the higher-order diffraction efficiencies of the grating. As an illustration of the method, the refractive index profile, the effective photovoltaic field, and the relative contributions of diffusion and drift are determined from experimental measurements for a lithium niobate holographic grating.

The authors are with the School of Electrical Engineering, Georgia Institute of Technology, Atlanta, Georgia 30332.

Received 28 February 1976.

I. Introduction

Volume (thick) holographic gratings have numerous applications. They can be used as highly efficient diffraction gratings, narrow band spectral filters, thick grating optical components such as lenses, imaging systems capable of spectral resolution of extended objects, and as a variety of components in integrated optics. The materials used for recording volume holograms, in general, exhibit light-induced changes in refractive index (photorefractive effect) or changes in optical absorption or both. Photorefractive materials include linear electro-optic crystals such as lithium niobate. In these materials, a sinusoidal light intensity pattern does not necessarily produce a sinusoidal change in the index of refraction or a change that is in phase with the recording intensity pattern. Depending on the crystals, the details of exposure, and the physical mechanisms in the process of hologram recording, different grating profiles and different spatial phase shifts may be generated.[1-4] Therefore, in the study of microscopic physical processes in these optically-induced phase gratings, a knowledge of the resultant gratings is of fundamental importance.

In this paper, a method for determining the grating profile of thick gratings in linear electro-optic crystals is presented. This method also determines the effective photovoltaic field and the relative contributions of diffusion and drift during hologram recording. The method requires only a knowledge of the modulation ratio during hologram recording and the fundamental and the higher-order diffraction efficiencies of the grating. Thus, simple external measurements reveal the microscopic internal properties.

To test the calculational accuracy of the method, the refractive index profiles of thick gratings are determined from the calculated diffraction efficiency data for some known grating profiles. Comparison of the determined profiles to the original profiles verifies that the method is very accurate. Further, as an illustration of the method, the refractive index profile, the

effective photovoltaic field, and the relative contributions of diffusion and drift are determined from experimental measurements for a lithium niobate holographic grating.

II. The Model

The geometry used for a thick optically-induced grating is presented in Fig. 1. The +x direction is chosen to coincide with the +c axis direction of the crystal and is in the plane of incidence and parallel to the surfaces of the crystal, the y axis is perpendicular to the page, and the z axis is perpendicular to the surfaces of the crystal. The crystal is assumed to be lossless and the grating is assumed to be pure phase grating. The light intensity producing the grating is the sinusoidal interference pattern produced by the intersection of two plane waves and is given by

$$I(x) = I_o (1 + M \cos Kx), \tag{1}$$

where I_o is the sum of the intensities of the two waves, $K = 2\pi/L$, L is the grating period given by $L = \lambda/2\sin\theta$, λ is the free space wavelength of the writing beams, θ is the angle of incidence, and M is the modulation ratio. The physical processes through which the grating is generated are known to be diffusion and drift of photoexcited electrons.[5] Also, an externally applied electric field and/or an effective photovoltaic field[6] may exist during the process of hologram recording. The grating profile inside the crystal is periodic (but not necessarily sinusoidal) in the x direction. For simplicity, the grating is assumed to be uniform in the z direction.

III. Determination of the Refractive Index Profile

A. Theoretical Analysis

The space-charge electric field patterns, and therefore the grating profiles, generated through diffusion and drift of electrons can be obtained for any given wavelength, exposure, material parameters, and geometrical

configuration either by analytical methods,[2,3] or by numerical methods.[4] An analytical expression for the space-charge field patterns can be shown to be

$$E_{sc}(x,t) = [(kT/e)\,MK \sin Kx + M E_o (1 - \cos Kx)]\,(1 + M \cos Kx)^{-1}$$
$$\times \{1 - \exp[(-e\mu_n \tau g_o t/\epsilon)(1 + M \cos Kx)]\}, \qquad (2)$$

where k is Boltzmann's constant, T is the absolute temperature, e is the magnitude of the electronic charge, μ_n is the electron mobility, τ is the lifetime of the photoexcited electrons, g_o is the electron photo-generation rate, t is the exposure time, ϵ is the permittivity of the crystal, and E_o is the effective electric field during hologram recording, which is the sum of the effective photovoltaic field and an externally applied field (if any). When multiplied by an appropriate electro-optic coefficient, Eq. (2) becomes a general expression for the grating profiles. The term containing sin Kx in Eq. (2) is due to diffusion and the term containing (1 - cos Kx) is due to drift. From Eq. (2), it is seen that, for a given wavelength and geometrical configuration in holographic recording, the controlling parameters are E_o and $\mu_n \tau g_o t/\epsilon$. The permittivity (a tensor) is well known for any given direction in most crystals. The exposure time t is externally controlled and is thus also known. Without accurate measurements of the material parameters in advance, the values of E_o and $\mu_n \tau g_o$ are usually not known during the process of holographic recording. Therefore, with E_o and $\mu_n \tau g_o$ unknown, Eq. (2) does not represent any particular grating profile but a family of grating profiles. However, Eq. (2) contains information about the allowed profiles. From Eq. (2), it is seen that the grating profiles generated through diffusion of electrons have odd symmetry with respect to x = 0 (intensity maximum during recording) and can be represented by a sine series. Likewise, the grating profiles generated through drift have even symmetry with respect to x = 0 and can be represented by a cosine series. The refractive index modulation amplitude,

which is proportional to $E_{sc}(x)$ at any time, is periodic and can be written as a Fourier series

$$\Delta n(x) \equiv n(x) - n_o = \sum_{h=1}^{\infty} [n_{sh} \sin(hKx) + n_{ch} \cos(hKx)], \qquad (3)$$

where $n(x)$ is the grating refractive index profile, n_o is the average value of $n(x)$, and n_{sh} and n_{ch} are the amplitudes of higher-order harmonic gratings due to diffusion and drift, respectively. The subscripts s, c, and h denote the quantities associated with the sine gratings, the cosine gratings, and the h th-harmonic grating, respectively. By use of Eq. (2), it can easily be shown that the higher-order harmonic gratings, n_{sh} and n_{ch}, can be expressed in terms of their corresponding fundamental gratings as

$$n_{sh} = n_{s1} f_{sh} = n_{s1} \int_0^{2\pi} g_1(v) \sin(hv)\, dv \Big/ \int_0^{2\pi} g_1(v) \sin v\, dv, \qquad (4)$$

and

$$n_{ch} = n_{c1} f_{ch} = n_{c1} \int_0^{2\pi} g_2(v) \cos(hv)\, dv \Big/ \int_0^{2\pi} g_2(v) \cos v\, dv, \qquad (5)$$

where

$$g_1(v) = \sin v\,(1 + M \cos v)^{-1}\{1 - \exp[(-eu/\epsilon)(1 + M \cos v)]\}, \qquad (6)$$

and

$$g_2(v) = (1 - \cos v)(1 + M \cos v)^{-1}\{1 - \exp[(-eu/\epsilon)(1 + M \cos v)]\}, \qquad (7)$$

where $u \equiv \mu_n \tau g_o t$ and $v \equiv Kx$. From Eqs. (4) through (7), it is observed that f_{sh} and f_{ch} are independent of E_o and K. They are functions of M and u only. That is, for a given value of M, $f_{sh} = f_{sh}(u)$ and $f_{ch} = f_{ch}(u)$. Using this property and the expression for diffraction efficiency,[7] the grating profile of a thick grating can be determined.

B. The Method

By the method of Ref. 7, the m th-order diffraction efficiency for an E mode incident wave (wave polarized in plane of incident) of free space wavelength λ' at the m th-order Bragg angle θ_m can be shown to be

$$DE_m = \sin^2\left(\left\{\left[\sum_h^m \left(\frac{L^{(m_h-1)}}{(m_h-1)!\,(h)^{(m_h-1)}}\right)^2 \left(\frac{\{[(n_{sh})^2 + (n_{ch})^2]^{\frac{1}{2}}\}^{m_h}}{(\lambda')^{(2m_h-1)}}\right)\right.\right.$$

$$\times (n_o)^{(m_h-1)} \cos[m_h \tan^{-1}(n_{sh}/n_{ch})]\Big]^2 + \left[\sum_h^m \left(\frac{L^{(m_h-1)}}{(m_h-1)!\,(h)^{(m_h-1)}}\right)^2\right.$$

$$\left.\left.\times \left(\frac{\{[(n_{sh})^2 + (n_{ch})^2]^{\frac{1}{2}}\}^{m_h}}{(\lambda')^{(2m_h-1)}}\right) (n_o)^{(m_h-1)} \sin[m_h \tan^{-1}(n_{sh}/n_{ch})]\right]^2\right\}^{\frac{1}{2}}$$

$$\left.\times \frac{\pi d \cos(2\theta_m)}{\cos\varphi_m}\right), \qquad (8)$$

where φ_m is the refraction angle given by $\varphi_m = \sin^{-1}[(\sin\theta_m)/n_o]$ and m_h is an integer representing the m_h th mode (with respect to the h th-harmonic grating) excited due to the h th-harmonic grating. The symbol $\sum_h^m$ denotes the summation over all of the values of h that divide evenly into the integer m. A detailed discussion of the relationships among the integers m, h, and m_h is given in Ref. 7 for both exact Bragg conditions and nearly exact Bragg conditions. The quantities n_o, λ', θ_m, and DE_m (m = 1, 2, 3, $\cdots$) are now given and the Fourier components n_{sh} and n_{ch} (h = 1, 2, 3, $\cdots$) are the quantities to be determined. The grating period, if not given, can be obtained by $L = \lambda'/2\sin\theta_1$.

From Eq. (8), the first- and second-order diffraction efficiencies are

$$DE_1 = \sin^2\{[(n_{s1})^2 + (n_{c1})^2]^{\frac{1}{2}} \pi d \cos(2\theta_1)/(\lambda' \cos\varphi_1)\}, \qquad (9)$$

and

$$DE_2 = \sin^2\Big[\Big(\{L^2 n_o[(n_{c1})^2 - (n_{s1})^2]/(\lambda')^2 + n_{c2}\}^2 + [2L^2 n_o n_{s1} n_{c1} /(\lambda')^2 + n_{s2}]^2\Big)^{\frac{1}{2}} \pi d \cos(2\theta_2)/(\lambda' \cos\varphi_2)\Big]. \quad (10)$$

Substituting Eqs. (4) and (5) into Eq. (10) with h = 2 gives

$$DE_2 = \sin^2\Big[\Big(\{L^2 n_o[(n_{c1})^2 - (n_{s1})^2]/(\lambda')^2 + n_{c1} f_{c2}\}^2 + [2L^2 n_o n_{s1} n_{c1} /(\lambda')^2 + n_{s1} f_{s2}]^2\Big)^{\frac{1}{2}} \pi d \cos(2\theta_2)/(\lambda' \cos\varphi_2)\Big] . \quad (11)$$

Since the values of f_{s2} and f_{c2} can be calculated for any given value of u via Eqs. (4) and (5), n_{s1} and n_{c1} can be obtained for the same value of u by solving Eqs. (9) and (11) simultaneously. Thus, solving Eqs. (9) and (11) using a particular value of u, say u_1, we get a pair of solutions denoted by $n_{s1}(u_1)$ and $n_{c1}(u_1)$. The signs of $n_{s1}(u_1)$ and $n_{c1}(u_1)$ must be carefully chosen.[8,9] Once $n_{s1}(u_1)$ and $n_{c1}(u_1)$ are obtained, the corresponding higher-order Fourier components, $n_{sh}(u_1)$ and $n_{ch}(u_1)$, h = 2, 3, ···, can be obtained by Eqs. (4) and (5). With this set of Fourier components, the corresponding set of higher-order diffraction efficiencies $[DE_m(u_1)$, m = 3,4, ···] are calculated. This entire process [starting from solving Eqs. (9) and (11)] is then repeated for other values of u. Using numerical techniques, a search is made for the particular u, say u_p, that gives the calculated higher-order diffraction efficiencies best matching the initially given values. The corresponding Fourier components $n_{sh}(u_p)$ and $n_{ch}(u_p)$, h = 1, 2, 3, ···, are the solutions desired, and the refractive index profile is obtained by inserting $n_{sh}(u_p)$ and $n_{ch}(u_p)$ into Eq. (3).

C. Calculational Accuracy of the Method

The method was numerically implemented and tested by determining the

Fourier components of three typical gratings from the calculated diffraction efficiencies [using Eq. (8)] of these gratings. The first few orders of the Fourier components of the refractive index profile of these gratings are listed in the "original" rows in Table I. The diffraction efficiencies of these gratings are calculated with $\lambda' = 514.5$ nm. With these diffraction efficiency data, the Fourier components of the refractive index profile of the gratings are then determined using the foregoing method. The Fourier components determined are listed in the "calculated" rows in Table I. From Table I, it is seen that the method yields excellent numerical accuracy. Other reading wavelengths ($\lambda' = 488.0$ nm and $\lambda' = 632.8$ nm) have also been used to perform these calculations and similar results were obtained. This shows that the reading wavelength λ' used in the method does not necessarily have to be equal to the writing wavelength λ and that the refractive index profile determined is independent of the reading wavelength.

D. Effect of Diffraction Efficiency Errors

In practice, the diffraction efficiencies are measured values, and therefore, some experimental error is unavoidable. These experimental errors will affect the refractive index profile determined by the method. However, if the errors are small, a reasonably accurate grating profile can still be obtained. This is illustrated in Fig. 2. The central curve in Fig. 2 represents the actual profile of a grating. The other curves in Fig. 2 represent the grating profiles determined from diffraction efficiencies which are 5% higher and 5% lower than those corresponding to the actual profile. From Fig. 2, it is observed that a several percent systematic error in the diffraction efficiencies results in a small change in the grating profile determined by the method. In addition to the grating profile presented in Fig. 2, other grating profiles produced with smaller exposure parameters have also been

analyzed. It is found that the error in the grating profile decreases with decreasing exposure parameters. If, instead of a systematic error, a random error of the same standard deviation is present, the determined profile similarly approximates the actual profile.

E. Effect of Boundary Reflections

The effect of boundary reflections was not included in the foregoing analysis. To include this, the measured diffraction efficiency at each Bragg angle must be corrected by dividing by the appropriate transmittance factor τ_m. When the surfaces of the grating are perfectly flat and perfectly parallel, this transmittance factor for the m th-order diffraction is given by[10]

$$\tau_m = (1 - R_m)^2[1 + 2R_m\cos(2\beta_m d) + (R_m)^2]/\{[1 - (R_m)^2]^2 + 4(R_m)^2 \times [\cos^2(2\nu_m d) + \cos^2(2\beta_m d)] - 4R_m[1 + (R_m)^2]\cos(2\nu_m d)\cos(2\beta_m d)\}, \quad (12)$$

where $R_m = \tan^2(\theta_m - \varphi_m)/\tan^2(\theta_m + \varphi_m)$, $\beta_m = 2\pi n_o(\cos\varphi_m)/\lambda'$, and $\nu_m d$ is the argument of the sine squared function in Eq. (8). In most practical cases, the surfaces of the grating are neither perfectly flat nor perfectly parallel. If the cosine factors in Eq. (12) average to zero due to variations in thickness over the illuminated region, the transmittance factor reduces to $\tau_m = (1 - R_m)^2/[1 + (R_m)^2]$.

IV. Determination of Effective Photovoltaic Field and Physical Processes

It has been shown in the preceding section that the refractive index profile of a grating in a linear electro-optic crystal can be determined by knowing the modulation ratio during hologram recording and the fundamental and the higher-order diffraction efficiencies of the grating. The information from Eq. (2) used in determining the grating profile was independent of the effective electric field E_o. Therefore, the value of E_o can be obtained by

a best fit of Eq. (2) to the grating profile determined by the method in the preceding section. The effective photovoltaic field can thus be obtained by subtracting the externally applied field (if any) from E_o.

The physical processes of diffusion and drift during hologram recording are conveniently quantified by the effective diffusion electric field E_D, which is given by $(kT/e)K$, and the effective electric field E_o. The relative magnitudes of the effective fields are a measure of the relative contributions of diffusion and drift. Thus,

$$(\% \text{ diffusion}) = [E_D/(E_D + |E_o|)] \times 100\%, \tag{13}$$

and

$$(\% \text{ drift}) = [|E_o|/(E_D + |E_o|)] \times 100\%. \tag{14}$$

V. Experimental Results

For illustration, the refractive index profile of a lithium niobate holographic grating is determined from measurements of its fundamental and higher-order diffraction efficiencies. The holographic grating was recorded in a 2.12-mm-thick 0.02-mole% Fe-doped lithium niobate crystal with the grating vector parallel to the c axis of the crystal. The hologram was written with a wavelength of 514.5 nm, a total power density of 8.77 mW/mm^2, external writing angles of $\pm$ 5.00°, a writing time of 187 sec, polarization in the plane of incidence, a modulation ratio of 0.994, and no externally applied field. The diffraction efficiencies were measured with a low power He-Ne laser (λ' = 632.8 nm). The measured diffraction efficiencies were DE_1 = 21.6%, $DE_2 = 8.64 \times 10^{-2}$%, and $DE_3 = 7.74 \times 10^{-3}$%. When corrected by their corresponding transmittance factors, the diffraction efficiencies became DE_1 = 29.7%, DE_2 = 0.123%, and $DE_3 = 1.08 \times 10^{-2}$%. These corrected diffraction efficiencies were then used in the method to determine the refractive index profile of the grating. The

exposure parameter for this grating was found to be $u_p = 4.74 \times 10^8$ $V^{-1}m^{-1}$ for $\epsilon = 30\epsilon_o$, where ϵ_o is the permittivity for free space. The resultant refractive index profile is shown in Fig. 3. This particular grating profile is nearly sinusoidal due to the relatively small exposure. By fitting Eq. (2) to the profile in Fig. 3, it was found that the effective electric field during hologram recording was $E_o = -1.06 \times 10^5$ V/m (in -c direction). This value is larger than the values reported by Cornish et al.[2] but smaller than the values reported by Glass et al.[6] The value of E_D was found to be 5.5×10^4 V/m. Thus, (% diffusion) = 34% and (% drift) = 66% for this particular grating.

For small exposures which produce sinusoidal or nearly sinusoidal refractive index gratings, the physical processes of diffusion and drift may be quantified by evaluating the parameter ϕ_n, which is the spatial phase difference between the hologram-forming light interference pattern and the resulting refractive index profile. The range of values for ϕ_n is from 0° (pure drift) to 90° (pure diffusion).[5] For a light interference pattern with a maximum at the coordinate system origin, diffusion contributes sine grating components and drift contributes cosine grating components. The value of the parameter ϕ_n is determined by the relative amplitudes of the fundamental sine grating and the fundamental cosine grating. Specifically, $\phi_n = |\tan^{-1}(n_{s1}/n_{c1})|$, where n_{s1} and n_{c1} are the fundamental sine and cosine components, respectively. For this experimental case it was found that $\phi_n = 27.3^\circ$.

Determinations of the grating profile and physical processes have also been performed for gratings recorded in an applied electric field. An external field during recording applied in the +c or -c axis directions of the crystal was found respectively to decrease or to increase E_o and thus to decrease or to increase the relative contribution of drift. The relative drift contribution has been experimentally altered by an external field from essentially 0% to nearly 100%.

VI. Discussion

Because the incident angle of the reading beam can not exceed 90.0°, the number of higher-order Bragg angles available is limited to the integer that is nearest to, but less than $2L/\lambda'$. If a suitably short wavelength source is available, the accessibility of higher-order Bragg angles is assured. However, the higher-order diffraction efficiencies are often small and thus the first three or so orders of the diffraction efficiency are usually sufficient.

The method presented in this paper can also be applied to the case in which the reading beam is polarized perpendicular to the plane of incidence (H mode). It can be shown straightforwardly that the grating profiles determined are independent of the polarization of the reading beam.

The phenomenon of birefringence must, in principle, also be taken into account. Here, the refractive index is a function of the angle of incidence, and therefore, the appropriate value for the average refractive index must be used in the foregoing formulations. However, for uniaxial crystals (such as lithium niobate), if the crystal is oriented in such a way that its optic axis is parallel to the x axis for the geometry used in this paper (Fig. 1), birefringence appears only in the case of E-mode polarization. In addition, since the amplitude of the spatial modulation of the refractive index would be 10^{-4} or smaller, the error in determining the grating profile is negligible due to the very small variations in the birefringence at different Bragg angles. For example, in the case of lithium niobate at $\lambda' = 514.5$ nm, changes in the amplitude of the fundamental grating do not exceed one tenth of one percent (using $n_0 = 2.337$ and $n_E = 2.243$, where n_0 and n_E are the principal indices of refraction for ordinary and extraordinary waves, respectively).

VII. Conclusions

A method for determining the refractive index profile, the effective

electric field, and the physical processes in optically-induced thick phase gratings in linear electro-optic crystals has been presented. This method utilizes a knowledge of the allowed family of grating profiles and a knowledge of the modulation ratio during hologram recording and the fundamental and the higher-order diffraction efficiencies of the grating. Thus, simple external measurements reveal the internal properties of the grating.

Acknowledgments

The authors would like to thank R. Magnusson for his help with the experimental measurements and L. Young for a prepublication copy of Ref. 2.

References

*Work supported by the National Science Foundation and by the National Aeronautics and Space Administration.

[1]J. J. Amodei, RCA Rev. 32, 185 (1971).

[2]W. D. Cornish, M. G. Moharam, and L. Young, J. Appl. Phys. 47, (1976) (in press).

[3]G. A. Alphonse, R. C. Alig, D. L. Staebler, and W. Phillips, RCA Rev. 36, 213 (1975).

[4]S. F. Su and T. K. Gaylord, J. Appl. Phys. 46, 5208 (1975).

[5]D. L. Staebler and J. J. Amodei, J. Appl. Phys. 43, 1042 (1972).

[6]A. M. Glass, D. von der Linde, and T. J. Negran, Appl. Phys. Lett. 25, 233 (1974).

[7]S. F. Su and T. K. Gaylord, J. Opt. Soc. Am. 65, 59 (1975).

[8]These, of course, depend on the physical propertities of the recording materials. For example, for lithium niobate, it can be shown[9] that negative signs must be chosen for both $n_{s1}(u_1)$ and $n_{c1}(u_1)$ when the +c axis of the crystal is directed in the +x reference direction, and that the positive sign for $n_{s1}(u_1)$ and negative sign for $n_{c1}(u_1)$ must be chosen when the +c axis is directed in the -x reference direction. No matter which direction (+x or -x) is chosen for the +c axis direction, the same refractive index profile in the lithium niobate crystal is obtained. This shows that there is no ambiguity in the solution.

[9]S. F. Su, Ph.D. thesis, Georgia Institute of Technology, 1976.

[10]H. Kogelnik, J. Opt. Soc. Am. 57, 431 (1967).

FIGURE CAPTIONS

Fig. 1 Geometry of thick grating showing recording beams. The spatial modulation of the refractive index is indicated by the line pattern.

Fig. 2 One grating period of the refractive index profile determined from diffraction efficiencies that are a) 5.0% too large and b) 5.0% too small compared to the actual profile.

Fig. 3 One grating period of the refractive index profile of a holographic grating recorded in a 2.12-mm-thick iron-doped lithium niobate crystal.

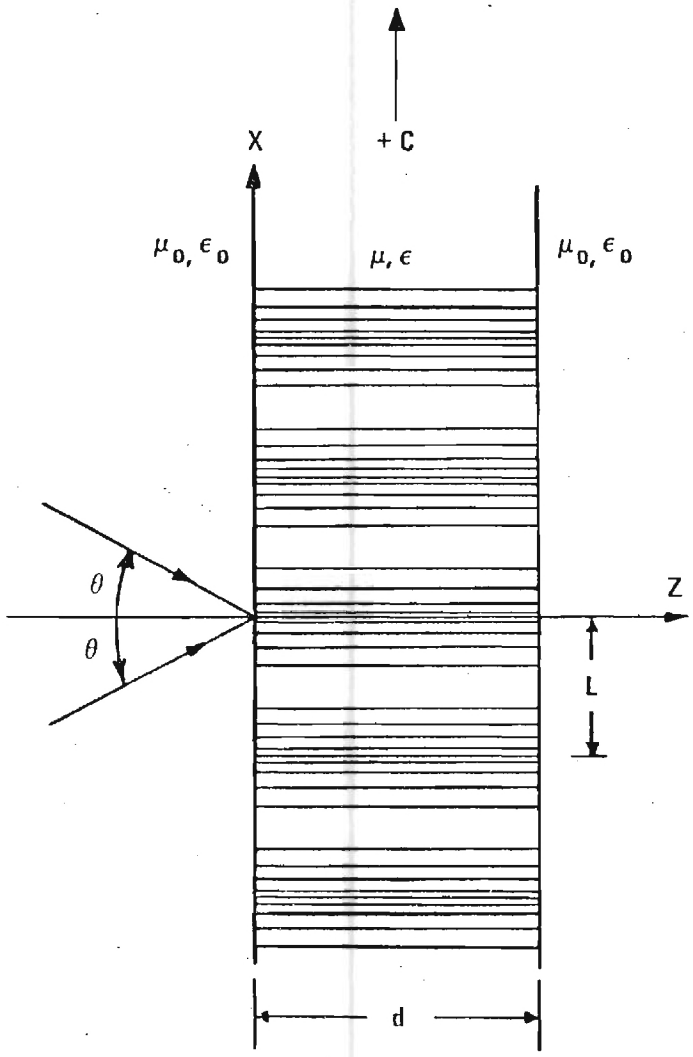

Fig. 1 Geometry of thick grating showing recording beams. The spatial modulation of the refractive index is indicated by the line pattern.

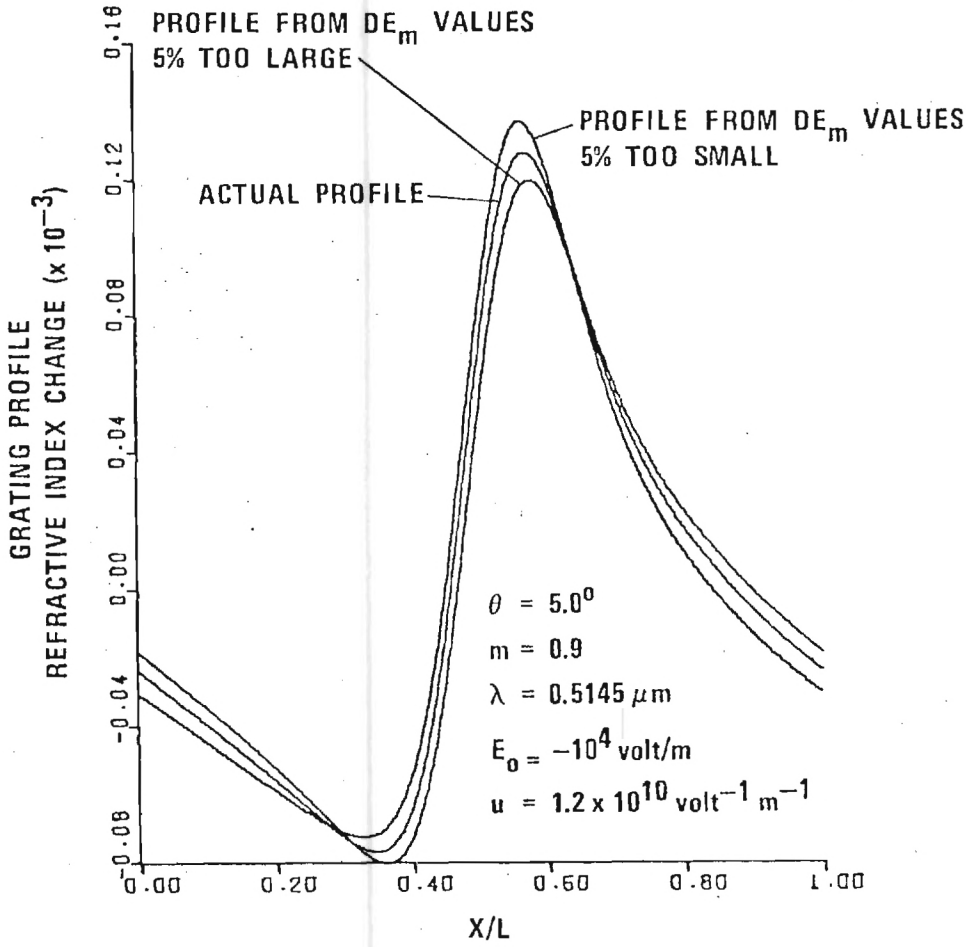

Fig. 2 One grating period of the refractive index profile determined from diffraction efficiencies that are a) 5.0% too large and b) 5.0% too small compared to the actual profile.

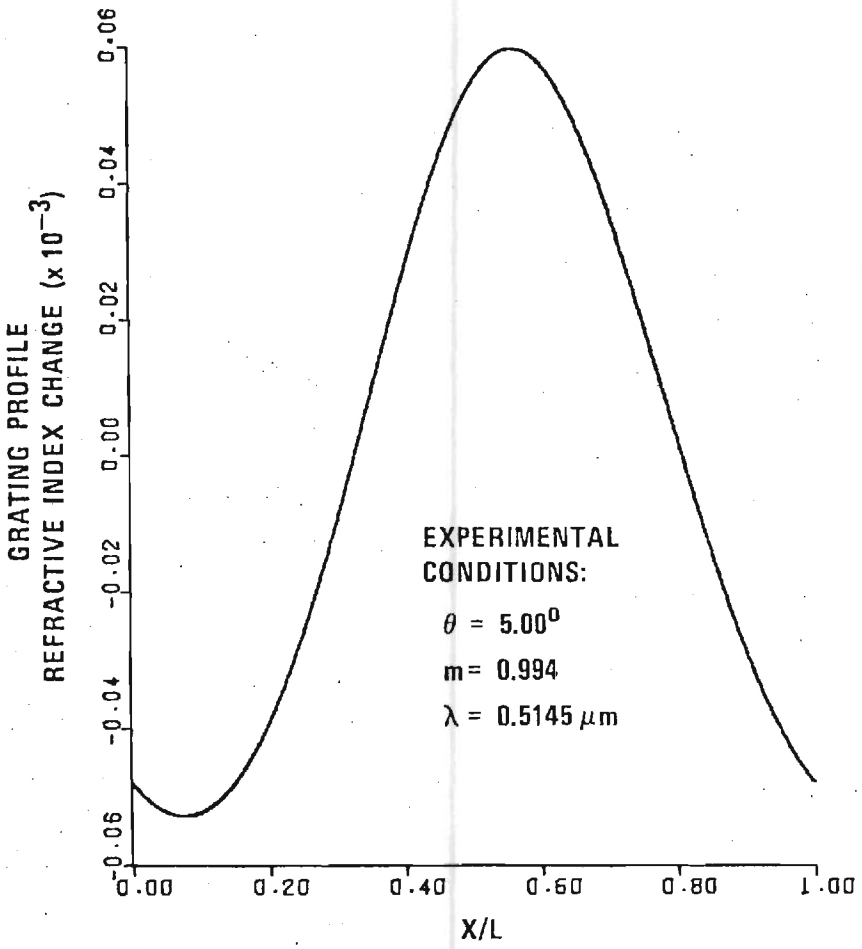

Fig. 3 One grating period of the refractive index profile of a holographic grating recorded in a 2.12-mm-thick iron-doped lithium niobate crystal.

TABLE I. Comparison of the original Fourier components and the calculated Fourier components of the gratings generated through diffusion of electrons, drift of electrons, and a combination of the two. The grating parameters are $n_o = 2.243$ and $L = 3.6303$ μm.

Physical mechanism		Refractive Index Fourier Component ($\times 10^{-5}$)									
		n_{c1}	n_{s1}	n_{c2}	n_{s2}	n_{c3}	n_{s3}	n_{c4}	n_{s4}	n_{c5}	n_{s5}
Diffusion	Original	0.000	-6.842	0.000	4.216	0.000	-2.566	0.000	1.536	0.000	-0.900
	Calculated	0.000	-6.842	0.000	4.216	0.000	-2.566	0.000	1.536	0.000	-0.899
Drift	Original	-4.997	0.000	2.988	0.000	-1.755	0.000	1.009	0.000	-0.566	0.000
	Calculated	-4.997	0.000	2.988	0.000	-1.755	0.000	1.009	0.000	-0.566	0.000
Diffusion & Drift	Original	-4.997	-6.842	2.988	4.216	-1.755	-2.566	1.009	1.536	-0.566	-0.900
	Calculated	-4.997	-6.842	2.988	4.216	-1.755	-2.566	1.009	1.536	-0.566	-0.899

III. DYNAMIC ANALYSIS OF THE RECORDING AND READING OF VOLUME HOLOGRAMS

Static diffraction characteristics of thick gratings have been analyzed by Burckhardt [5] by solving the exact electromagnetic boundary-value problem and by Kogelnik [6] by employing a coupled-wave theory. In these theories, the thick grating is assumed to exist already and is not affected by the reconstruction process. The grating is assumed to be uniform through the thickness of the material. Much experimentally observed behavior only can be explained by a dynamical theory that allows the interference of an incident light beam with its own diffracted beam inside the material. The results of the dynamical theory developed by Magnusson and Gaylord are included in Reference [7], which is reproduced on the following pages of this report.

Use of dynamic theory to describe experimental results from volume holography*

R. Magnusson and T. K. Gaylord

School of Electrical Engineering, Georgia Institute of Technology, Atlanta, Georgia 30332
(Received 1 July 1975)

The general applicability of dynamic theory to the description of the recording and readout characteristics of volume (thick) hologram gratings is indicated. In dynamic theory (as opposed to static theory), the volume nature of the thick holographic grating allows the interference of an incident light beam with its own diffracted beam inside the recording medium. This effect causes the continuous recording of another grating that alters the initial one, producing a resultant grating that is not uniform through the thickness of the recording material and a grating whose writing and reading characteristics may vary dramatically depending on the recording material and the experimental conditions. A large number of diverse types of writing, reading, and angular selectivity behavior have been reported in the published literature. The dynamic theory of thick hologram writing and reading is shown to predict qualitatively all of these various types of experimental behavior.

PACS numbers: 42.40.D, 42.30.N

I. INTRODUCTION

Thick gratings and thick holograms have numerous applications based on their properties of high diffraction efficiency,[1] wavelength selectivity,[1] angular selectivity,[1] and reduced noise.[2] Thick gratings may be used as highly efficient diffraction gratings, narrow-band spectral filters,[3] thick grating lenses,[4] imaging systems capable of spectral resolution of extended objects,[2] wave guides for surface waves,[5] frequency-selective grating reflectors for thin-film distributed feedback lasers,[6] thin-film waveguide couplers,[7,8] and as deflectors and modulators.[9] Thick (volume) holograms are of interest due to their use in high-capacity information storage,[10] color holography,[11] and in white light reconstruction of holograms.[12]

The static diffraction characteristics of a thick grating have been analyzed by Burckhardt[13] by solving the exact electromagnetic boundary-value problem and by Kogelnik[1] by employing a coupled-wave theory. In these theories, the thick grating is assumed to exist already (as opposed to analyzing the recording process); it is assumed to be uniform through the thickness of the material; and it is assumed to be unaffected by the reconstruction process. These theories have been applied successfully to a large number of experimental situations. There remain, however, numerous types of experimentally observed behavior that are not predicted with these static theories. These include certain writing effects, reading effects, and angular selectivity effects (to be discussed in this paper).

It has been recognized[14] that the volume nature of thick holograms permits the interference of an incident light beam with its own diffracted beam inside the recording medium. This effect causes the continuous recording of a new grating that may add to or subtract from the initial grating producing a resultant grating that is not uniform through the thickness of the material. As is shown in this paper, the explanation of the resulting characteristics, in general, requires a dynamical theory such as that developed by Ninomiya.[15]

Among the materials used for recording volume holograms are those that exhibit light-induced refractive-index changes (photorefractive materials), those that exhibit light-induced changes in optical absorption (photochromic materials), and those that exhibit both of these effects. Numerous recording materials exist in each of these categories.[16]

II. ANALYTICAL TECHNIQUES

The coupled-wave theory used here originated in acoustics.[17] This method has since been adapted to the analysis of volume holograms. Kogelnik[1] analyzed diffraction from sinusoidal hologram gratings and Su and Gaylord[18] analyzed nonsinusoidal gratings. These authors assumed the existence of a uniform grating through the thickness of the medium. Further, they assumed that the hologram grating can be addressed with a light beam without affecting the grating. Thus, these approaches are essentially static.

A more general approach, combining and extending the initial efforts of Kogelnik[1] and Kermisch,[19] has been presented by Ninomiya.[15] He included in the basic coupled-wave formalism, the dynamic behavior of holograms during recording and reading. That is, during recording, the development of the hologram continuously affects the diffraction process (feedback). Similarly, during reading, the incident beam is diffracted inside the medium and the resultant two beams interfere with each other producing changes which may either add to or subtract from the existing holographic grating.

There has been little study of the characteristics of hologram gratings that are not uniform in the direction perpendicular to the hologram surface. Kermisch[20] and Uchida[21] have theoretically analyzed the case of an exponentially attenuated grating, the latter using the coupled-wave approach. In the present work, nonuniformity is shown to occur for photorefractive materials as a result of the spatial phase difference (represented by ϕ_n) between the hologram-forming light interference pattern and the resulting index-of-refraction grating. Also, of course, an attenuated profile is produced if α_0, the average absorption coefficient of the material, is nonzero. It is found that the index profiles can have

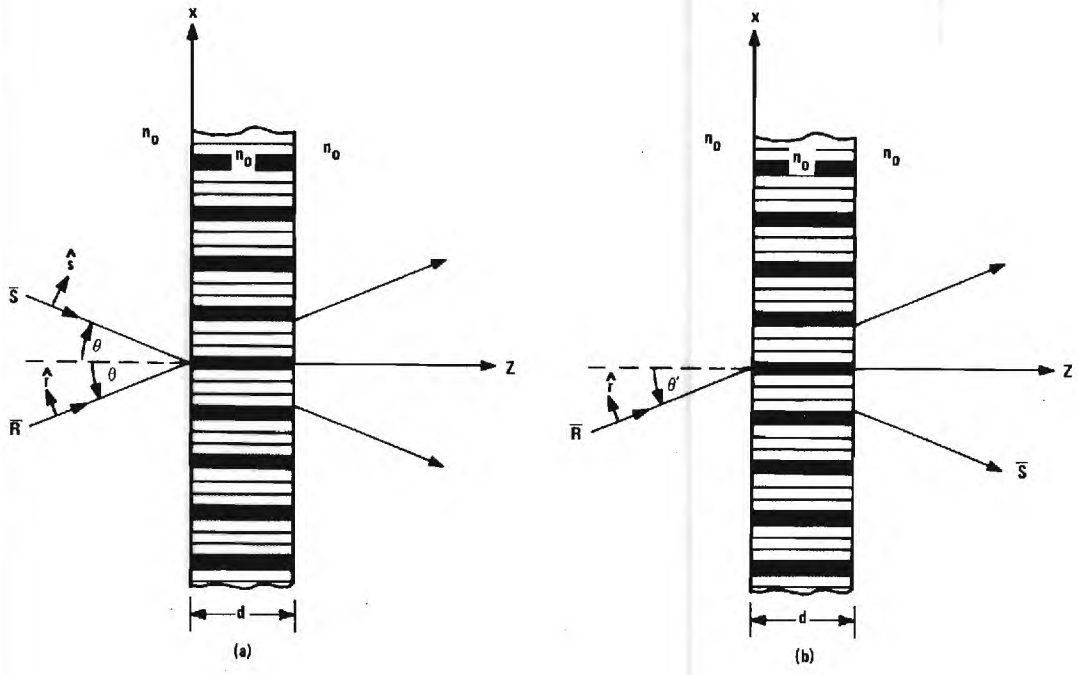

FIG. 1. Model for (a) hologram recording and (b) hologram reading.

many forms in addition to exponential. The above theories[1,15,18–21] have been presented without experimental results.

In this paper, the dynamical coupled-wave equations have been generalized to allow deviations in the angle of incidence and the wavelength, and are given for the *E*-mode polarization. These are then used to calculate the grating profiles and the writing, reading, and angular selectivity characteristics of unslanted phase volume holograms. Numerous types of experimental behavior cited in the literature as well as new experimental results presented here are shown to be predicted by the dynamical theory.

III. MODEL AND DYNAMIC THEORY

A. Model

The thick hologram gratings treated here are assumed to be recorded by the intersection of two coherent light waves in a thick photosensitive medium. They are read by a single wave incident upon the hologram. The recording and reading configurations are shown in Fig. 1. The signal and reference beams represented by the vectors $\mathbf{S}$ and $\mathbf{R}$, respectively, are taken to be infinite plane waves. They are polarized in the plane of incidence of the grating (*E* mode) with polarization vectors $\hat{\mathbf{s}}$ and $\hat{\mathbf{r}}$. The medium is unbounded in the x and y directions. It is to be noted that, during recording, the waves are symmetric in their angle of incidence and, therefore, the grating fringes are normal to the material surface (unslanted). The extension to slanted gratings is straightforward but little additional insight is gained. For convenience, it is assumed that the same average refractive index exists inside and outside the grating (this is a common simplification; see, e.g., Ref. 1) and thus no reflections or deviations occur.

B. Equations

Ninomiya[15] developed the dynamic coupled-wave equations that describe the writing, reading, and erasure of thick holograms for exact Bragg conditons and *H*-mode polarization ($\hat{\mathbf{s}} \| \hat{\mathbf{r}}$). Here the dynamical equations for *E*-mode polarization (electric field in the plane of incidence) are used because the available experimental data are primarily for the *E*-mode configuration. In addition, the equations have been generalized to permit deviations in the incident angle from the writing angle and deviations in the wavelength from the writing wavelength. The notation used here is that of Ninomiya.[15]

Following Ninomiya's development, the wave equation for the total electric field,

$$\nabla^2\mathbf{E} - \nabla(\nabla \cdot \mathbf{E}) + K^2\mathbf{E} = 0, \tag{1}$$

where K is the propagation constant, is used as a starting point. The total electric field in the grating may now be expressed by the vector

$$\mathbf{E}(\mathbf{r},t) = \mathbf{R}(\mathbf{r},t)\exp(-j\boldsymbol{\rho}\circ\mathbf{r}) + \mathbf{S}(\mathbf{r},t)\exp(-j\boldsymbol{\sigma}\circ\mathbf{r}), \tag{2}$$

where $\boldsymbol{\rho}$ and $\boldsymbol{\sigma}$ are the wave vectors of the reference and signal beams, respectively, and $\mathbf{r} = (x,y,z)$. The exposure is thus $\int_0^T \mathbf{E}\cdot\mathbf{E}^*\,dt$, where t is time and T is exposure time. From Eqs. (1) and (2), the following coupled equations are obtained for the wave amplitudes R and S (functions of z and t):

$$\cos\theta\frac{\partial R}{\partial z} + \gamma R = -j\Gamma_1 S(\hat{\mathbf{r}}\cdot\hat{\mathbf{s}})^2, \tag{3}$$

$$\cos\theta\frac{\partial S}{\partial z} + (\gamma + j\vartheta)S = -j\Gamma_2 R(\hat{\mathbf{r}}\circ\hat{\mathbf{s}})^2, \tag{4}$$

where

$$\gamma = (j2\pi a/\lambda + b)\int_0^T (RR^* + SS^*)\,dt + \alpha_0, \tag{5}$$

$$\Gamma_1 = [(2\pi a/\lambda)\exp(j\phi_n) - jb\exp(j\phi_\alpha)]\int_0^T RS^*\,dt, \tag{6}$$

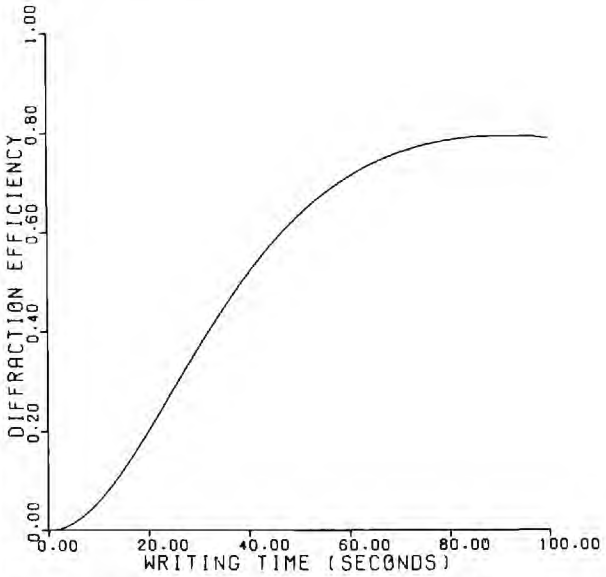

FIG. 2. Calculated hologram writing characteristic exhibiting a saturationlike appearance. Hologram thickness is 2.00 mm, $a = 10^{-12}$ $(\mathrm{V/m})^{-2}$ sec^{-1}, $\phi_n = 90°$, $\alpha_0 = 0$, and other parameters as given in Sec. IV.

$$\Gamma_2 = [(2\pi a/\lambda)\exp(-j\phi_n) - jb\exp(-j\phi_\alpha)]\int_0^T SR^*\,dt, \quad (7)$$

$$\vartheta = (\beta_0^2 - \sigma'^2)/2\beta_0, \quad (8)$$

$$\beta_0 = 2\pi n_0/\lambda, \quad (9)$$

$$\hat{\mathbf{r}}\cdot\hat{\mathbf{s}} = \cos 2\theta, \quad (10)$$

and λ is the free-space wavelength, n_0 is the average index of refraction, α_0 is the average absorption constant, ϕ_n and ϕ_α are the phase differences between the hologram-forming light interference pattern and the resulting refractive-index and absorption gratings, respectively, and a and b are the exposure sensitivities of the refractive-index changes and absorption changes, respectively. The quantity ϑ is the dephasing factor introduced by Kogelnik.[1] The magnitude of the propagation vector of the diffracted wave upon reading is

$$\sigma' = (\beta_\delta^2 - 4\beta_0\beta_\delta\sin\theta\sin\theta' + 4\beta_0^2\sin^2\theta)^{1/2}, \quad (11)$$

where $\beta_\delta = 2\pi n_\delta/\lambda'$. The primed quantities represent the values associated with the reading process.

Equations (3) and (4) can be solved numerically on a digital computer. It is shown that the solutions thus obtained qualitatively describe the various types of externally measurable diffraction behavior of volume holograms that have been experimentally measured and reported in the literature (sometimes with very little explanation).

IV. CALCULATED RESULTS AND EXPERIMENTAL BEHAVIOR

A. Calculational procedure

In this section, numerical results obtained by solving Eqs. (3) and (4) are presented for selected sets of hologram parameters. The solutions are seen to compare favorably with published experimental results. For writing, the equations are solved with $\vartheta = 0$ (no dephasing) and the boundary conditions $R(0,t) = R_0$ and $S(0,t) = S_0$. For reading, ϑ can be nonzero. Deviations in wavelength and/or incident angle from the corresponding writing quantities result in $\vartheta \neq 0$. The boundary conditions $R(0,t) = R_\delta$ and $S(0,t) = 0$ are used for the case of readout with the R beam and $R(0,t) = 0$ and $S(0,t) = S_\delta$ are used for readout with the S beam. Diffraction efficiency is then defined as $\eta = S(1,T)S^*(1,T)/R_\delta^2$ for R-beam readout and $\eta = R(1,T)R^*(1,T)/S_\delta^2$ for S-beam readout.

The computer algorithm employs a fourth-order Runge-Kutta method to solve the equations with respect to the z variable. The integrations in t were performed by replacing the integrals by the corresponding sums and using increments, Δt, small enough for convergence. The actual incremental step sizes used were $\Delta z = 0.01$ (the equations are normalized with respect to the thickness so that $0 \leq z \leq 1$) and $\Delta t = 0.5$ sec. The numerical accuracy was tested by decreasing the step sizes Δz and Δt until the improvements in convergence were insignificant.

The calculations presented are for a 1.66- and a 2.00-mm-thick crystal of $LiNbO_3$ with its optic axis (c axis) in the plane of incidence of the writing beams. The writing and reading waves are polarized in the plane of incidence and have a wavelength of $\lambda = 0.5145$ μm. The angles of incidence for the writing beams are $\pm 2.23°$ (corresponding to external angles of incidence of $\pm 5.00°$ for the grating surrounded by a unity refractive-index medium). For this wavelength, polarization, angle of incidence, and orientation of the lithium niobate crystal, the index of refraction is $n_0 = 2.2426$. For writing $R_0 = S_0 = 1000$ V/m. Reading is done with $R_\delta = 1000$ V/m. Only transmission phase holograms are considered, that is, b is set equal to zero (no photochromic effect).

B. Writing

With a few exceptions, the experimental diffraction efficiency writing characteristics (η vs t) reported in the literature for volume holograms begin with zero initial slope and increase in a parabolic fashion. The magnitudes of the diffraction efficiencies reported, however, vary considerably. Several workers[22–25] report relatively low efficiencies (e.g., $<1\%$) exhibiting saturating behavior or a very small rate of increase. Others[26–31] have reported higher efficiencies, also showing saturation behavior. At times, instead of saturation, an oscillatory diffraction efficiency is observed.[2,27,28,30,31] It seems that experimental oscillatory writing characteristics are observed primarily for relatively high-efficiency holograms. In many papers,[2,14,24,27,32–38] the writing is terminated before the onset of oscillation or saturation.

The types of behavior indicated above can be straightforwardly predicted using the dynamic theory. The oscillatory behavior is seen to be inherent in the theory because of the assumption of constant refractive-index exposure sensitivity. The material is thus assumed to respond continuously to the interaction of the wave fields at all times. Physically, the quantity a may be time depen-

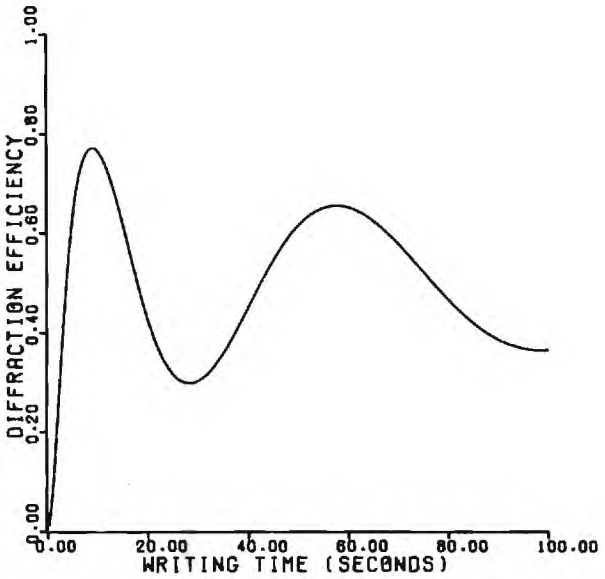

FIG. 3. Calculated oscillatory hologram writing characteristic with decreasing amplitude and increasing period of the diffraction efficiency oscillations. Hologram thickness is 2.00 mm, $a = 10^{-11}$ $(V/m)^{-2}$ sec^{-1}, $\phi_n = 90°$, $\alpha_0 = 0$, and other parameters as given in Sec. IV.

dent since the physical mechanism(s) (such as photochemical effects, drift of charge carriers, diffusion of charge carriers, etc.) that produce the sensitivity may be self-limiting in some materials. Therefore, saturation at low or high efficiency may be brought about by a vanishing sensitivity. At the turning point toward saturation, $|d\eta/dt|$ is strongly affected by $|da/dt|$. Thus, depending on the material and the experimental situation, gradual [22,24–28,30,31] or abrupt [23,29] turning points are observed in $\eta(t)$. Figure 2 demonstrates that an approximately saturating behavior may be predicted by the dynamic equations even with a constant refractive-index exposure sensitivity (Fig. 2 is similar to Fig. 6 in Ref. 15). Calculated oscillatory behavior is shown in Fig. 3.

Figure 3 exhibits behavior similar to that experimentally observed by the authors in lithium niobate and shown in Fig. 4. Note the decreasing amplitude and increasing period of the diffraction efficiency oscillations with exposure in both of these figures. Figure 3 also bears qualitative resemblance to Fig. 6 in Ref. 27 and to Fig. 2 in Ref. 28. Figure 5 illustrates large increasing diffraction efficiency oscillations with minima near 0%. This behavior is like that depicted in Fig. 5 of Ref. 2 for a 1.8-mm-thick photopolymer hologram grating.

The exceptional cases for which writing starts with an apparently linear $\eta(t)$ characteristic [23,25,28,39] (rather than parabolic) may possibly be reconciled by the fact that the zero-slope initial portion of the $\eta(t)$ is sometimes of very brief duration (see, for example, Fig. 4 of this paper, Fig. 2 in Ref. 22, Fig. 5 in Ref. 27, Fig. 1 in Ref. 35, etc.) and thus the curve appears to be approximately linear when in fact it may not be.

C. Reading

The application of a reading beam to a thick hologram may continually change its characteristics. Experimentally, the most commonly observed result seems to be exponentiallike decay of the diffraction efficiency. [14,22–24,27,28,30,32–34,36,37,40,41] Oscillatory diffraction efficiency readout behavior has also been reported. In rhodium-doped $LiNbO_3$, for example, vivid oscillations have been observed during readout. [28] An iron-doped sample of $LiNbO_3$ has shown an initial rise and a subsequent decay of diffraction efficiency upon readout. [33] Oscillatory behavior at low efficiency following an exponentiallike decay has also been noted. [33] Self-enhancement (an increase of diffraction efficiency upon reading) of Fe-doped $LiNbO_3$ holograms has been observed. [42] In this case, erasure and enhancement were produced depending on which of the original writing beams was used for readout. Behavior such as this has been theoretically predicted by Staebler and Amodei. [14] We present here further experimental results for volume holograms that show this type and other effects upon

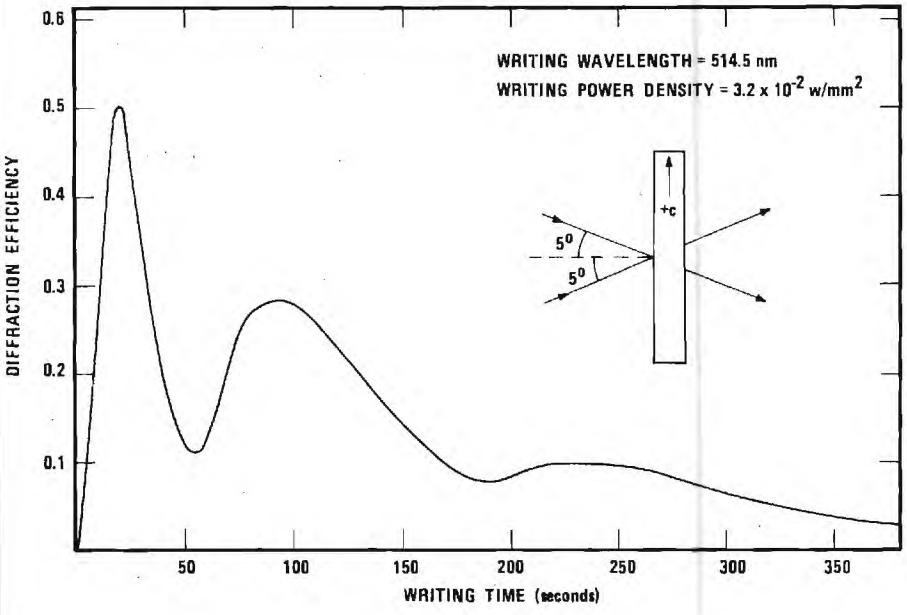

FIG. 4. Experimental oscillatory hologram writing characteristic for a 1.66-mm-thick iron-doped lithium niobate crystal. Writing beam polarizations are in the plane of incidence and the experimental configuration is as shown in the figure inset.

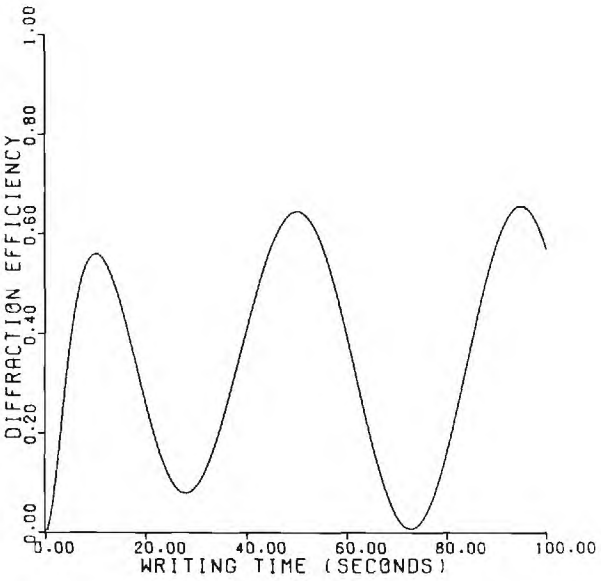

FIG. 5. Calculated oscillatory hologram writing characteristic with diffraction efficiency minima near 0%. Hologram thickness is 2.00 mm, $a = 10^{-11}$ $(V/m)^{-2}$ sec^{-1}, $\phi_n = 60°$, $\alpha_0 = 10^2$ m^{-1}, and other parameters as given in Sec. IV.

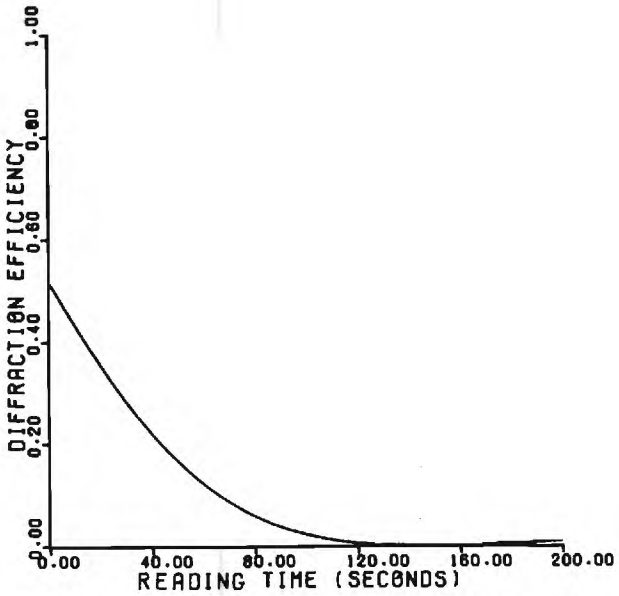

FIG. 6. Calculated exponentiallike reading characteristic. Note slight rise in efficiency at a reading time of 200 sec. Hologram thickness is 2.00 mm, $a = 10^{-12}$ $(V/m)^{-2}$ sec^{-1}, $\phi_n = 90°$, $\alpha_0 = 0$, readout with R beam, and other parameters as given in Sec. IV. The original hologram was recorded using these same parameters and an exposure time of 40 sec.

changing the reading beam from the R beam to the S beam (see Fig. 1).

The various types of behavior discussed above are all predicted by the dynamic theory. In Fig. 6, for example, a calculated exponentiallike decay of the hologram efficiency is shown. Note that, eventually, the efficiency rises again (as experimentally reported in Ref. 33 and in Fig. 4 of Ref. 41). Figure 7 depicts the experimentally recorded decay of the efficiency of a hologram written in a 1.66-mm-thick iron-doped crystal of $LiNbO_3$ for the beam configuration indicated in the inset of Fig. 7. Note the slight oscillations at low efficiency. Figures 8 and 9 illustrate the calculated effect of switching the reading beam to the symmetrical angular location. In Fig. 8, an initial decrease in diffraction efficiency is predicted, whereas in Fig. 9 an initial increase is predicted (like experimental data in Fig. 6 of Ref. 33, in Fig. 2 of Ref. 42, and in Fig. 12 of this paper). Figure 8 also clearly predicts oscillations at low efficiency such as have been experimentally observed. Figure 10 shows the behavior of efficiency oscillations followed by monotonic decay as calculated by the dynamic theory. This is qualitatively like the experimental readout behavior observed in rhodium-doped $LiNbO_3$ by Ishida *et al.*[28] Figure 11 illustrates calculated diffraction efficiency

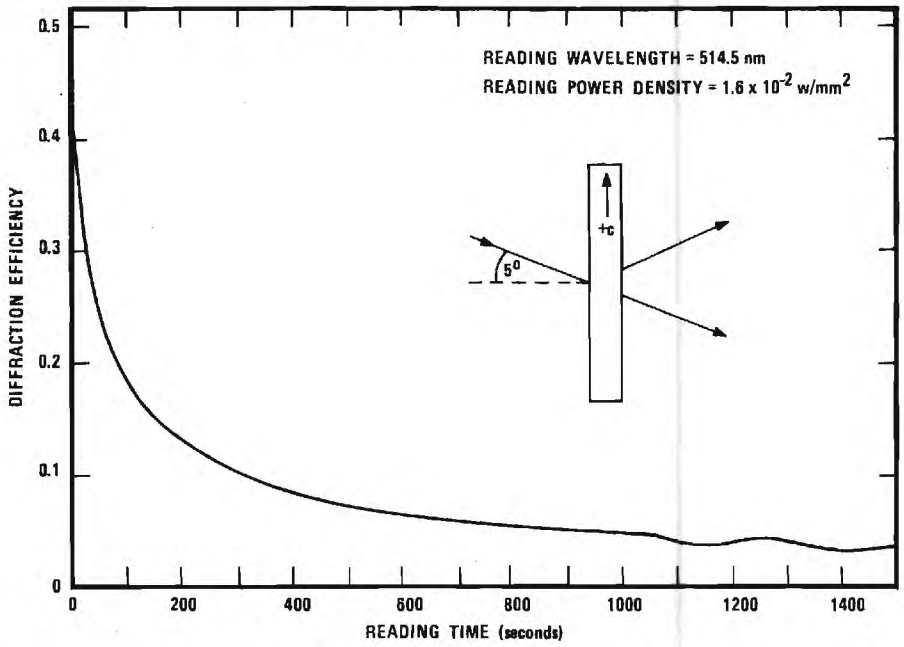

FIG. 7. Experimental exponentiallike reading characteristic for a 1.66-mm-thick iron-doped lithium niobate crystal. Small amplitude diffraction efficiency oscillations are present at low efficiencies. Reading beam polarization is in the plane of incidence and the experimental configuration is as shown in the figure inset.

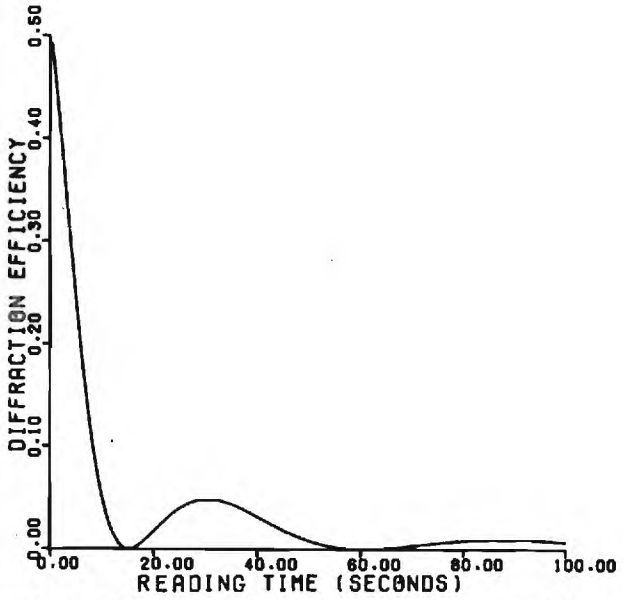

FIG. 8. Calculated reading characteristic showing diffraction efficiency oscillations at low efficiencies. Hologram thickness is 2.00 mm, $a = 10^{-11}$ $(V/m)^{-2}$ sec^{-1}, $\phi_n = 90°$, $\alpha_0 = 10^2$ m^{-1}, readout with R beam, and other parameters as given in Sec. IV. The original hologram was recorded using these same parameters and an exposure time of 10 sec.

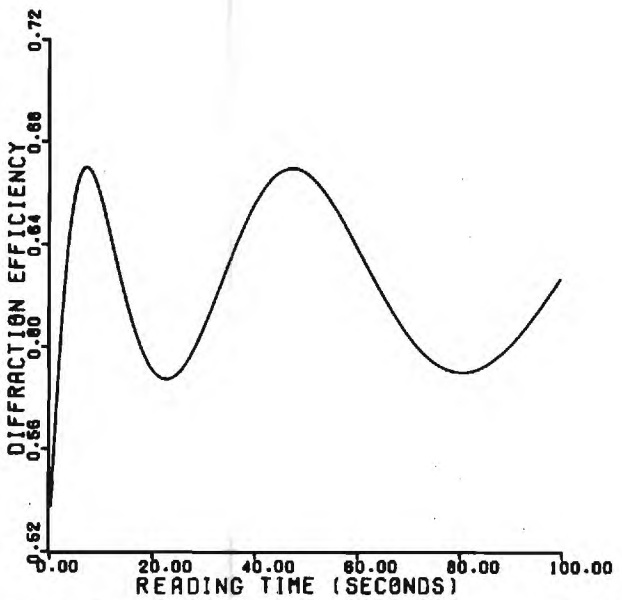

FIG. 9. Calculated enhancement and oscillatory reading characteristic resulting from S-beam readout as opposed to normal R-beam readout. All other conditions and parameters are identical to those of Fig. 8.

oscillations that both decrease and increase as a function of readout exposure. In Fig. 12, we show experimentally measured oscillatory reading behavior for the same hologram grating used in Fig. 7 except that reading is done with the beam at the symmetric recording angle (reading with the S beam instead of the R beam in the notation of Fig. 1). Large variations in both the amplitude and the period of the efficiency oscillations are observed. This behavior is qualitatively similar to the predicted readout diffraction efficiency of Fig. 11.

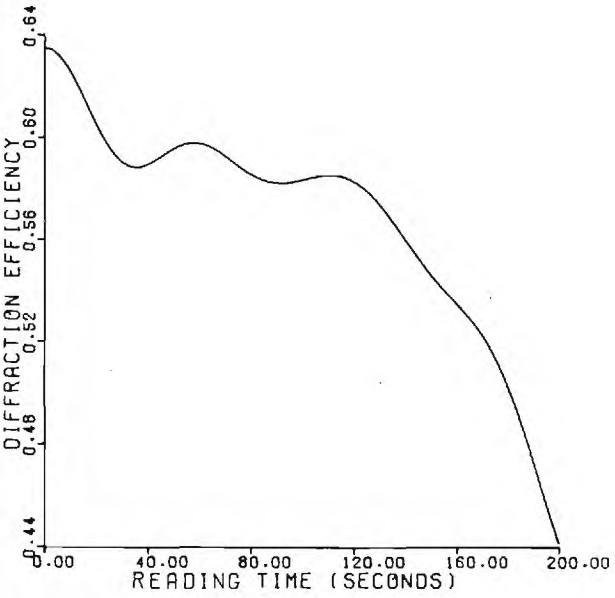

FIG. 10. Calculated reading characteristic showing diffraction efficiency oscillations followed by rapid decay. Hologram thickness is 2.00 mm, $a = 10^{-11}$ $(V/m)^{-2}$ sec^{-1}, $\phi_n = 0°$, $\alpha_0 = 0$, readout with R beam, and other parameters as given in Sec. IV. The original hologram was recorded using these same parameters and an exposure time of 35 sec.

D. Angular selectivity

Angular selectivity refers to the variation of diffraction efficiency as a function of angle of incidence of the reading wave. In experiments measuring this property of thick hologram gratings, a low power reading beam or a reading beam of a wavelength at which the material is insensitive is generally used so as not to affect the hologram by the process of measurement.

Experimental angular selectivity results are somewhat less plentiful than the other terminally measured

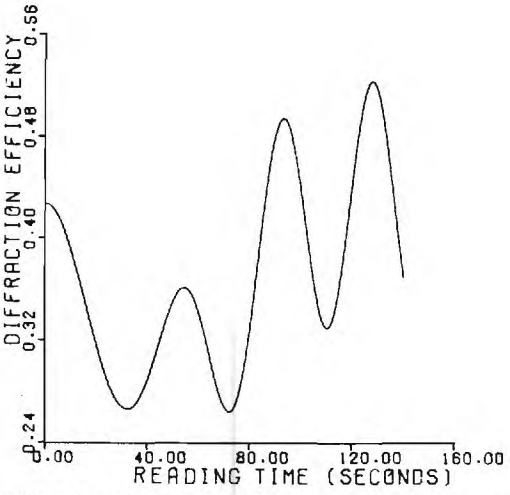

FIG. 11. Calculated oscillatory reading characteristic showing large variations in the amplitude and period of the diffraction efficiency oscillations. Hologram thickness is 2.00 mm, $a = 10^{-11}$ $(V/m)^{-2}$ sec^{-1}, $\phi_n = 0°$, $\alpha_0 = 0$, readout with R beam, and other parameters as given in Sec. IV. The original hologram was recorded using these same parameters and an exposure time of 10 sec.

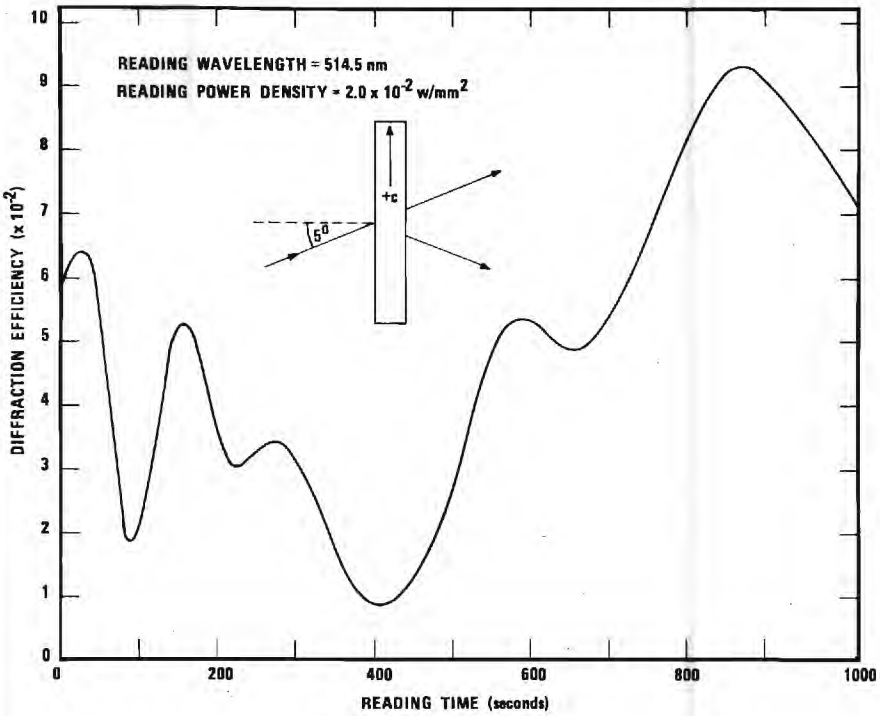

FIG. 12. Experimental oscillatory reading characteristic for a 1.66-mm-thick iron-doped lithium niobate crystal. A wide variation in the amplitude and period of the diffraction efficiency oscillations is apparent. Reading beam polarization is in the plane of incidence and the experimental configuration is as shown in the figure inset.

characteristics of thick holograms. Some of the existing experimental results exhibit a series of nonzero minima in place of the nulls [43–47] predicted by static hologram theories. Some experimental data show no minima in the angular selectivity. [43,48] It is now well established [20,21,43] that nonuniformity of the grating with material thickness produces nonzero diffraction minima or the complete disappearance of the minima in the angular selectivity.

The dynamic theory straightforwardly predicts the various types of angular selectivity behavior of volume holograms. Here, grating nonuniformity arises if $\phi_n \neq 0$, or $\alpha_0 \neq 0$, or if both ϕ_n and α_0 are nonzero. Nonuniformity, and the corresponding disappearance of angular selectivity minima for low-loss materials ($\alpha_0 \cong 0$), is explained here by the dynamic theory but cannot be explained by the static theories. In Fig. 13, a logarithmic plot of experimental data is presented for a hologram written in a 1.66-mm-thick 0.05-mole% Fe-doped crystal of $LiNbO_3$ and compared to the solution of Eqs. (3) and (4) for the same conditions. Due to the short writing time and the low efficiency ($\cong 1\%$), the grating is still quite uniform through the thickness of the material (z direction) and thus the grating exhibits well-defined nulls in the diffraction efficiency for a series of reading angles. Theory and experiment both show these nulls. Figure 14 indicates the vanishing of the angular selectivity nulls as the grating develops and begins to show nonuniformity in the amplitude of the refractive index modulation with z (see inset in Fig. 14). Figure 15 shows the angular selectivity and the index profile for the hologram grating after further exposure. Note that $\alpha_0 = 0$. Figure 15 illustrates that the absolute maximum diffraction intensity peak now occurs off the Bragg angle. The pattern is symmetric with respect to the Bragg angle and thus a second peak occurs for an angle of incidence on the other side of the Bragg angle.

V. DISCUSSION

The prediction of a very wide variety of results in volume holography is possible with the dynamic theory. Writing and reading characteristic curves (usually presented as η vs t) may have an infinitude of possible magnitudes and shapes. The calculated curves presented in this paper are typical results taken from a much larger number of cases that have been analyzed by the authors. Many rapidly varying experimental writing and reading results (such as the data shown in Fig. 12) have previously informally been attributed to "experimental problems". It is now apparent that these types of oscillatory results are "normal" and are to be expected.

The dynamic theory is an important aid in identifying the "significant" parameters in volume holographic recording and readout. Relatively few parameters are needed in the dynamic theory. The role of each of these parameters can be determined in a given situation. This indicates the possibility of using the dynamic theory (1) as an aid in synthesis and (2) as a diagnostic tool.

As an aid in synthesis, the dynamic theory serves as an indicator of the parameter values that are needed to produce a particular desired situation (e.g., uniformity of induced change through the thickness of a hologram, a certain type of angular selectivity, an enhancing readout, a rapidly erasing readout, etc.). The dynamic theory parameters in some materials, indeed, may be controlled in a fairly direct manner. For example, in iron-doped lithium niobate, α_0 and a may be dramatically changed by heat treating the material in various environments. [32,33] Microscopically, this has been shown to control the relative Fe^{2+} and Fe^{3+} concentrations in iron-doped lithium niobate. [32,33] In addition, the phase difference between the light and the refractive-index

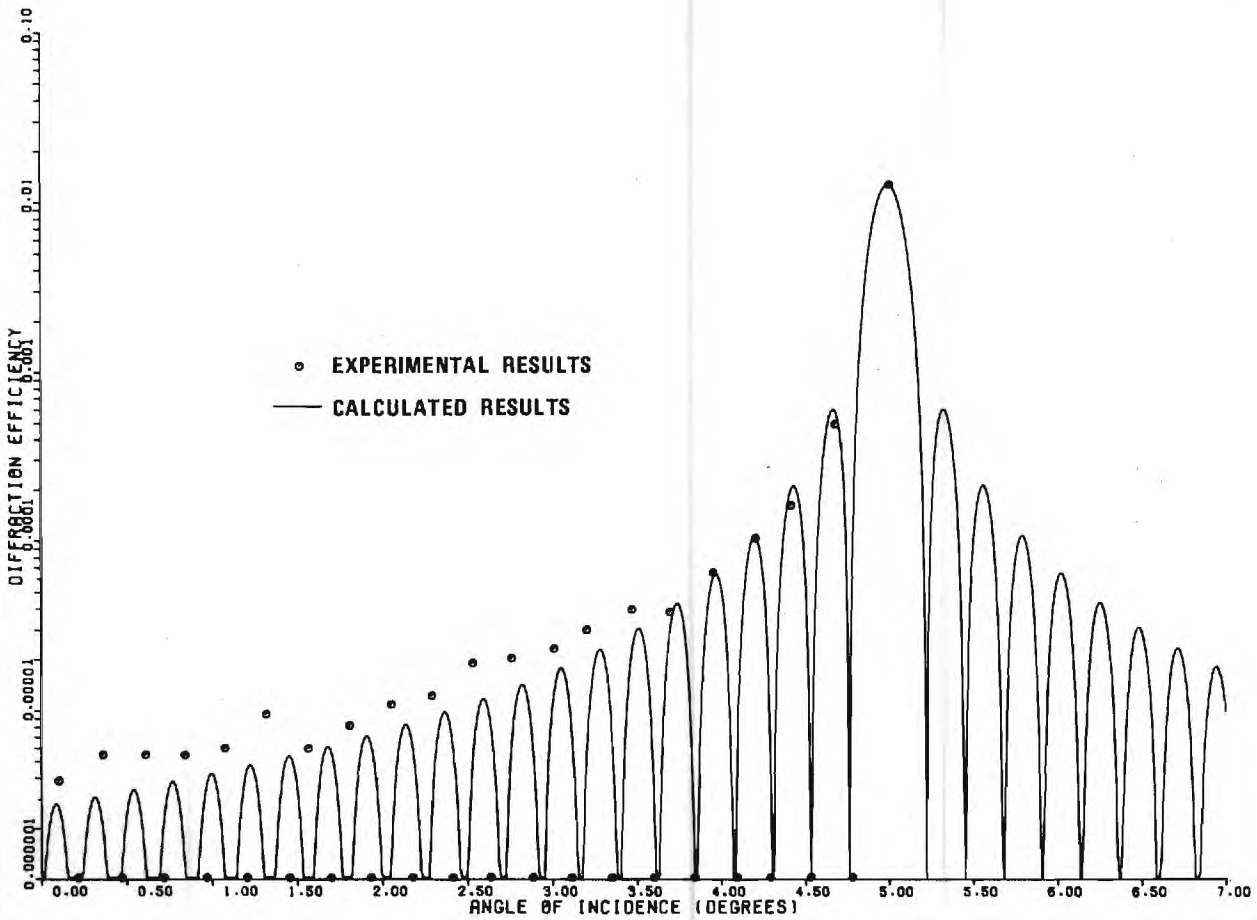

FIG. 13. Experimental and calculated angular selectivity exhibiting zero diffraction efficiency at minima. The hologram is a 1.66-mm-thick iron-doped lithium niobate crystal. Experimentally, hologram was written with a wavelength of 514.5 nm, a total power density of 3.5 mw/mm^2, external angles of incidence of $\pm$ 5.00°, a writing time of 5 sec, polarization in the plane of incidence, and the configuration shown in the inset of Fig. 4. Experimentally, the angular selectivity was measured with a low power beam of the same wavelength. The calculated curve is for a hologram of thickness of 1.66 mm, written with $R_0 = 571$ V/m, $S_0 = 518$ V/m, for 5 sec with $a = 3.8 \times 10^{-12}$ (V/m)$^{-2}$ sec^{-1}, $\phi_n = 0°$, and $\alpha_0 = 0$, these parameters being estimated from the experimental conditions.

grating, ϕ_n, approaches 0° when drift of the photoexcited electrons dominates[14] (which may be induced by externally applying an electric field). The phase difference approaches 90° when diffusion of the electrons dominates[14] (which may be induced by using a small fundamental grating spacing).

As a diagnostic tool, the dynamic theory, when coupled with experiment, is capable of determining certain material and hologram characteristics. By experimentally holding constant some of the dynamic theory parameters, other parameters and properties may be found. For example, the variations with grating thickness of the refractive index may be determined knowing the conditions of recording. This would allow the direct determination of the index profile (in the z direction) as opposed to assuming a uniform grating or an exponential variation with thickness (both of which may be totally incorrect). As another example, the variation with exposure of the refractive-index exposure sensitivity, a, may be measured. By holding the other dynamic theory parameters constant and measuring the hologram writing characteristic, the time dependence of the index exposure sensitivity may be determined.

Chronologically, in the literature, the earlier thick recording materials tended to show a saturating-type writing characteristic indicating a rapidly decreasing value of a. More recently, higher-sensitivity materials have tended to show an oscillatory writing characteristic indicating a larger dynamic range for these materials (and thus the dynamic theory is valid in these cases with essentially a constant value of a).

VI. CONCLUSION

A large number of different types of recording and reading behaviors have been reported for thick (volume) holograms in a wide variety of recording materials. Writing, reading, and angular selectivity experimental data from approximately 25 published articles are cited in this paper as being representative of the known types of behavior. The dynamic theory of thick hologram recording and reading qualitatively predicts all of these various types of experimental behavior. Thus, the dynamic theory is potentially very powerful (1) in determining the material and recording parameters needed to produce a certain desired hologram characteristic

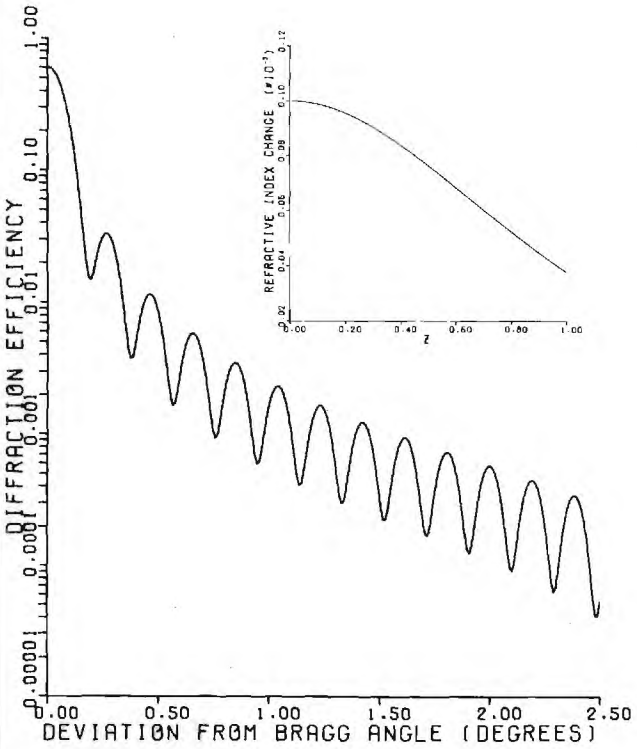

FIG. 14. Calculated angular selectivity exhibiting nonzero diffraction efficiency at minima. Nonzero minima are characteristic of phase holographic gratings having a variation in index of refraction through the thickness of the material. The refractive-index profile is shown in the inset. Hologram thickness is 2.00 mm, $a = 10^{-11}$ $(V/m)^{-2}$ sec^{-1}, $\phi_n = 90°$, $\alpha_0 = 0$, and writing time is 5 sec.

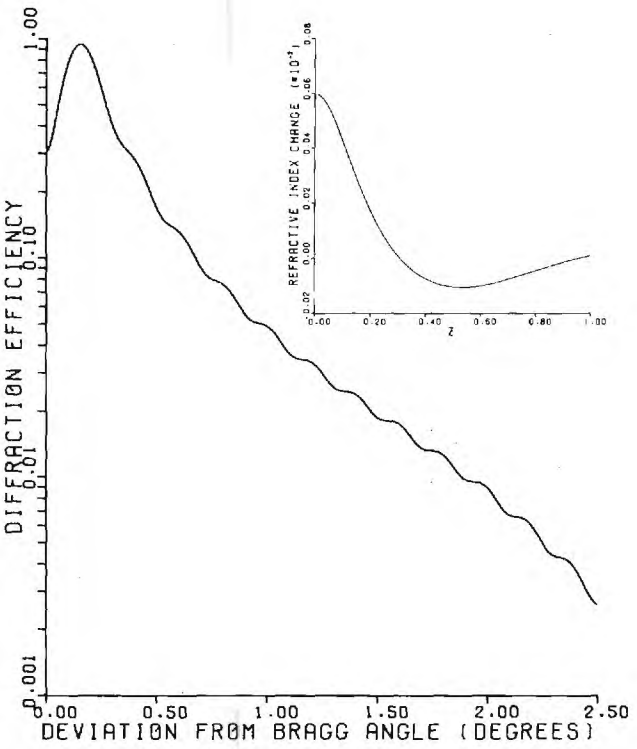

FIG. 15. Calculated angular selectivity showing the disappearance of diffraction efficiency minima. The same conditions as Fig. 14 prevail but with a longer writing time of 30 sec. The increased nonuniformity of the grating profile is shown in the inset.

and (2) as a diagnostic tool to analyze the parameters of thick photosensitive recording materials.

Note added in proof. An oscillatory diffraction efficiency upon readout has also been shown theoretically and experimentally to be possible due to changes in the multiple internal reflections as a result of crystal thermal expansion caused by the absorption of laser light. These results are reported in the work by W. D. Cornish and L. Young, J. Appl. Phys. 46, 1252 (1975). In our experimental case (Figs. 4, 7, 12, and 13), we have found by the reflectance test given in the above reference that our crystals do not satisfy the flatness-and-parallelism requirements necessary for such effects to occur. Laser-induced thermal expansion, therefore, does not significantly affect our experimental results.

ACKNOWLEDGMENTS

The authors would like to thank S. F. Su for his help with the numerical analysis in this paper and W. R. Callen for his help with the experimental measurements.

*Work supported by the National Science Foundation and by the National Aeronautics and Space Administration.

[1]H. Kogelnik, Bell Syst. Tech. J. 48, 2909 (1969).
[2]M. R. B. Forshaw, Opt. Laser Technol. 6, 28 (1974).
[3]B. H. Crawford, J. Sci. Instrum. 31, 333 (1954).
[4]J. N. Latta and R. C. Fairchild, J. Opt. Soc. Am. 63, 487 (1973).
[5]R. Shubert and J. H. Harris, J. Opt. Soc. Am. 61, 154 (1971).
[6]H. Kogelnik and C. V. Shank, Appl. Phys. Lett. 18, 152 (1971).
[7]H. Kogelnik and T. P. Sosnowski, Bell Syst. Tech. J. 49, 1602 (1970).
[8]M. L. Dakss, L. Kuhn, P. F. Heidrich, and B. A. Scott, Appl. Phys. Lett. 16, 523 (1970).
[9]J. M. Hammer, Appl. Phys. Lett. 18, 147 (1971).
[10]P. J. Van Heerden, Appl. Opt. 2, 393 (1963).
[11]K. S. Pennington and L. H. Lin, Appl. Phys. Lett. 7, 56 (1965).
[12]G. W. Stroke and A. E. Labeyrie, Phys. Lett. 20, 368 (1966).
[13]C. B. Burckhardt, J. Opt. Soc. Am. 56, 1502 (1966).
[14]D. L. Staebler and J. J. Amodei, J. Appl. Phys. 43, 1042 (1972).
[15]Y. Ninomiya, J. Opt. Soc. Am. 63, 1124 (1973).
[16]See, for example, T. K. Gaylord, Opt. Spectra 8, 29 (1974).
[17]P. Phariseau, Proc. Indian Acad. Sci. A 44, 165 (1956).
[18]S. F. Su and T. K. Gaylord, J. Opt. Soc. Am. 65, 59 (1975).
[19]D. Kermisch, J. Opt. Soc. Am. 61, 1202 (1971).
[20]D. Kermisch, J. Opt. Soc. Am. 59, 1409 (1969).
[21]N. Uchida, J. Opt. Soc. Am. 63, 280 (1972).
[22]T. K. Gaylord, T. A. Rabson, and F. K. Tittel, Appl. Phys. Lett. 20, 47 (1972).
[23]F. Micheron and G. Bismuth, Digest of Technical Papers, 1972 IEEE International Solid-State Circuits Conference, p. 104 (unpublished).
[24]W. Phillips, J. J. Amodei, and D. L. Staebler, RCA Rev. 33, 95 (1972).

[25]L.H. Lin, Proc. IEEE **57**, 252 (1969).
[26]F.S. Chen, J.T. LaMacchia, and D.B. Fraser, Appl. Phys. Lett. **13**, 223 (1968).
[27]J.J. Amodei, W. Phillips, and D.L. Staebler, Appl. Opt. **11**, 390 (1972).
[28]A. Ishida, O. Mikami, S. Miyazawa, and M. Sumi. Appl. Phys. Lett. **21**, 192 (1972).
[29]R.W. Damon, D.H. McMahon, and J.B. Thaxter, Electro-Opt. Syst. Des. **2**, 68 (1970).
[30]F. Micheron and G. Bismuth, Appl. Phys. Lett. 23, 71 (1973).
[31]T.A. Shankoff, Appl. Opt. **7**, 2101 (1968).
[32]W. Phillips and D.L. Staebler, J. Electron. Mater. **3**, 601 (1974).
[33]D.L. Staebler and W. Phillips, Appl. Opt. **13**, 788 (1974).
[34]J.P. Huignard, J.P. Herriau, and F. Micheron, Appl. Phys. Lett. **26**. 256 (1975).
[35]D.L. Staebler, W.J. Burke, W. Phillips, and J.J. Amodei, Appl. Phys. Lett. **26**, 182 (1975).
[36]J.J. Amodei, D.L. Staebler, and A.W. Stephens, Appl. Phys. Lett. **18**, 507 (1971).
[37]F. Micheron and G. Bismuth, Digest of Technical Papers, Optical Storage of Digital Data, MB3-1, 1973 (unpublished).
[38]T.K. Gaylord, T.A. Rabson, F.K. Tittel, and C.R. Quick, Appl. Opt. 12, 414 (1973).
[39]R.L. Townsend and J.T. LaMacchia, J. Appl. Phys. **41**, 5188 (1970).
[40]J.J. Amodei and D.L. Staebler, Appl. Phys. Lett. 18, 540 (1971).
[41]D.L. Staebler and J.J. Amodei, Ferroelectrics 3, 107 (1972).
[42]T.K. Gaylord, T.A. Rabson, F.K. Tittel, and C.R. Quick, J. Appl. Phys. **44**, 896 (1973).
[43]E.N. Leith, A. Kozma, J. Upatnieks, J. Marks, and N. Massey, Appl. Opt. 5, 1303 (1966).
[44]K. Biedermann, S.I. Ragnarsson, and P. Komlos, Opt. Commun. **6**, 205 (1972).
[45]V.V. Aristov and V.Sh. Shekhtman, Sov. Phys. Usp. **14**, 263 (1971).
[46]R.G. Zech, Ph.D. thesis (University of Michigan, 1974) (unpublished).
[47]D.R. Bosomworth and H.J. Gerritsen, Appl. Opt. **7**, 95 (1968).
[48]T.K. Gaylord and F.K.Tittel, J. Appl. Phys. **44**, 4771 (1973).

IV. NEW MASS DATA STORAGE ARCHITECTURES

The development of a high capacity computer memory with a multi-port simultaneous access capability may require new computer architectures for efficient computation. The implications of this are discussed in Reference [7], which is reproduced on the following pages of this report.

THE POTENTIAL OF MULTI-PORT OPTICAL MEMORIES IN DIGITAL COMPUTING

C. O. Alford and T. K. Gaylord
School of Electrical Engineering
Georgia Institute of Technology
Atlanta, Georgia 30332

Summary

A high-capacity memory with a relatively high data transfer rate and multi-port simultaneous access capability may serve as the basis for new computer architectures. The implementation of a multi-port optical memory is discussed. Several computer structures are presented that might profitably use such a memory. These structures include (1) a simultaneous record access system, (2) a simultaneously shared memory computer system, and (3) a parallel digital processing structure.

Introduction

It is widely recognized that the characteristics of optical memories are different from those of conventional computer memories. Thus, they may play roles that are different from the roles played by existing magnetic and semiconductor memories. One potential capability of optical holographic memories as suggested by Rajchman [1] is the replacement of a large fraction of the conventional computer memory hierarchy. In this situation a series of slow and large, and fast and small memory devices would be replaced by a single optical memory unit. This may be possible due to the potential coexistence of both high capacity and fast access times in an optical memory--two features that do not exist together in conventional memories.

In addition, there are other ways that optical memories may be distinctly different from conventional memories. One of these is the multi-port capability--the capability of stored data in the memory to be accessed simultaneously by multiple users through each of the memory's ports. This is to be contrasted with space multiplexed (interleaved) and time multiplexed conventional memories which are sometimes represented as being "multi-port." However, a true multi-port memory allows simultaneous access to its data through each memory port.

Multi-Port Optical Memories

Multi-port optical memories could be of a variety of designs. A possible example of a multi-port holographic memory is shown in Fig. 1. In this diagram, the recording medium is being used as a two dimensional store rather than a three dimensional store [2]. There is one page of binary data stored in holographic form at each x-y location of the recording medium. This memory is basically the same as a conventional optical holographic memory [3] except that 1) there are three extra beam deflectors and 2) there is one read-out detector matrix for each memory port. The extra beam deflectors are of key importance in this memory system. The first reference/read-out beam deflector produces N beams deflected by varying amounts in the y direction. The second reference beam deflector is a one dimensional array of deflectors to produce deflection of the reference beams by varying amounts in the x direction. Finally, the readout deflector array is a two dimensional array of deflectors directly behind the recording medium to steer the reconstructed data beam to the appropriate memory port [4]. Notice that this memory configuration uses a single page composer for writing in data at all x-y hologram locations in the recording medium.

The complexity of a multi-port optical memory is thus greater than that of a single port optical memory. However, the cost of additional memory ports beyond the second port would be relatively small. For each additional port, the primary additions would be another read-out detector matrix and an increase in laser power. There would be one reference/read-out beam for each of the N ports. With additional ports, the basic object beam and reference/read-out beam configurations as illustrated in Fig. 1 would not be changed. An upper limit on the number of ports would obviously be imposed by the amount of usable space available behind the inverse Fourier transform lens.

Simultaneous Record Access System

One of the prime purposes of a high-capacity optical memory is to store vast quantities of records or information such as libraries, insurance data, medical data, seismic data, criminal data, defense data, tax information, patent records, telephone numbers, stock market information, etc. Users of such a storage bank would need to have access to page information. Further, multiple user capability is required to make such a system cost effective. A possible structure for this system is shown in Fig. 2.

Data is stored in page format in the multi-port optical memory. Access to any page is via a terminal (CRT type) through one of the memory access ports. The data requirements of each terminal are, in some applications, low enough to have one memory port support several terminals through a multiplexer. Since a single page access may require on the order of 1 μsec and since each human user would take on the order of 1 minute to scan a page and reach a decision on the next access, a single port operating through a multiplexer could theoretically support 10^6 terminals. However, maximum data rates between the port and the terminal will reduce this number to the order of probably 100. Thus ten ports could support 1000 users and this could be extended to more users by increasing the data rates on the external circuitry.

Trade-offs are between port speed, multiplexer speed and numbers of ports. The most effective system would match the total number of users at one port to an economical multiplexer such that the average access time for any user is reasonable (approx. 1 min.). This access time divided by the number of users per port fixes the multiplexer speed and memory access time per page. If a slower memory access time can result in a less expensive memory or if this can be traded for additional memory ports at the same expense, these would make desirable trade-offs.

The normal mode of page read-out is a binary pattern of a discrete number of bits. It is conceivable, however, that certain information, such as pictures and figures, would be read out of the optical

memory in a non-encoded format. The transfer of this type of information to a readable display for multiple users, presents a number of new design problems and trade-offs.

The user terminals are normally used in the read-only mode and are not allowed to perform write operations to memory. Writing would be done by an input terminal through a separate memory port. Since this is also a low speed operation, this port could be multiplexed to other terminals for further read-only usage.

Simultaneously Shared Memory Computer System

The record access application did not require any transformations on the data accessed by the user. If such transformations are necessary, arithmetic logic units must be added to the architecture. One such structure is shown in Fig. 3. The system is essentially the same as most current time-sharing structures. Several users are allowed access to a processing unit. Primary memory is allocated and user programs are executed independently of the multi-port secondary memory, if possible. Calls to special application programs and large blocks of data are achieved by swapping that data in and out from the multi-port memory.

The secondary memory serves as a backing store mass memory device. Its multi-port structure, however, makes it functionally equivalent to several disk drives and its transfer rate makes it superior to the parallel operation of disk units. The possibility exists of placing most of the operating system in the optical memory and decreasing the size of the primary memory units for each central processor unit (CPU).

Some of the parameters needed to characterize such a system are number of bits per page, number of pages, number of ports, access time, primary memory size, write protection scheme, and division of the operating system between the primary memory and the multi-port memory. Trade-offs exist between these parameters and it would appear that if primary memory can be effectively reduced by utilizing the optical memory, a more cost efficient time sharing system would result. Since swapping of information between memories is a common problem in time-sharing systems, the potential access ease and speed of moving pages in and out of the optical memory would be a definite improvement. Other trade-offs exist between the number of ports and number of users and the port speed necessary for a single CPU.

Parallel Digital Processing

There are many scientific problems which require an enormous number of computations. One approach to this problem has been a multi-processor parallel computation technique. Essentially all processors are dedicated to solving one step of the problem. The results are then transfered to the appropriate processor that is dedicated to solving the next step of the problem. Likewise, the first processor also receives new input data and the step-wise computation continues. Problems arise from synchronization and system reliability when the parallelism is carried as far as that in Illiac IV. While no structure is being proposed which would duplicate the Illiac IV performance, it is believed the multi-port memory with a minicomputer multiprocessor structure could give surprising performance.

A possible structure based on a single bus (Unibus) architecture similar to the Lockheed Sue computer is given in Fig. 4. Each minicomputer (module) contains its own processor, data source, and instruction memory. The Unibus allows this module to function as a separate computer independent of the other processors and the multi-port memory. Each module is connected to the multi-port memory through a port and a page memory buffer. This buffer is then tied to the Unibus for transfers to the processor and other memory units. Transfers between modules are made on an outer bus connecting each module.

An alternate configuration which places control of all processors under the direction of one control computer (CPU) is shown in Fig. 5. Instructions are kept in the optical memory and fetched by the control computer. These instructions are sent along the outer bus to selected CPU modules. Modules can then execute similar instructions or different instructions according to the demands of the control computer. All data on which the modules will operate moves through the ports, page buffers, and data memories to be transformed by the processors.

Some of the characteristic parameters of these systems are number of bits per page, number of pages, number of ports, page transfer rates, bus transfer rates, and types of synchronization signals. Trade-offs exist between computational speed of the processors, number of ports and access time. It would seem that the control computer of Fig. 5 would have to be considerably faster than the other processors and possibly the port under its control, port 0, would have to have a higher speed than other ports.

Acknowledgements

This work was supported in part by the National Science Foundation under Grant No. GK-37453 and by the National Aeronautics and Space Administration under Contract No. NAS8-30246.

References

1. J. A. Rajchman, "Promise of Optical Memories," J. Appl. Phys., vol. 41, pp. 1376-1383, March 1, 1970.
2. e.g. L. d'Auria, J. P. Huignard, C. Siezak, and E. Spitz, "Experimental Holographic Read-Write Memory using 3-D Storage," Appl. Optics, vol. 13, pp. 808-818, April 1974.
3. e.g. W. C. Stewart, R. S. Merzrich, L. S. Cosentino, E. M. Nagle, F. S. Wendt, and R. D. Lohman, "An Experimental Read-Write Holographic Memory," RCA Review, vol. 34, pp. 3-44, March 1973.
4. A possible technology for this is described in Y. Ninomiya, "High s/n-Ratio Electrooptic Prism-Array Light Deflectors," IEEE J. Quantum Electron, vol. QE-10, no. 3, pp. 358-362, March 1974.

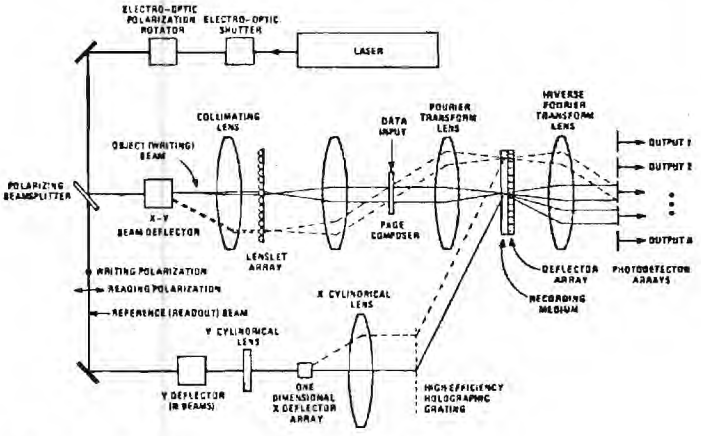

Fig. 1. A multi-port optical memory.

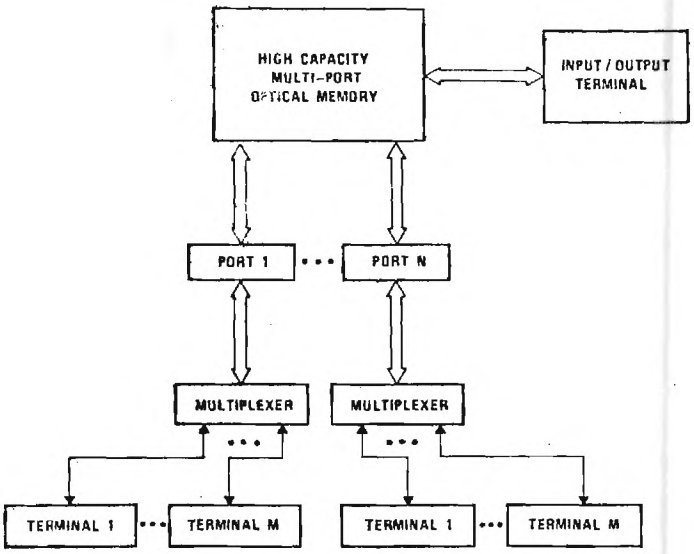

Fig. 2. Computer architecture for a record access system.

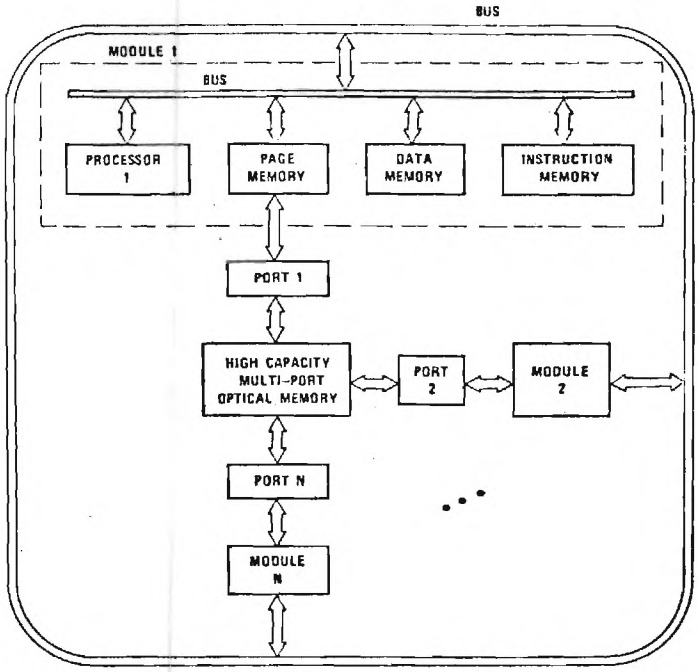

Fig. 4. Computer structure for parallel processing.

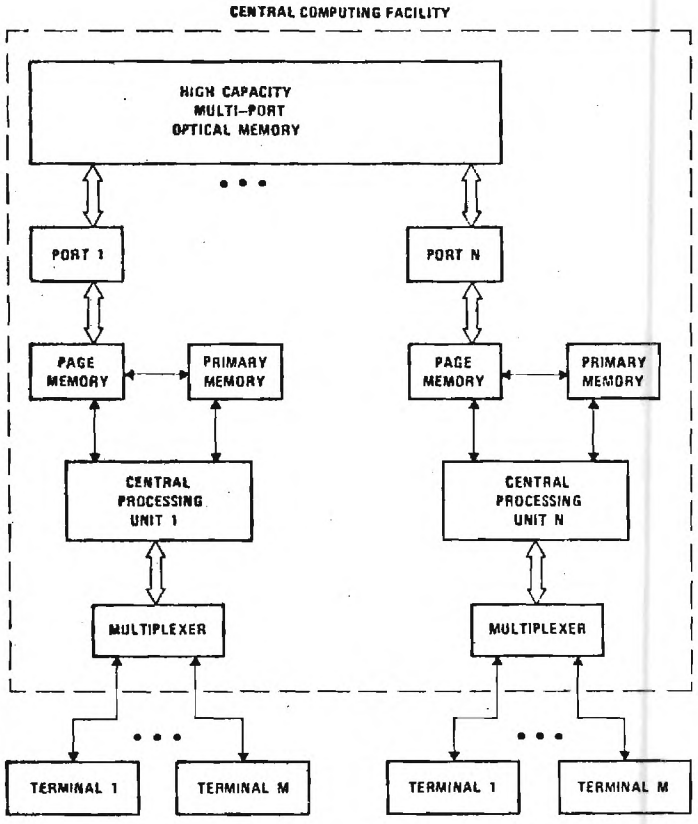

Fig. 3. Simultaneously shared memory computer system.

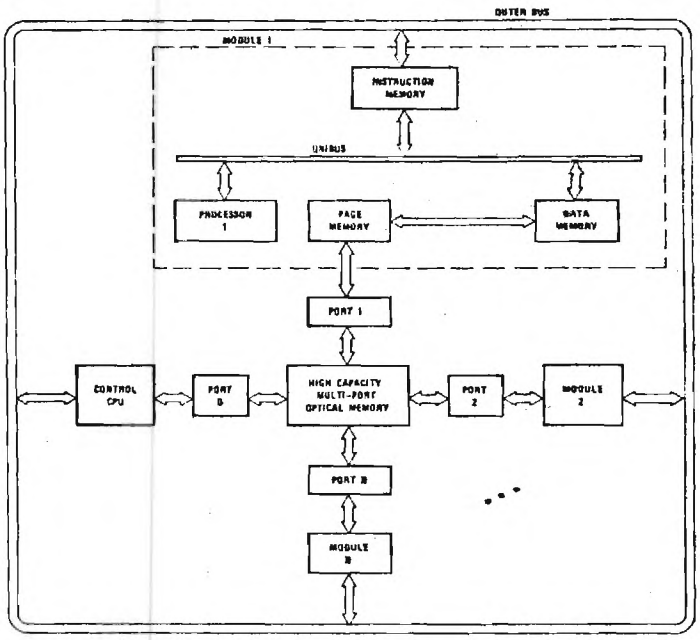

Fig. 5. Synchronized parallel processing computer structure.

V. MULTIPLE RECORDING OF HOLOGRAMS

This section of the report details experimental efforts to store multiple holograms at a single location in a crystal of lithium niobate. Seven holograms of different data masks with an angular separation of 2.97 milliradians were successfully written at a single location and reconstructed, and ten holograms of the same data mask with an angular separation of 4.75 milliradians were successfully written at a second location and reconstructed.

MULTIPLE RECORDING OF HOLOGRAMS

J. E. Weaver and W. R. Callen

APPARATUS

The experimental configuration depicted in Figure 1 was used in all experiments described in this section of the report. The entire experimental arrangement is mounted on an air suspension stable table. The laser used to perform the multiple recording is a 5mW Spectra Physics HeNe gas laser. The crystal was mounted in a modified commercial lens positioner. The modifications included an x-y stage that allowed crystal movement only, in order to vary the location of the interference pattern on the crystal. The retransform lens was rigidly mounted to the entire assembly, which was capable of xyz displacement and capable of deflection in the ϕ and θ (horizontal and vertical) planes. This crystal mount allowed the retransform lens to remain fixed relative to the crystal. By moving the crystal-retransform lens assembly and keeping the reference (R) beam fixed, it was possible to duplicate optically the effect of motion of the R beam relative to a stationary crystal and transform lens assembly. The advantage of this approach is that a stationary R beam may be easily spatially filtered and controlled in diameter. The wavefront does not undergo the distortion produced by an actual deflector. Although in any working memory system, beam deflectors will probably be used, the arrangement used here enables one to study the multiple storage effects in isolation from beam deflection considerations.

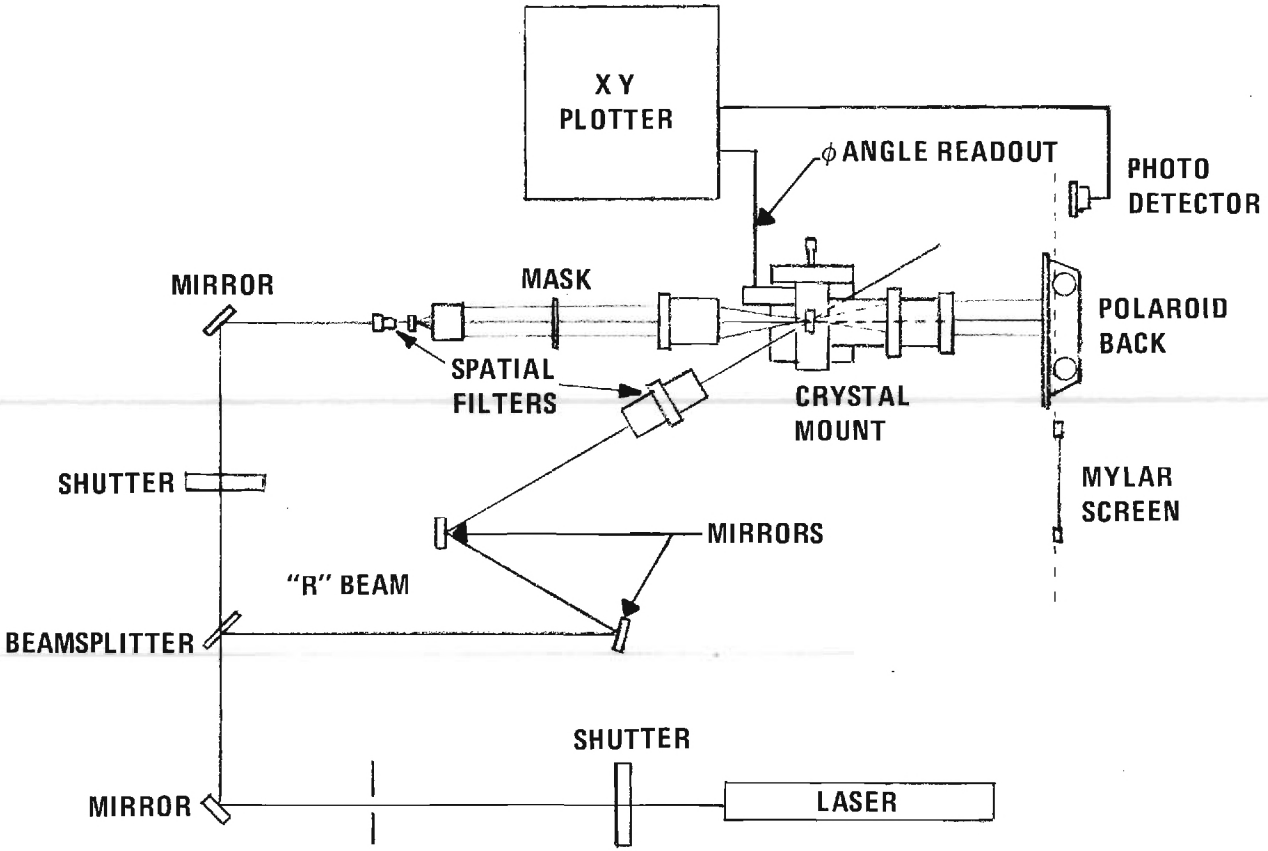

FIGURE 1. Experimental configuration for study of multiple hologram recording.

The transform optics employed were two f/3.5, 200 mm diameter Cooke triplets. The signal beam is formed by passing the laser beam, after spatial filtering and collimating, through a square aperture framing a transparency. The reference beam is also spatially filtered and collimated.

The effective waist diameter of the transformed signal (S) beam as a function of distance along the optical axis (Z direction) is shown by the curve indicated by (0) data points in Figure 2. This waist is defined by visual determination, as opposed to the $1/e^2$ definition employed for Gaussian beams. The width of the central spot of the transform is indicated by (x) data points in Figure 2. The effective diameter of the collimated and spatially filtered reference beam can be determined from Figure 3, which shows a plot of transmitted power versus position of a knife edge that is movable in the y direction.

The region of the holographic grating occurs where both the signal and the reference beams are of approximately equal intensity. This region may be approximated by the first few orders of the one dimensional Fourier transform of the checkerboard-type mask, as shown in Figure 4.

Since the pattern of the mask is similar in both x and y directions, we can characterize it by considering a one-dimensional transmissivity function:

$$t(x) = \mathrm{rect}\left(\frac{x}{16a}\right)\left[\mathrm{comb}\left(\frac{x}{2a}\right) * \mathrm{rect}\left(\frac{x}{a}\right)\right], \qquad (1)$$

using the notation of reference [1]. The actual data mask had 16 squares in each dimension.

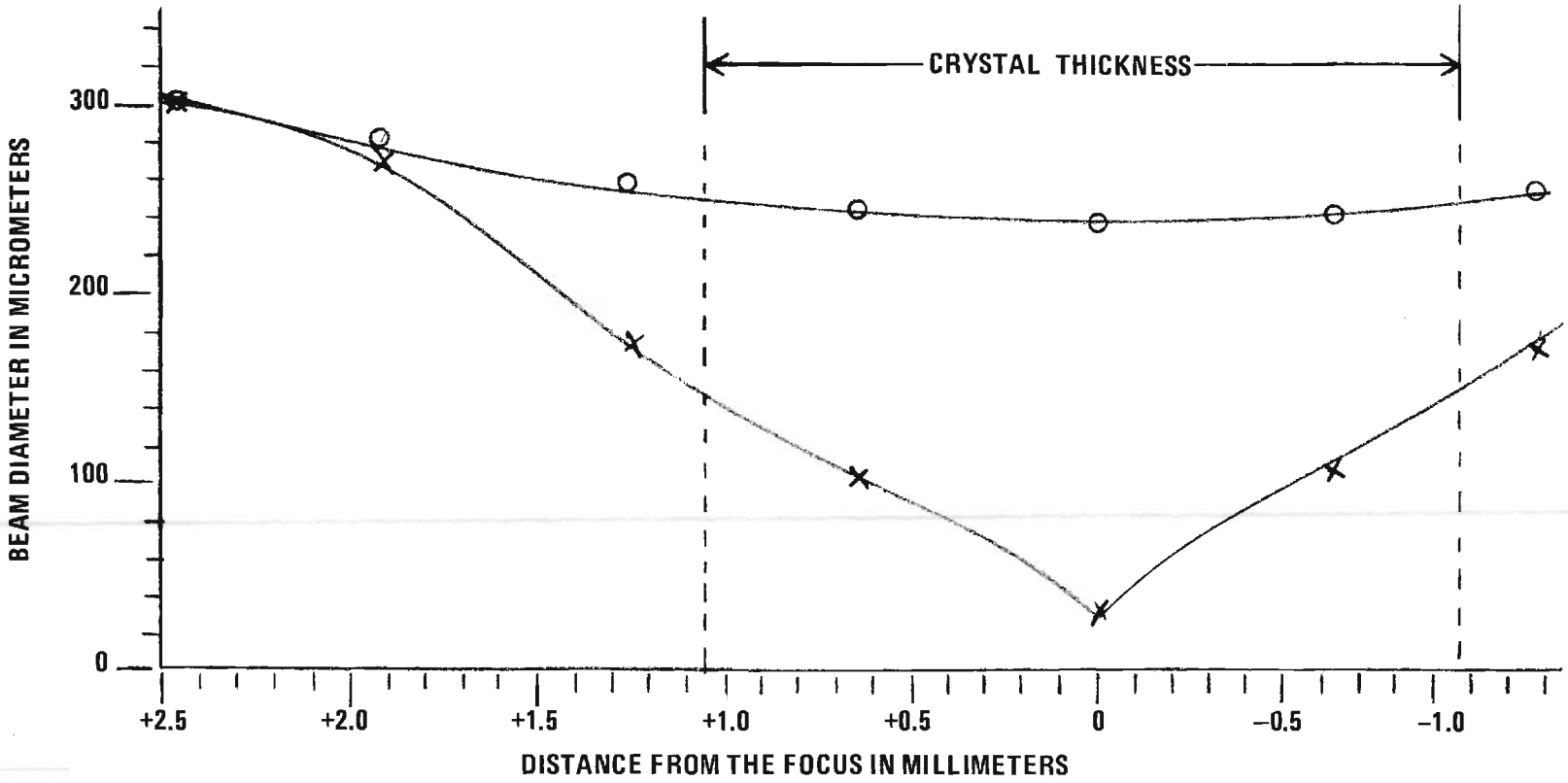

FIGURE 2. Signal ("S") beam diameter as a function of position along the optical axis.

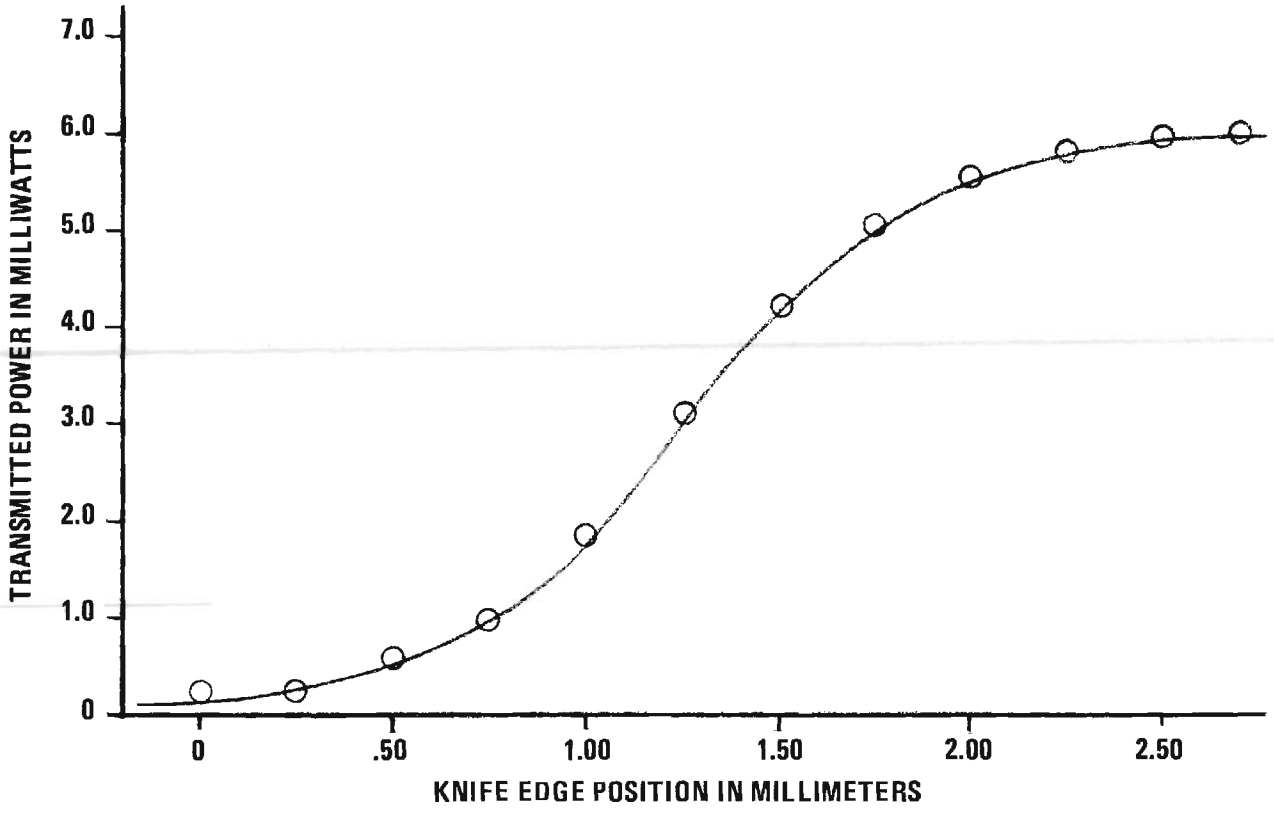

FIGURE 3. Reference ("R") beam diameter determination.

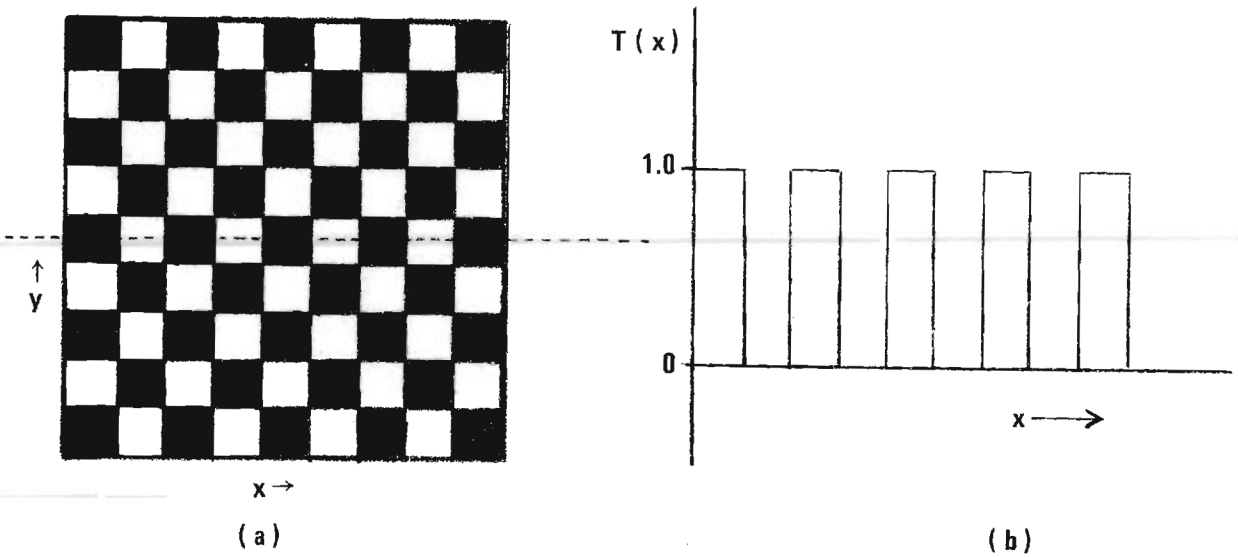

FIGURE 4. (a) Checkerboard mask used to produce signal beam pattern
(b) One-dimensional transform of checkerboard mask (at one value of y)

The transform of Equation (1) is

$$\{t(x)\} = 32a^3 \text{sinc}(16af_x) * [\text{comb}(2af_x)\text{sinc}(af_x)] \qquad (2)$$

where $f_x = x_2/\lambda f_\ell$, with λ as the wavelength of light and f_ℓ the focal length of the transform lens. The transform describes the electric field distribution in a line described by the spatial variable x_2 and positioned one focal length from the transform lens on the opposite side from the data mask. For our experiment, $a=1.06\text{x}10^{-3}$m, $f_\ell=2\text{x}10^{-1}$m, and $\lambda=6.33\text{x}10^{-7}$m. For a perfect thin lens, the power in the first n orders is confined to a circular region that is $(2n+1)\Delta$ in diameter, where Δ is the distance in the (x_2,y_2) plane between any two adjacent orders. For the transform defined by equations (1) and (2), we have

$$\Delta = \frac{\lambda f_\ell}{2a} = 59.7\ \mu\text{m}.$$

The region of the first three orders exists within a region of diameter [2(2)+1][59.7] μm = 298.5 μm. Therefore, we may assume that the hologram exists within a cylinder 300 μm in diameter, which is substantiated by Figure 2.

EXPERIMENTAL PROCEDURE

The crystal used for all experiments was an iron-doped lithium niobate ($LiNbO_3$) crystal (.1 mole per cent F_e in melt). The crystal was 2.12 mm thick, with an average absorption coefficient of 3.15 cm^{-1} and exhibited extremely high light sensitivity.

Two experiments were conducted to illustrate multiple recording of images in $LiNbO_3$. In the first experiment, seven different high contrast images were written at one location in the crystal. The

reconstructed images and the angular separations were recorded. In the second experiment, diffraction efficiency was measured as a function of angle for the reconstruction of the same mask recorded ten times at the same location. The total diffracted power and angular position of the R beam was recorded.

First Experiment. The S beam was attenuated by approximately 30 db and positioned on the crystal. A photograph of the image of the S beam only was made, shown in Figure 5a. The neutral density filter was removed, and the ratio of power of the R beam to that of the S beam was adjusted to fifty; the total beam power was 3.5×10^{-5} watts. A ten second exposure was made with both beams. The reconstruction of the R beam was photographed (Figure 5b). The crystal was displaced in the ϕ direction as the attenuated reconstruction was observed. When the reconstruction was extinct, the change in ϕ was calculated to be .17 degrees (2.97 milliradians). Without further change in crystal orientation, the mask was changed, and a second exposure of ten seconds was made with both S and R beams. The crystal was displaced again in the ϕ direction by .17 degrees, the mask was changed, and another ten second exposure was made with both beams. This procedure of crystal displacement, mask changing, and dual beam exposure was repeated until seven holograms of different masks were written at the same location. Using the R beam only, the reconstructions of all seven holograms were photographed (Figures 5b through 5h).

The results illustrate that the high constrast masks were reconstructed. The noise present in the reconstruction may be divided into three sources: 1) spatial noise present in the optical system;

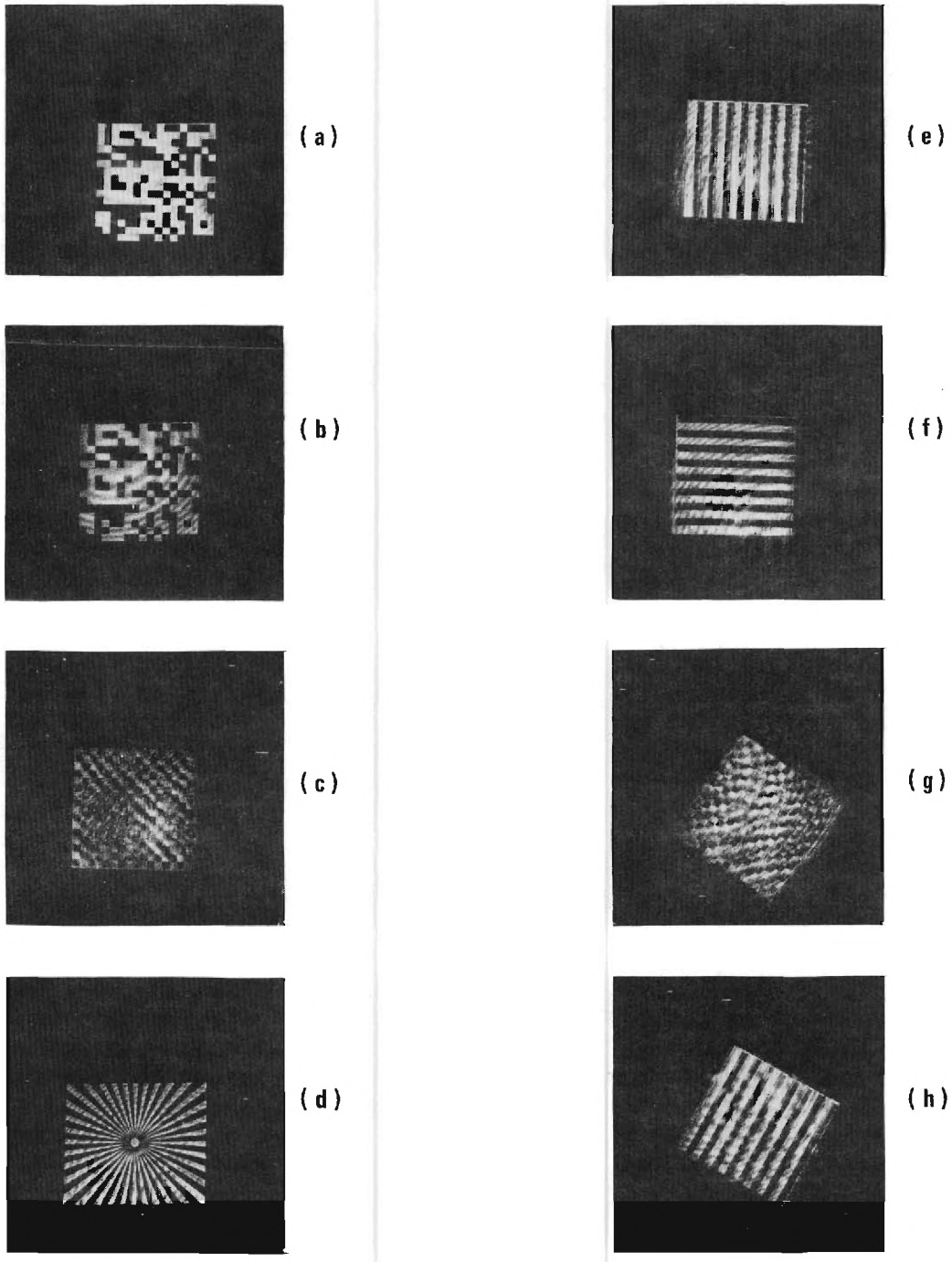

FIGURE 5. Photographs of (a) signal beams, (b)-(h) reconstruction of seven holograms.

2) scattering and aberrations present in the recording medium, and 3) cross-talk from adjacent holograms.

Optical system noise produces the concentric ring pattern that may be seen in all images. This pattern remains fixed as the crystal is rotated, which indicates that this pattern is not produced by the recording medium. This ring pattern is also observed using the S beam only, which indicates that holographic reconstruction noise and aberrations are not contributing.

Noise due to scattering and aberrations of the recording medium are exhibited as 1) blurring or fringes around the high contrast-high spatial frequency edges; 2) dark regions in the center of extended light areas and vice-versa; and 3) speckle noise distributed through the circular region corresponding to the clear aperture of the lens.

Cross-talk due to adjacent holograms is not inherent in the reading operation, but is due to poor repeatability in the Φ positioning operation.

Second Experiment. Using the same experimental arrangement as in the first experiment, but without changing the mask, ten holograms were written. The angular separation between holograms was 4.75 milliradians (.272°). The total diffracted power and diffraction efficiency for each of the ten holograms is shown in Table 1. A plot of the diffracted power versus angle is shown in Figure 6. The approximate diffraction efficiency based on an estimate of hologram size is shown on the right side of Figure 6. The typical base width of each reconstruction is 3.8×10^{-3} radians and the half power width is 1.9×10^{-3}

TABLE I. Multiple Hologram Data (Second Experiment)

Hologram (in order of writing)	Total Diffracted Power (μ watts)	Diffraction Efficiency (%)
1	1.45	3.4
2	3.75	8.6
3	1.46	3.4
4	2.44	5.6
5	2.98	6.9
6	3.27	7.6
7	2.53	5.8
8	3.78	8.7
9	2.16	5.0
10	2.88	6.6

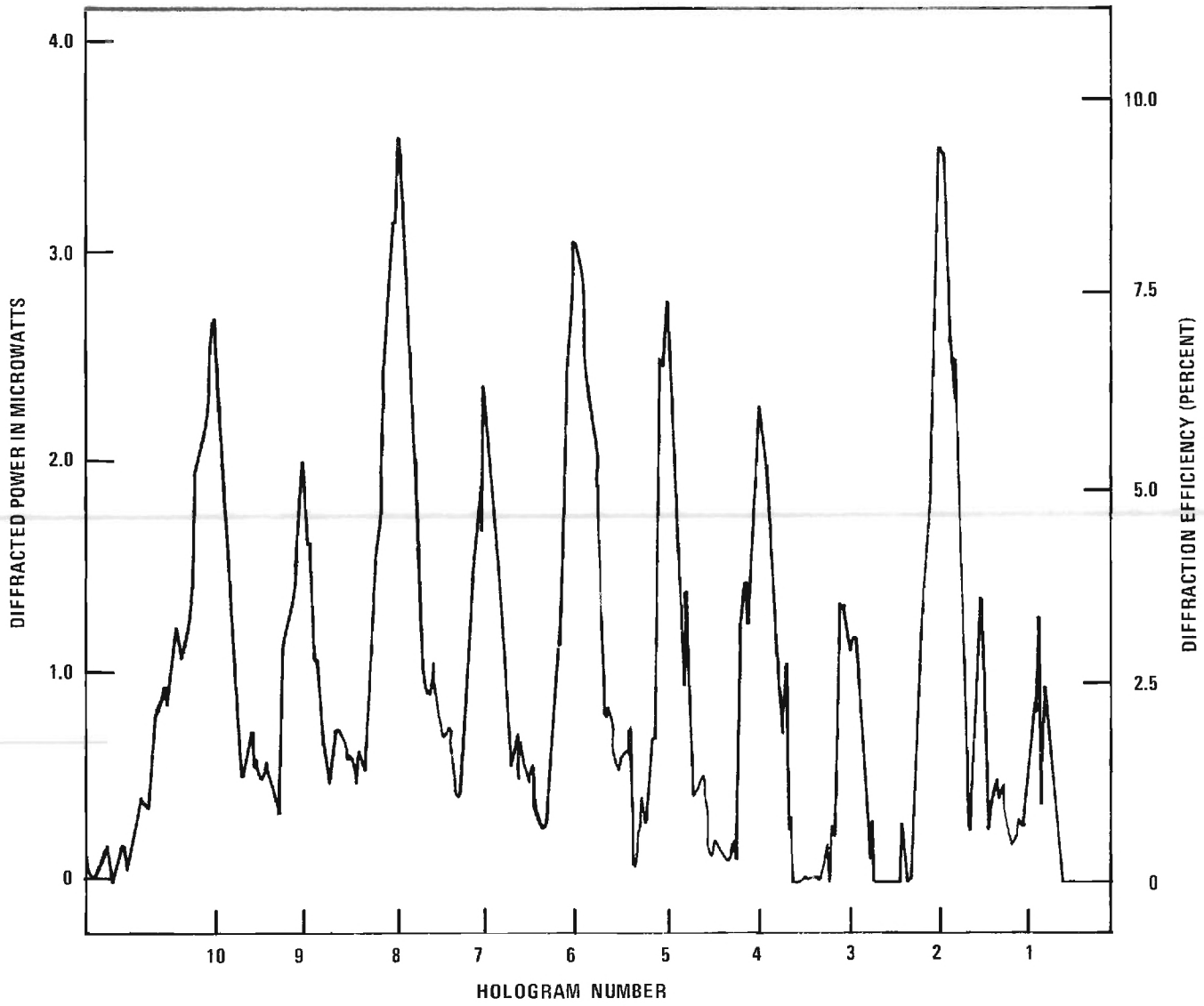

FIGURE 6. Plot of diffracted power versus angle.

radians. The first hologram (extreme right of Figure 6) is noisy and reduced in diffraction efficiency, because this hologram was exposed longer than were the other holograms while the quality of the reconstuction was examined visually with the full power R beam.

FUTURE WORK

Future work in this area will be to reduce the spatial noise in the recording system, calculate and measure the R beam positioning sensitivity, develop an optimum mask for the storing of data, and examine the relationship between the relative strength of object and reference beam and diffraction efficiency.

REFERENCES

[1] J. W. Goodman, Introduction to Fourier Optics, New York: McGraw-Hill, 1968, pp. 9-17.

REFERENCES

[1] J. J. Amodei, "Analysis of transport processes during holographic recording in insulators," RCA Review, vol. 32, pp. 185-199, June 1971.

[2] S. F. Su and T. K. Gaylord, "Unified approach to the formation of phase holograms in ferroelectric crystals," J. Appl. Phys., vol. 46, no. 12, pp. 5208-5213, December 1975.

[3] S. F. Su and T. K. Gaylord, "Determination of physical parameters and processes in hologram formation in ferroelectrics," J. Appl. Phys., vol. 47, no. 6, pp. 2757-2758, June 1976.

[4] S. F. Su and T. K. Gaylord, "Refractive-index profile and physical process determination in thick gratings in electro-optic crystals," Appl. Optics, vol. 15, no. 8, August 1976 (to appear).

[5] C. B. Burckhardt, "Diffraction of a plane wave at a sinusoidally stratified dielectric grating," J. Opt. Soc. Am., vol. 56, pp. 1502-1509, November 1966.

[6] H. Kogelnik, "Coupled-wave theory for thick hologram gratings," Bell Syst. Tech. J., vol. 48, no. 9, pp. 2909-2947, November 1969.

[7] R. Magnusson and T. K. Gaylord, "Use of dynamic theory to describe experimental results from volume holography," J. Appl. Phys., vol. 47, no. 1, pp. 190-199, January 1976.

[8] C. O. Alford and T. K. Gaylord, "The potential of multi-port optical memories in digital computing," Proc. of the International Optical Computing Conference, Washington, D.C., April 1975.